LBNL-41464

ERNEST ORLANDO LAWRENCE BERKELEY NATIONAL LABORATORY

The Oxidation Behavior of SiC Sintered with Al-B-C and Improved Oxidation Resistance via Heat Treatments

Mark Sixta

Materials Sciences Division
Center for Advanced Materials

December 1997

M.S. Thesis

REFERENCE COPY
Does Not
Circulate

Bldg. 50 Library - Ref.
Lawrence Berkeley National Laboratory

LBNL-41464
Copy 1

DISCLAIMER

This document was prepared as an account of work sponsored by the United States Government. While this document is believed to contain correct information, neither the United States Government nor any agency thereof, nor the Regents of the University of California, nor any of their employees, makes any warranty, express or implied, or assumes any legal responsibility for the accuracy, completeness, or usefulness of any information, apparatus, product, or process disclosed, or represents that its use would not infringe privately owned rights. Reference herein to any specific commercial product, process, or service by its trade name, trademark, manufacturer, or otherwise, does not necessarily constitute or imply its endorsement, recommendation, or favoring by the United States Government or any agency thereof, or the Regents of the University of California. The views and opinions of authors expressed herein do not necessarily state or reflect those of the United States Government or any agency thereof or the Regents of the University of California.

The Oxidation Behavior of SiC Sintered with Al-B-C and Improved Oxidation Resistance via Heat Treatments

Mark Sixta

(M.S. Thesis)

Department of Materials Science and Mineral Engineering
University of California, Berkeley

and

Materials Sciences Division
Lawrence Berkeley National Laboratory
University of California
Berkeley, CA 94720-1760

December, 1997

This work was supported by the Director, Office of Energy Research, Office of Basic Energy Sciences, Materials Sciences Division of the U.S. Department of Energy under Contract No. DE-AC03-76SF0098.

The Oxidation Behavior of SiC Sintered with Al-B-C and Improved Oxidation Resistance via Heat Treatments

by

Mark Eldon Sixta

B.S. (University of California, Berkeley) 1994

A thesis submitted in partial satisfaction of the

requirements for the degree of

Master of Science

in

Engineering:

Materials Science and Mineral Engineering

in the

GRADUATE DIVISION

of the

UNIVERSITY OF CALIFORNIA, BERKELEY

Committee in charge:

Professor L.C. De Jonghe, Chair
Professor J.W. Evans
Professor R.O. Ritchie

Fall 1997

Abstract

The Oxidation Behavior of SiC Sintered with Al-B-C and Improved Oxidation Resistance via Heat Treatments

by

Mark Eldon Sixta

Master of Science in Materials Science and Engineering

University of California, Berkeley

Professor Lutgard C. De Jonghe, Chair

The oxidation behavior of high strength and high toughness SiC, sintered with Al, B, and C (ABC-SiC), was examined. Kinetic data were acquired and the parabolic rate constant for oxidation was determined and compared with literature data on various SiC materials. The role of secondary phases on the oxide morphology was explored. ABC-SiC was compared to commercially available SiC, Hexoloy, and SiC sintered with 10% yttrium aluminum garnet (YAG). Two-step sintering (pre-coarsening) was employed with holds for 48 hours at 600-1600°C, prior to the typical hot-pressing conditions of 1900°C for 1 hour, to change the chemistry and reduce the number of bubbles in the silica scale. The effects on the oxide thickness and integrity was examined as a function of the pre-coarsening heat treatment temperature. Additionally, the hot-pressed ABC-SiC was subjected to heat treatments (anneals) at 1800°C for 1 hour in nitrogen, Ar, and vacuum environments, and the effects on subsequent oxidation were evaluated. The Ar and vacuum heat treatments dramatically improved the oxidation resistance of ABC-SiC. Finally, reoxidation experiments were performed to try to alter the surface chemistry of the SiC to improve the oxidation resistance. The four-point bend strengths and two-

parameter Weibull plots of the most successful heat treatments were compared with the standard ABC-SiC to ensure that significant degradation did not result from altering the processing of the material.

TABLE OF CONTENTS

Acknowledgments v

I. INTRODUCTION

A. SiC sintered with Al, B, & C (ABC-SiC) 1
B. Types of corrosive attack 4
C. Fundamental steps in SiC oxidation 6
D. Oxidation rate-limiting step 7
E. Physical properties of silica 9
F. Effects if water on silica 11
G. Crystallization of silica 12
H. Issues of bubbles in the oxide 14
J. Possible sources of bubble formation 16
K. Objectives of the current work 19

II. EXPERIMENTAL PROCEDURE

A. Starting materials/processing 20
B. Hot-pressing conditions 21
C. Two-step processing 21
D. Heat treatments 22
E. Microstructure evaluation 23
F. Oxidation parameters 24
G. Mechanical testing 26

III. RESULTS AND DISCUSSION

A. Oxidation kinetics for ABC-SiC (1200°C) 27
B. Effects of impurities on the oxidation behavior 30
C. Oxide morphology of ABC-SiC 33
D. TEM of oxides 35
E. Bubbles in ABC-SiC 36

F. Oxidation of two-step processed SiC 37

G. Comparison of ABC-SiC oxidation with other silicon carbides 39

H. Oxidation behavior of SiC annealed in various environments 40

J. Oxide morphology and chemistry after heat treatments 42

K. Effects of annealing on chemistry and surface morphology 45

L. Microstructure after annealing 47

M. Mechanical properties 48

IV. CONCLUSION 51

V. REFERENCES 53

VI. FIGURES 57

Acknowledgements

I owe Professor De Jonghe many thanks for supporting this project and providing valuable discussions. Dr. Warren MoberlyChan had an integral role in completing this thesis. His countless hours spent teaching, advising, amusing, and preparing and examining TEM samples were invaluable.

Drs. Joe Cao, Mani Gopal, and Yanping Ma, were instrumental in helping me become acclimated with the laboratory and provided endless guidance. They were always willing to help and frequently interrupted their own activities to help me with this project. For all their help I am extremely grateful.

I. INTRODUCTION

A. SiC sintered with Al, B, & C (ABC-SiC)

SiC has received much attention as a high temperature structural material. The high thermal stability and high strength of SiC, compared to many metals, makes it a candidate material for various applications such as components for gas turbines, piston engines, and heat exchangers.[1] However, the inherently low fracture toughness of SiC has limited the implementation of structural components fabricated with SiC.

The covalent nature of the bonding in SiC is responsible for the high strength and hardness exhibited by this material, and coupled with high temperature stability makes SiC attractive as components for engines, heat exchangers, etc. However, the strong covalent bonds, while necessary for the excellent material properties, introduce considerable difficulty in the fabrication process. Consequently, sintering additives are typically introduced in SiC to facilitate fabricating components. The role of the additives is generally to promote the formation of a liquid phase, which leads to enhanced mass transport and hence enables densification. Without sintering additives it is not feasible to densify SiC. While the inherent oxidation resistance of SiC is high, the additives have deleterious effects on the oxidation behavior, and leave an intergranular glassy phase. As seen in Figure 1, lines F, G, and H correspond to SiC processed with various additives, and thus the oxidation rate is enhanced in these materials relative to high purity SiC. The additives typically affect the viscosity of the intergranular glass and also influence crystallization of the oxide scale that develops in oxidation, thereby altering the oxidation behavior. Typically, SiC forms a silicon rich oxide on the surface upon oxidation. This oxide invariably contains bubbles that further degrade oxidation resistance.

The primary limitation to implementation of SiC as a structural material is the inherent brittleness. Extensive research has been conducted to increase the fracture toughness of SiC. The approaches have included both monolithic and composite silicon carbides. For monolithic SiC the various methods all utilize the β-SiC (cubic) to α-SiC (hexagonal) phase transformation to produce a microstructure with elongated, plate-like, grains akin to toughening in the Si_3N_4 system, where needle like grains are obtained. The sintering additives actually serve a dual role for these monolithic materials. They provide a liquid phase to facilitate densification and in most cases enhance the phase transformation. The primary additives used to toughen SiC are Al_2O_3, yttrium aluminum garnet (YAG)[2,3,4], or Al-B-and C.[5]

The current research studies the oxidation behavior of SiC with Al, B, and C sintering additives. The fracture toughness of SiC with these additives is the highest reported in the literature, ~ 9 MPa√m.[5] The toughness is largely derived from various crack bridging processes in the wake of the crack.[6] Additionally, unlike what would be expected for toughened ceramics, the strength is not sacrificed for the ABC-SiC. In fact, the interlocking-grain microstructure enhances the strength of the material. The final microstructure consists of large grains with an aspect ratio of ~ 7 surrounded by a thin grain boundary phase, which primarily consists of Al-O-C. Additionally, the remaining sintering additives form bulk secondary phases and also triple point phases. These have been identified as $Al_4B_7C_8$ and Al_4O_4C.[5,7,8] The grain boundary phase permits intergranular fracture, which is necessary to obtain a tortuous crack path promoting crack bridging and high toughness, but it has adverse effects on the high temperature properties of SiC. Both the oxidation resistance and the creep properties of SiC with Al, B, and C

additives are diminished. Additionally, the bulk secondary phases are likely the source of bubbles in the oxide scale.

Numerous ceramics, like Al_2O_3 and ZrO_2, are thermodynamically stable in air. In contrast, while SiC and other non-oxide ceramics like Si_3N_4 exhibit high temperature stability, they are not inherently resistant to oxidation. However, in oxidizing environments SiC forms a thin layer of silicon dioxide (SiO_2) which effectively passivates the surface and protects the material from further reactions. Unlike metal oxidation, transport of oxygen through the SiO_2 scale is the important diffusion process since platinum-marker experiments show the new oxide grows at the SiC/SiO_2 interface.[57] The permeability of oxygen through SiO_2 is the lowest among the common oxides that form to serve as protective coatings.[9] The low oxygen permeability suggests that the performance of SiC at high temperatures in oxidizing environments could exceed that of metals. Superalloys for such applications utilize the same concept of a protective coating to improve the high temperature stability. The analogous coatings for superalloys are Al_2O_3 and Cr_2O_3.[10]

SiC is not thermodynamically stable in air since a reaction with oxygen is accompanied by a negative change in the free energy of the system. However, for practical purposes the material is stable since the rate of the reaction is kinetically limited by the formation of a protective silica scale (SiO_2). The various reactions between SiC and O_2, with the respective free energy changes, are provided in Table 1.[11] While the first of these reactions may seem more likely to occur, based solely on an evaluation of the free energy of the reactions, the second reaction is believed to be the most common reaction. Gas chromatography has shown that CO is generated at the oxide/ceramic

interface.[12] However, the further oxidation to CO_2 cannot be excluded.[13] The exact reaction(s) that occurs is dependent on the oxygen partial pressure of the environment.

	ΔF (kcal.)	ΔF (kcal.)
Reaction	25°C	1627°C
$SiC + 2O_2 \rightarrow SiO_2 + CO_2$	-279.2	-215.4
$SiC + 3/2O_2 \rightarrow SiO_2 + CO$	-217.7	-187.2
$SiC + O_2 \rightarrow SiO_2 + C$	-184.9	-120.7
$SiC + 3/2O_2 \rightarrow SiO + CO_2$	-110.1	-144.5
$SiC + O_2 \rightarrow SiO + CO$	-48.6	-116.3
$SiC + 1/2O_2 \rightarrow SiO + C$	-15.8	-49.8
$SiC + O_2 \rightarrow Si + CO_2$	-81.9	-86.5
$SiC + 1/2O_2 \rightarrow Si + CO$	-20.4	-58.3

Table 1: Free energies for oxidation reactions

Should the third reaction in Table 1 take place, a subsequent reaction of C with oxygen would immediately occur and generate CO through reaction (1).

$$C(s) + 1/2O_2(g) \rightarrow CO(g) \qquad (1)$$

There is only limited evidence that an oxycarbide forms between the silica and SiC.[14]

B. Types of Corrosive Attack

There are several types of corrosive attack that may occur at elevated temperatures for SiC. Figure 2 indicates the various regions, which include passive oxidation, active oxidation, scale/substrate reaction, and scale volatility.[1] While the exact position of the lines separating the regions is dependent on the specific system, such as types and amounts of sintering additives, this figure provides an approximate account of the particular degradation which is likely for a given pressure and temperature. The active oxidation regime is characterized by the generation of SiO(g). This gas is generated by the reaction.

$$SiC(s) + O_2(g) = SiO(g) + CO(g) \quad (2)$$

Active oxidation is particularly detrimental to the life of a SiC component since the advantageous passivating SiO_2 layer does not have an opportunity to form. Active oxidation will lead to rapid degradation but this will only occur at low oxygen partial pressures and high temperatures, as seen in the volatility diagram of Figure 3.[15] Fortunately, many environments where SiC is being considered, like combustion environments, are oxidizing and should possess appreciable partial pressures of oxidants such as oxygen, CO_2, or H_2O.[1] However, as shown in Figure 2, when extremely high temperatures are reached the volatility of the silica scale and reactions between the SiO_2 and SiC become a major concern regardless of the oxidant pressure. At elevated temperatures, the following reaction becomes important for SiC.[1]

$$SiC(s) + 2SiO_2 = 3SiO(g) + CO(g) \quad (3)$$

This reaction may lead to high gas pressures at the SiC/SiO_2 interface; these high pressures could compromise the integrity of the scale. This would cause the passivating effects of the SiO_2 to be diminished if not destroyed.

Evaluation of the interfacial reaction can be performed with aid of the Si-C-O predominance diagram, Figure 4.[1] The SiC/SiO_2 coexistence line (AB) provides the gas pressure. Comparison of the gas pressure from Figure 4 with the total vapor pressure of the system (as it varies with temperature), Figure 5, yields the temperature at which the system becomes unstable for a carbon-saturated, stoichiometric, and silicon-saturated system. Thus, for a carbon-saturated system, taking 1 atm as the criterion for instability, the SiC/SiO_2 interface becomes unstable at ~ 1800 K. For the other systems the pressure approaches 1 atm at a temperature near the melting point of SiO_2. For systems that are

carbon-saturated, the stoichiometric composition is obtained by releasing large amounts of CO(g) and also forming a secondary SiC.[16] Thus, systems with a carbon-saturated interface are more susceptible to bubble formation in the oxide. Therefore, it is clear that SiC applications are only suitable for situations where the passive oxidation regime is the dominant degradation mechanism. The current work focuses on development of SiC for temperatures in the range of 1300°C to 1500°C, thus passive oxidation is the region of most interest, and the following experiments will deal with this issue.

C. Fundamental Steps in SiC Oxidation

Oxidation of SiC involves five fundamental steps: (1) transport of molecular oxygen gas to the surface of the oxide, (2) oxygen diffusion through the oxide towards the oxide/ceramic interface, (3) reaction of the ceramic with the oxygen at the interface, (4) diffusion of gaseous products (CO) through the oxide scale, (5) diffusion of gas(es) away from the oxide surface. Since platinum-marker experiments show the new oxide forming at the SiO_2/SiC,[57] Si and C diffusion through the scale are not the fundamental steps in the oxidation process. The oxidation process is shown schematically in Figure 6. From the five processes that occur during the oxidation of SiC, steps (1) and (5) can be eliminated as possible rate limiting steps since they involve diffusion of species through a gas. Therefore, the possible rate limiting steps are the inward diffusion of oxygen through the oxide to the interface, interface reaction, or diffusion of CO from the interface to the surface or mixed control. Numerous groups have performed extensive studies to identify and evaluate the kinetically limiting step. However, there is still no consensus on the rate-controlling step, but there is general agreement that SiC oxidation follows parabolic kinetics after a short linear region that is dominated by the oxidation

reaction. The parabolic kinetics indicates that the reaction is diffusion controlled. Each of the possible rate-controlling, or slowest, steps are now evaluated in turn.

D. Oxidation Rate-Controlling Step

One complication in evaluating the oxidation of SiC is the presence of impurities (or sintering additives). Figure 1 compares the parabolic rates for SiC, fabricated with a variety of additives and techniques, and Si. Motzfeld[17] reviewed the early work on SiC oxidation and showed that the rate constants for SiC and Si are very similar after correcting for the stoichiometric difference between the two reactions, (4) and (5). SiC consumes 1.5 moles of O_2 compared to 1 mole for Si during oxidation.

$$Si(s) + O_2(g) = SiO_2(s) \tag{4}$$

$$SiC(s) + 3/2O_2(g) = SiO_2(s) + CO(g) \tag{5}$$

This indicates that the same rate-controlling step is present for Si and SiC. The rate-controlling step for Si is the inward diffusion of oxygen.[18] Examination of the activation energy can provide additional insights into the limiting diffusion mechanism. As reported by Deal and Grove,[18] the activation energy for Si oxidation is 119 kJ/mole. Table 2 compares this activation energy, for oxygen diffusion through silica, with the activation energy reported by several investigators. These activation energies for SiC are ~ 120-140 kJ/mole for $T < 1350°C$ and greater than 200 kJ/mole for $T > 1350°C$. The lower temperature regime corresponds to the activation energy of molecular oxygen through silica.

The increase in the activation energy with temperature suggests that the mechanism is different at elevated temperatures. Diffusion may occur by network-ion

Material	Temperature Range (K)	Activation Energy (kJ/mol)
Si	1073-1473	119.3
Controlled-nucleation, thermally deposited SiC	1473-1673	142
Single crystal SiC	1673-1773	293
C face	1473-1623	120
C face	1623-1773	260
Si face	1473-1773	223-298
CVD SiC	1640-1820	125.5
CVD SiC	1823-1948	345

Table 2: Activation energies for SiC oxidation.

exchange in addition to molecular diffusion. Thus, Zheng et al.[19,20] suggest that a mixture of molecular oxygen diffusion and network exchange are present at higher temperatures and this leads to a higher activation energy. An alternative interpretation of these results is that the diffusion is governed by a different gaseous species, i.e. CO, which could account for a change in activation energy. Additionally, crystallization of the silica will result in a change in the activation energy.

Since the oxidation of SiC follows parabolic kinetics, the other possibility for the rate limiting step is outward diffusion of CO(g). The increase in the activation energy above ~ T>1350°C has been attributed to the diffusion of CO.[12,21,22] Luthra[22] contends that the oxidation rate of SiC cannot be limited by oxygen diffusion alone. Otherwise, CO gas bubbles should never form and CO permeability should be much higher than oxygen permeability. Comparing the molecular sizes, C-O is 0.1128 nm and O-O is 0.1208 nm,[23] the diffusivities should be similar. However, should the oxidation rate be limited by outward diffusion of CO a concentration gradient of CO across the silica would exist. However, Zheng et al.[19] examined oxides using SIMS and no concentration

gradient was present. An additional difficulty with accepting CO as the rate-controlling is that a pressure of ~ 10^{27} bar (1 bar = 10^5 Pa) at the SiC/SiO_2 interface would be generated should the equilibrium gas pressure be obtained.[1] A pressure of this magnitude would likely cause the scale to blow off, but this behavior is not observed.

The premise that CO diffusion is limiting the oxidation is predicated on the presence of bubbles in the SiO_2. However, as discussed earlier, there are additional reactions that may occur which could account for bubble formation. Also, the secondary phase inclusions may account for bubbles in polycrystalline SiC. Luthra[22] does not consider these possibilities while concluding the reaction is CO diffusion limited.

The final possibility for the rate limiting step is interfacial reaction. If the interfacial reaction is governing the oxidation rate the kinetics would follow a linear behavior. Literature data clearly show that the oxidation reaction follows parabolic kinetics, which eliminates the reaction as the possible limiting step. However, it is likely that the early stages of oxidation are linear until a sufficient oxide is formed to limit the transport of the gaseous species. The experiments in the current work were not directed towards determining the exact kinetic information for SiC. Rather the goal was to minimize the oxidation rate and thus an understanding of the possible rate limiting steps is valuable to review. Since the oxidation is limited by diffusion, efforts to improve the oxidation resistance are therefore targeted at slowing diffusion rates. Ultimately, the effect of the oxide chemistry and morphology on the oxidation rate must be determined.

E. Physical Properties of Silica

The nature of the passivating SiO_2 scale on SiC is primarily dependent on the temperature and chemistry of the system. The oxide scale is typically amorphous at the

beginning of oxidation and at low temperatures. Even at lower temperatures, the SiO_2 tends to crystallize for longer times and, naturally, elevated temperatures result in a crystalline (or partially crystalline) oxide. The presence of some impurities can enhance the crystallization process,[24] which could also explain the higher activation energy at higher temperatures.

Vitreous (amorphous) silica forms at lower temperatures and is characterized by the absence of order on a scale larger than a few tetrahedra. Glasses are viewed as three-dimensional networks or arrays which do not repeat any unit of the structure at regular intervals since it lacks symmetry and periodicity. For the case of SiO_2, the networks are composed of silicon and oxygen tetrahedra. According to the hypothesis of Zachariasen[25] the oxygen tetrahedra will share corners and not edges or faces. Additionally, at least three corners of each polyhedra should be shared. Figure 7 provides a schematic representation of a crystalline form and random-network glassy form of silica. Gases tend to dissolve molecularly in vitreous silica as a consequence of the open structure.[26] Often the mass transport through silica is evaluated by the permeability. The permeability is the product of the solubility of the gas, s, and the diffusion coefficient, D, equation (6).

$$P = s \cdot D \tag{6}$$

As the size of the molecule increases the concentration of the dissolved gas will decrease and hence the permeability is lower for larger molecules. The viscosity of the silica is also directly related to the impurities present. Since the oxygen diffusivity is inversely proportional to the viscosity, through the Stokes-Einstein equation (7), the oxidation rate will increase should impurities lower the viscosity.

$$D = \frac{k_B T}{4\pi R \eta} \tag{7}$$

D is the diffusivity, η is the viscosity, k_B is Boltzmann's constant, R is the effective molecular radius of the spheres, and T is the temperature. Common oxidants such as water also lower the viscosity of the silica. Of importance in the current research is the addition of B_2O_3 to silica. Boron from the sintering additives may be oxidized and incorporated into the scale and reduce the viscosity.[26] The dependence of viscosity on temperature also follows an inverse relationship. The glass oxidation layer behaves more like a liquid at higher temperatures, which results in the mass transport through the passivating layer being facilitated.

F. Effects of Water on Oxides

H_2O is generally agreed to accelerate the rate of oxidation.[27,28,29,30,31] Previously mentioned was the deleterious effect of the viscosity of the glass, but also reactions with the SiC must be considered.

$$SiC(s) + 3H_2O(g) = SiO_2(s) + CO(g) + 3H_2(g) \tag{8}$$

Tressler *et al.*[24] showed that the effect of water vapor on single-crystal and sintered α-SiC is that the oxidation rate is accelerated approximately 10 to 20 times. The presence of steam presumably results in rapid permeation of H_2O molecules through the incorporation of $(OH)^-$ and $(H_3O)^+$ into the SiO_2. The effect of H_2O on the isothermal oxidation of pure Si is noted by Deal and Grove[18] and is attributed to a higher solubility of H_2O in SiO_2, ~3.4 x 10^{19} molecules/cm^3, versus molecular oxygen solubility in SiO_2, ~ 5.5 x 10^{16} molecules/cm^3. Additionally, Deal and Grove[18] show that the oxidation rate is the same in a mixture of H_2O/O_2 and H_2O/Ar, suggesting that water may actually be the

primary oxidizing species. The presence of water may also disrupt the SiO_2 network by forming nonbridging SiOH groups.[32] Thus, even if water is not the primary oxidizing species it may reduce the viscosity of the SiO_2 and hence the oxidation rate would increase since the molecular oxygen can diffuse at a higher rate.

G. Crystallization

Crystallization of the silica scale occurs for long times and higher temperatures since vitreous silica is metastable below its melting point. The equilibrium diagram for SiO_2 is provided in Figure 8. Since many of the transformations are sluggish it is useful to include the metastable phases in the diagram, Figure 9. In Figure 9 the most stable phase, that with the lowest vapor pressure, is the equilibrium phase and is shown as the dark line. The crystalline silica exists as several different polymorphic forms corresponding to the various ways the tetrahedra can be arranged with all of the corners shared. The three basic structures are quartz, tridymite, and cristobalite; the structure of cristobalite is shown in Figure 10. Also, each of these three phases possess in turn two or three modifications, typically a high-low or α and β phase. The high-low transformation corresponds to a change in the secondary coordination by a distortion of the structure, which does not require breaking bonds or changing the number of nearest neighbors. Since these transformations occur by merely displacing the tetrahedra from their previous position they occur rapidly, and at a definitive temperature, since there is no activation barrier for the displacement.[33] In contrast, a reconstructive transformation requires interatomic bonds to be broken as the atoms are displaced and this energy is recovered when the new structure is formed. Thus, these reconstructive transformations can occur by nucleation and growth in the solid state, or the unstable modification can vaporize and

condense as the more stable phase if there is an appreciable vapor pressure. These transformations can be accelerated by the presence of a liquid phase. The liquid phase, should it possess a higher solubility for the unstable phase, allows the unstable phase to go into solution and precipitate out in the stable form, as seen in the β-SiC (cubic) to α-SiC (hexagonal) transformation. Since these transformations are kinetically sluggish many of the high temperature phases, like cristobalite, exist in a metastable form even at room temperature. The most stable of these phases is detailed in Figure 8. While cristobalite is not the densest of the crystalline forms (ρ_{quartz} = 2.65 g/cm^3, $\rho_{cristobalite}$ = 2.32 g/cm^3),[33] crystallization of the silica scale to cristobalite has been shown to reduce the oxidation rate of SiC.[24,34,35] Additionally, impurities serve a vital role in determining the phase of silica that will form. Figure 11 illustrates the effects of impurities on the possible phases.[36]

Crystallization is beneficial for improving oxidation resistance if only diffusion is considered. The diffusion rates are lower for crystalline SiO_2, but this is only true provided no cracks develop in the oxide. Cracks in a crystalline oxide film arise when the material is cooled due to thermal expansion mismatch with the substrate, but cracks may also be introduced during phase transformations. The high-low inversion, a cubic to tetragonal transformation at 270°C for cristobalite, is accompanied by a three percent volume change. Consequently, crystalline silica is sensitive to thermal shock where high-low inversions occur. Should a high quartz silica scale form and subsequently transform to cristobalite the transformation would result in a 15% volume expansion.[26] An expansion of this order would likely result in cracks in the passivating oxide which would inhibit the protective nature of the scale.

The stability of vitreous silica is less than crystalline SiO_2. Above about 1350°C a vitreous silica will begin to vaporize by the following reaction:[26]

$$SiO_2(s) = SiO(g) + 1/2O_2(g) \quad (9)$$

The vaporization reaction is enhanced in reducing atmospheres but must still be considered when evaluating the long term high temperature exposure of SiC components. A benefit of a crystalline oxide, for instance cristobalite, is that the scale should provide similar protection as the temperature is raised to the melting point of ~ 1740°C. Naturally, the oxidation rate would still increase as the temperature is raised since the diffusivity, and hence permeability of oxygen, increases with temperature. The parabolic rate constant will thus be greater for vitreous silica since the viscosity is decreasing and this further enhances the increase in the diffusivity at higher temperatures. Overall, a crystalline scale is more likely to provide greater oxidation resistance, but in practice the scales typically exhibit both vitreous and crystalline regions and thus an understanding of the diffusion relationships for both is necessary.

H. Issues of Bubbles in the Oxide

The aforementioned oxidation behavior relates to SiC with a thin passivating layer of SiO_2. However, in many silicon carbides bubbles are observed in the silica scale. It is hypothesized that bubbles in the oxide scale are a significant source of concern since they would be expected to compromise the integrity of the protective layer of SiO_2. Bubbles in the oxide are a concern since the rate controlling step for this reaction is the diffusion of a gaseous species through the silica. The mass transport of the rate limiting species, presumably oxygen, suggests that bubbles will greatly accelerate the rate of oxidation since the oxygen can diffuse fast through the gaseous environment of the

bubbles and this rate should be vastly enhanced compared to solid state diffusion. Even if a liquid phase, or a lower viscosity glass, is formed as a result of impurities in the system, as Singhal and Lange[44] suggested, the presence of bubbles would likely increase the oxidation rate since the bubbles would still provide a faster diffusion path than diffusion through the liquid. The parabolic kinetics are not necessarily compromised by the formation of gas bubbles, but this is only true should the integrity of the scale still be maintained with the bubbles.

New substrate material would continuously be exposed if the bubbles rupture during oxidation. The resultant kinetics for this case would likely tend more towards a linear region that is governed by the rate of the reaction. Costello and Tressler[57] report that the oxidation rate was increased for samples with ruptured bubbles. With ruptured bubbles, and linear kinetics, the SiC would lose all protection against further attack in oxidizing environments since all of the oxidation reactions, Table 1, are thermodynamically favorable and at such high temperatures the oxidation reaction will not be kinetically limited. Therefore, a SiC with bubbles that burst during oxidation, as a result of escaping gaseous by-products, would have no meaningful lifetime as a high temperature structural material. By comparison, parabolic kinetics allow an initial oxide to form relatively fast, but with longer times the increase in the oxide thickness for a high quality passivating layer becomes negligible. Thus, in concept, silicon carbides with bubbles in the oxide scale should exhibit a higher oxidation rate, and ultimately a thicker oxide than pure SiC, but the passivating effects of the silica scale likely would not be sacrificed and should be able to tolerate long term exposure in oxidizing environments at elevated temperatures. However, in practice the bubbles probably are not acceptable for

an actual component. Many of the environments under consideration for SiC are likely to be abrasive in nature or the SiC, in turbine blade applications, may be subjected to collisions with particles in the atmosphere. Either case would likely result in the bubbles bursting. Hence, various processing steps are necessary to eliminate bubble formation.

However, the current investigation will show that, in the absence of ruptured bubbles, the chemistry and degree of crystallinity of the silica scale have a more dramatic impact on the oxidation rate than bubbles.

J. Possible Sources of Bubble Formation

Many studies demonstrate that often the integrity of the oxide is compromised by the formation of gas bubbles in the oxide.[21,37,38,,39,40] However, in most studies bubble formation is not witnessed for CVD and single-crystal SiC[19,24,41] Since the oxidation reaction is limited by diffusion, the detrimental effects of bubbles can be twofold. First, the bubbles may be generated and then rupture. This would lead to rapid degradation of the SiC since the role of the passivating silica scale would be effectively eliminated as new surfaces for oxidation would be continuously exposed. Secondly, even if the bubbles do not rupture to expose unpassivated material they will naturally serve as fast diffusion paths since they are filled with gas and thus the oxidation rate is expected to be accelerated when bubbles are present.

While the detrimental effects of bubbles are readily observed, the source of these bubbles is still not agreed upon in the literature. The oxidation reaction generates CO(g), as shown in Table 1, and this may or may not be further oxidized to CO_2(g). Therefore, the formation of bubbles in the oxide has been attributed to the gaseous products of the oxidation reaction.[40,42,43,44] However, the absence of bubbles in the oxide for CVD and

single-crystal SiC, until temperatures where reactions between the SiC and SiO_2 begin to occur, suggests that the origin of bubbles is not from the reaction but rather is a function of the secondary phases that are present in sintered and hot-pressed SiC. For the oxidation reaction of SiC alone to be responsible for the bubbles the polycrystalline and single-crystal material should exhibit similar behavior.

The formation of bubbles in polycrystalline SiC has been attributed to C inclusions.[21] Free carbon will readily oxidize and produce CO gas through the reaction (1). Comparison of this reaction with the SiC oxidation reaction (5) shows that the oxidation of C inclusions produces 3 times as much CO(g) per molecule of O_2 than the SiC reaction. For a bubble to grow in the oxide scale, the reaction must occur rapidly relative to the rate of CO diffusion to enable the pressure to build at the SiC/SiO_2 interface. The pressure of the gas at the interface must exceed the ambient pressure and the force exerted by the surface energy of the oxide. Thus, the oxidation of C inclusions will be more likely to provide such a pressure buildup at the interface since it occurs rapidly and provides a large volume of gas. In non-stoichometric CVD-SiC bubbles are seen in the oxides. Excess carbon has been identified as the source of the pressure buildup in CVD SiC that exhibited bubbles in the oxide.[45] However, Fergus and Worrell[38] discount the possibility of excess carbon accounting for the increase in pressure at the SiC/SiO_2 interface for CVD SiC. According to their thermodynamic calculations the gas pressure at the interface could not reach 1 atm until 1515°C for CVD SiC with excess C, and not until 1817°C for silicon-saturated SiC. Recall, the gas pressure would have to be greater than 1 atm since the force from the surface energy must also be overcome for bubbles to form. Fergus and Worrell[38] maintain that since the sintered α-

SiC (hexagonal), also with excess carbon, exhibits bubbles but the carbon rich CVD SiC does not display bubbles, carbon cannot be the source of the excess gas. However, the sintered SiC would likely have significantly larger amounts of C and also large inclusions are present in these materials. In contrast, CVD SiC, despite being carbon-saturated, will contain much less carbon and the carbon will be more homogeneously distributed than in sintered materials. Thus, it seems possible that the larger inclusions in sintered SiC could be responsible for the localized pressure increase at the interface due to the generation of CO(g).

In contrast to the explanation of carbon alone being responsible for bubbles, Fergus and Worrell[38] suggest that impurities are the cause of gas bubbles. Both gases evolved from reactions of the impurities and the effects of impurities on the properties of the silica influence the silica morphology. If impurities decrease the viscosity of the glass then bubbles are more likely to form for a given gas pressure. Fergus and Worrell[38] studied sintered material with B and C additives and suggest that the boron is oxidized, and B_2O_3 is formed. Thus, to calculate the boron activity where B_2O_3 would be stable in carbon-saturated SiC and not react with SiO_2 the following reaction is used:

$$3SiC(s) + 2B_2O_3(s,l) = 3SiO_2(s) + 4B(s) + 3C(s) \qquad (10)$$

For 0.5 wt% B (~ 0.02 mole fraction), the B activity coefficient would have to be ~ 1.5, or greater, to ensure the activity exceeds the equilibrium value (at room temperature) of 0.03 calculated using equation (10). Thus, the B_2O_3 should be stable. The presence of B_2O_3 could promote bubble formation by reacting or locally decreasing the viscosity of the glass. A subsequent reaction between B_2O_3 and water vapor could generate $H_3BO_3(s)$ at room temperature.[46] The volatilization of the boron hydroxide could occur through

vaporization to $H_3BO_3(g)$ or decomposition (i.e., $H_2O(g) + HBO_2(g)$ or $H_2O + B_2O_3(l)$). These reactions would lead to a gas volume sufficient to generate bubbles at the interface. This sequence of reactions, while energetically feasible, does not appear to be the dominant mechanism for bubble formation. Since large gas volumes can be generated by the carbon oxidation, the role of excess carbon in sintered materials should not be overlooked; however, reactions of the various impurity species (compounds) should also be considered. It seems clear that each of the impurities in SiC must be considered as sources of gas and these impurities can enhance bubble formation in the oxide scale.

K. Objectives of the Current Work

The oxidation behavior of high toughness and high strength SiC, processed with Al, B, and C, is evaluated to determine whether or not the sintering additives have deleterious effects on the high temperature properties.

Two types of heat treatments were evaluated to improve oxidation rate and the oxide morphology: two-step processing and post hot-pressing anneals. Since the various sintering additives are essential for densification and enhancement of the phase transformation necessary for excellent mechanical properties, processing steps to improve the oxidation resistance must not be directed at eliminating these elements. Thus, several different heat treatment schedules were utilized to alter the oxidation rate of SiC with Al, B, and C sintering additives. Precoarsening, or two-step sintering, and heat treatments (anneals) after hot-pressing were employed to improve the oxidation behavior of SiC.

Since any processing steps directed towards reducing the oxidation must not compromise the mechanical properties, the strength of the standard processed SiC was compared with material that was subjected to a heat treatment.

II. EXPERIMENTAL PROCEDURE

A. Starting Materials/Processing

The starting SiC powder was cubic submicrometer β-SiC (H.C. Starck) with a mean particle size of 0.15 μm. The SiC powder was mixed with 3 wt% aluminum metal powder (H-3, Valimet, Stockton, CA), ~ 3 μm average particle size, and 0.6 wt% boron (Callery Chemical, Callery, PA), and ~ 4 wt% carbon Apiezon wax (Biddle Instruments, Plymoth Metting, PA). The Apiezon wax was dissolved in toluene, and yielded approximately 2 wt% C upon conversion by pyrolysis.[47] The slurry of SiC with the additives was ultrasonically agitated for ~ 10 minutes to break up agglomerates, and the mixture was stir-dried in air using a magnetic stir plate. The dried powders were reground using a porcelain mortar and pestle (Coors) and passed through a 200 mesh sieve (~ 75 μm). Then, the green compact was formed by cold pressing at 35 MPa (uniaxial compression) in a metal die set. The compact dimensions were approximately 38 mm in diameter and 6 mm high, corresponding to a green density of ~ 58%. These compacts were loaded into a graphite die lined with graphite foil. When several disks were processed simultaneously (up to a maximum of three disks) the compacts were separated by graphite spacers, with graphite foil adjacent to both faces of the SiC. A chart of the processing procedure and characterization is provided in Figure 12.

B. Hot-Pressing Conditions

The standard material was hot-pressed at 1900°C, for 1 hour, in an Ar atmosphere, with a pressure of 50 MPa, and was designated ABC-SiC . The hot-press furnace was heated to 400°C in vacuum and left overnight to remove the organics and any residual water in the sample. After backfilling with Ar, the furnace temperature was increased at a rate of 10°C/minute (temperature regulated with a Honeywell controller) and the pressure was started at 1000°C. A ramp rate of 250 lb/minute was used and the pressure was released at 150 lb/minute when 5 minutes where left in the 1900°C hold. The cooling rate was also 10°C/minute and the temperature of the furnace was monitored with a W-Rh thermocouple below 1300°C, while a double wavelength optical pyrometer, sighted on the graphite die, was employed for elevated temperatures.

The YAG-SiC, for comparing oxidation rates with ABC-SiC, was fabricated with 10% additives. A 6:4 wt% mixture of Al_2O_3:Y_2O_3 was wet mixed in acetone and stir dried. The powders were prepared the same as for ABC-SiC and hot-pressed at 1900°C for 1 hour in Ar. Again, the pressure was 50 MPa.

C. Two-Step Processing

The presintering heat treatment, or precoarsening, of powder compacts was introduced by Stutz *et al.*[48] and consists of holding the material for an extended time at a temperature lower than the sintering temperature. The final microstructure produced a more uniform microstructure as a result of a better distribution of the sintering aids. This concept of two-step sintering was extended by Chu *et al.*[49] to MgO and Al_2O_3 systems while increasing the hold time up to 90 hours, compared to a maximum of 5 hours as studied by Stutz *et al.*.[48] The advantage of two-step sintering again was attributed to an

increase in the uniformity of the powders (green compact), which resulted in the sintering damage being minimized. Initial powder compacts typically exhibit structural inhomogeneity and this leads to numerous complications in the processing of ceramics. The inhomogeneity leads to local non-uniform, or differential densification. The resultant transient stresses affect the pore development and particle rearrangements, and thus flaws can be introduced or enlarged.[50] Since the strength of ceramics is governed by the size of the pre-existing flaws, the inhomogeneous powders have deleterious effects on the strength. Ohji and De Jonghe,[50] applied the two-step sintering process to SiC, holding at 1400°C or 1600°C for 24 or 48 hours prior to isochronal sintering at 2000°C. They showed that both the strength and density of the material are enhanced with this heat treatment. In the current work, the bulk secondary phases could be correlated with the formation of bubbles in the oxide, and may compromise the passivating qualities of the silica scale. Therefore, two-step processing was applied to SiC hot-pressed with Al, B, and C sintering additives to try to achieve a more uniform distribution of the phases that would minimize bubble formation and oxidation rate.

Two-step processing utilized holds at 600, 1000, 1200, 1400, and 1600°C for 48 hours prior to reaching the hot-pressing temperature. A schematic of the heating schedule for two-step processing is shown in Figure 13.

D. Heat Treatments

The post hot-pressing heat treatments were based on the concept of thermally etching, or modifying the surface region, to eliminate volatile species, which are responsible for bubble formation and hence impact the oxidation resistance of SiC. Heat treatments at 1800°C for 1 hour in Ar are standard conditions for etching SiC to reveal

the grain structure since the grain boundary phases are preferentially attacked.[51] Thus, by removing the phases, which are detrimental to the high temperature performance, a passivating layer of higher quality may be achieved.

An alternative heat treatment process is to heat SiC in an atmosphere of N_2 at elevated temperatures to induce a thin Si_3N_4 surface layer that would serve as an excellent oxidation barrier.

After hot-pressing, the samples were placed on a diamond wheel surface grinder and ~ 500 μm was removed from each side and the SiC disks were polished to a 1 μm diamond finish. For the heat treatments following hot-pressing, SiC disks were annealed for 1 hour at 1800°C in N_2, vacuum (pressure ~ 2×10^{-4} torr), and Ar. A schematic of the heating schedule is shown in Figure 14.

A reoxidation experiment was conducted by oxidizing at 1300°C for 25 hours in air. This oxide was removed by soaking the sample in a 2% HF: water solution for 20 hours. Additionally, a polished ABC-SiC sample was added to the HF solution to monitor the effects on the subsequent oxidation rate. Both of these samples were then oxidized at 1300°C for 75 hours in air.

E. Microstructure Evaluation

X-ray diffraction (XRD) was performed on the polished surfaces of the disks over the range $2\theta = 20°$ to 50° at steps of 0.05° and an acquisition time of 1 second. The quantity of the SiC polytypes in specimens was calculated using the series of equations presented by Ruska *et al.*,[52] Table 3. The peak intensities substituted into the equations of Table 3 were determined by integrating the areas under the peaks, with the background subtracted, using DIFFRAC AT software (SOCABIM SARL, Paris, France). If the

solution to the equations provided a negative value for one of the polytypes, the values for that polytype were set to zero and equations were resolved. The designations 15R, 6H, 4H, and 3C represent the various structures for the polytypes. R, H, and C stand for rhombohedral, hexagonal, and cubic, respectively. The number preceding the letter for the structure indicates the number of layers in the stacking sequence of the close-packed planes.

15R		6H		4H		3C	Peak	d(nm)
3.2a			+	9.9c			= A	0.266
11.2a	+	19.4b					= B	0.263
26.0a			+	38.9c			= C	0.257
31.1a	+	59.2b	+	25.1c	+	100.0d	= D	0.251
		18.1b	+	34.1c			= E	0.235
2.4a	+	6.5b			+	13.1d	= F	0.217

Table 3: Equations to calculate the SiC polytypes.[52]

F. Oxidation Parameters

The oxidation of SiC was performed under several different conditions. The first oxidization experiments were to ascertain the governing kinetics of the system so the samples were oxidized at 1200°C for 25, 50, and 75 hours. The thickness, measured in the SEM, versus the square root of time for the standard ABC-SiC was plotted to determine if parabolic kinetics (diffusion control) were governing oxidation.

The standard ABC-SiC was oxidized with the various two-step processed materials at 1400°C for 20-25 hours to evaluate the effectiveness of the additional processing step. Oxidation at 1400°C was performed in a Lindberg/Blue M box furnace with a temperature ramp rate of 10°C/min for both heating and cooling. Additionally, since the kinetics of the system may be affected by the presence of impurities in the

reaction tube, commercial polycrystalline SiC, Hexoloy (Carborundum, Co., Niagra Falls, N.Y.), and SiC with yttria and alumina (YAG) were also oxidized along with the hot-pressed SiC so that relative oxidation rates could be determined. The oxidation samples were prepared by cutting the sample into beams ~ 3 mm thick, identical to the beams for the mechanical test, and then the beam were cut into sections ~ 7-10 mm long. A notch was cut into the sample prior to the oxidation experiment, and the specimens were broken after oxidation at the notch so that the oxide could be evaluated in cross-section.

Samples with a post hot-pressing heat treatment were oxidized, along with the standard material, at 1300°C for ~ 75 hours. Oxidation studies below 1400°C were performed in a Lindberg tube furnace equipped with SiC heating elements. The SiC heating elements dictated that the furnace was normally lowered only to 500°C and thus the oxidation specimens were introduced into the furnace at this temperature. The controller was manually increased to 600, 700, and 800°C with a soak for 30 minutes to 1 hour at each of these temperatures to minimize anisotropic heating effects in the heating elements. After 800°C the furnace controller was set to the oxidation temperature of 1300°C. The time to ramp to this temperature was negligible compared to the oxidation time (when factoring the enhanced kinetics at elevated temperatures). The furnace temperature was calibrated with a Pt-Pt+10%Rh thermocouple. The tube was made of mullite ($3Al_2O_3 \cdot 2SiO_2$) and the crucible holding the SiC samples was Al_2O_3 (reactions do take place between SiC and Al_2O_3 at these temperatures, but only the very bottom of the samples appeared to be effected). All of the oxidized materials were examined in cross-section in the SEM to measure the oxide thickness (25 points were measured along the

scale and an average value of these measurements was reported). Additionally, the oxides were examined in plan view in the SEM at 15 kV to evaluate the morphology and ascertain if bubbles, and or crystallization (and cracks), were present.

Scanning electron microscopy (SEM), in conjunction with energy-dispersive spectrometry (EDS) and wavelength-dispersive spectrometry (WDS), was used to characterize the oxide thickness and evaluate the distribution of secondary phases in the SiC. Additionally, XRD and transmission electron microscopy (TEM) were used to further characterize the nature of the oxide.

G. Mechanical Testing

The strength of the standard SiC and the materials subjected to a post hot-pressing heat treatment was evaluated on beams of ~ 2.7 mm by 3 mm by 30 mm sectioned from the polished SiC disks. The tensile edges were beveled to reduce the edge flaws using a 6 μm diamond wheel. The flexural strength was tested using a four-point bending jig with an inner span of 9.5 mm and an outer span of 25.4 mm. The crosshead speed during the test was 0.05 mm/minute and the strength was calculated from the following relation:

$$\sigma = \frac{3Pa}{bh^2} \tag{11}$$

where P is the load at fracture, a is one-half of the distance between the inner and outer spans, b is the width of the beam, and h is the height of the beam. The bend strength for the materials was averaged over eight beams and, in addition, a two-parameter Weibull distribution was fit to the data to determine the Weibull modulus, m.

III. RESULTS AND DISCUSSION

A. Oxidation Kinetics for SiC with Al, B, and C

Evaluation of the kinetics of the SiC was performed by oxidizing at 1200°C for various times, and the oxide thickness results were plotted versus the square root of time, Figure 15. A linear least squares regression was used to fit the data, and the minimal amount of scatter indicated that the oxidation followed parabolic kinetics for SiC with Al, B, and C. The parabolic rate was obtained by taking the square of the slope from Figure 15.

The parabolic rate, the square of the slope in Figure 15, was 2.7×10^{-2} μm^2/hour (7.5×10^{-18} m^2/s). This rate constant is significantly higher than $k = 1.82 \times 10^{-2}$ μm^2/hour for CVD SiC at 1200°C.[53] The larger rate is likely the result of the impurities, or residual phases from the sintering additives, present in the hot-pressed SiC. However, a comparison of the rate for the current material with the values in Figure 1 show excellent agreement. A temperature of 1200°C corresponds to a reciprocal temperature of 6.8×10^{-4} (K) and $\log_{10}$ (7.5×10^{-18} m^2/s) = -17.1. Plotting this point on Figure 1, the top of the shaded region, shows that this point, for SiC hot-pressed with Al, B, and C, appears to lie on, or very close to, line F for sintered α-SiC.[24] (Since the α-SiC was a commercial material, from Carborundum, the quantities of the sintering additives is not known but it is believed to contain small amounts of B and C.) Additionally, extrapolating line G,[42] for hot-pressed SiC with Al_2O_3, the value of k_p for this material appears to be very close to the value measured in the current experiment at 1200°C. Polycrystalline materials consistently exhibit a higher oxidation rate for a given temperature than single-crystal or high-purity CVD SiC.

To illustrate that parabolic kinetics indicate that diffusion is the rate-controlling step, consider the following simplified model based on representations in standard text books. Assuming that the inward diffusion of oxygen is the rate limiting step in the system, steady-state diffusion can be used to model the system since the concentration of the diffusing species is held constant at the surface and interface of the oxide. The assumption of steady-state oxidation dictates that the flux must be equal at any point within the oxide, dJ/dx = 0. Thus, the concentration profile is illustrated in a linear fashion, Figure 16. Fick's first law states (12):

$$J = -D\frac{dC}{dx} \tag{12}$$

where J is the flux of oxygen, D is the diffusion coefficient (exponential dependence on temperature), and dC/dx is the concentration gradient, which also is equal to $\Delta C/\Delta x$ for this steady state problem. The diffusion flux, J, is defined as the mass, or number of atoms, M, diffusing through and perpendicular to a unit cross-sectional area of solid per unit time. Thus, the flux can be mathematically represented in differential form by (13), where A is the area.

$$J = \frac{1}{A}\frac{dM}{dt} \tag{13}$$

Thus, the units for the flux will be $kg/m^2 \cdot s$ or $atoms/m^2 \cdot s$. For determining kinetic data a relationship for the change in thickness with time, dx/dt, is necessary. Therefore, the flux of oxygen can be rewritten in terms of dx/dt by introducing a constant, a, (14):

$$J_{oxygen} = a\frac{dx}{dt} \tag{14}$$

Substituting equation (14) into Fick's first law (12) and integrating both sides of the equation we arrive at the following equations (after some rearrangement):

$$x^2 = -2 \cdot D \cdot a \cdot \Delta C \cdot t \tag{15}$$

$$x^2 = B \cdot t \tag{16}$$

where B is the parabolic rate constant. This illustrates that parabolic kinetics will govern systems which are controlled by diffusion. The above solution is an approximation due to the assumption that the concentration of oxygen in the atmosphere is the same as the concentration of oxygen in the surface layer of the oxide. A more rigorous solution to the oxidation kinetics was provided by Deal and Grove[18] for Si oxidation. Here, the concentration gradient would appear as shown in Figure 17, and a more accurate description of the oxidation kinetics for diffusion through an oxide is provided by (21):

$$x^2 + Ax = B(t + \tau) \tag{21}$$

where B is the parabolic rate constant and τ corresponds to a shift in the time coordinate if an initial oxide is present. Thus, solving the quadratic equation (21) and evaluating the limiting cases for long and short times can elucidate the governing kinetics for oxidation. For short times the reaction follows linear kinetics, (22), while longer times can be described by equation (23).

$$x \cong \frac{B}{A}(t + \tau) \tag{22}$$

$$x^2 \cong B \cdot t \tag{23}$$

Equation (23) corresponds to the kinetic relationship derived in (20). The physical interpretation of short times is that the oxidation is limited by the rate of the interfacial reaction in the early stages since the oxide is thin and the diffusion rates are

comparatively fast. However, subsequent to the initial linear region, the kinetics follow a parabolic behavior governed by diffusion rates.

B. Effects of Impurities on the Oxidation Behavior

The exact kinetics of the ABC-SiC system were not studied extensively. The primary limitation to performing detailed kinetic studies was the presence of impurities in the system. It has been shown that impurities in the reaction tubes can alter both the oxidation rate and the oxide scale phase and microstructure.[54] A common impurity in these tubes is Na, and Zheng *et al.*[55] demonstrated that increasing the Na content increased the oxidation rate. Opila[54] showed that holding the alumina reaction tube at elevated temperatures for a couple of thousand hours resulted in oxidation rates similar to those in high purity fused quartz reaction tubes. Thus, the equipment for the present study did not allow for accurate determination of the kinetics of the oxidation reaction. However, to ensure that the impurities did not adversely effect the conclusions for the oxidation experiments, a sample of the standard ABC-SiC was always oxidized with samples which had been subjected to a heat treatment; this allowed the relative oxidation kinetics to be discerned.

The acceleration of the oxidation rate in the presence of H_2O is another reason that the precise kinetics for ABC-SiC was not attainable with the current apparatus. In addition to having a clean reaction tube, the effects of various amounts of water vapor present in the system (i.e. variations in the relative humidity of the air) will likely cause the actual kinetic information to be altered. Although these deviations should not be extremely large, the exact oxidation rates should be determined by oxidizing in a furnace with a controlled atmosphere as well as a clean reaction tube. Meaningful oxidation

kinetic data would only be achieved should the oxygen partial pressure and water content be known (many researchers use dry oxygen for such kinetic experiments). The box furnaces used in these experiments cannot be setup for flowing gases through the chamber.

The presence of impurities in SiC results in the lowering of the oxidation resistance. The effect may arise from a couple of sources that may or may not be interrelated. The impurities may lower the viscosity of the glass and/or affect the crystallization of the silica scale. Impurities tend to be redistributed during the oxidation of SiC. This phenomenon has been observed with B impurities and is characterized by a segregation of boron in the oxide near the interface and consequently a corresponding decrease in boron concentration in the substrate SiC near the interface.[56] The presence of boron presumably altered the oxidation behavior by forming a low-viscosity oxide, likely a borosilicate glass. A lower viscosity glass resulted in enhanced oxygen transport through the oxide scale; therefore, the oxidation rate was accelerated. The driving force for the redistribution of impurities in the substrate material, and subsequent transport across the interface into the oxide, is the difference in the chemical potentials for the impurities in the two regions. The ratio of the activity coefficients in the substrate and oxide determines if the impurity will remain in the substrate or redistribute into the oxide. Also, the rate at which the segregation will occur is governed by the relative magnitudes of flux of the impurity in the substrate, oxide, and from the oxide into the ambient gas phase.

A similar effect of impurities was reported by Singhal and Lange[44] for hot-pressing SiC with alumina additives. The parabolic rate constant increased as the

alumina content was increased. The accelerated oxidation in the presence of alumina was attributed to the formation of a low-viscosity oxide, aluminosilicate in this case, just like the oxidation with B additives. It was concluded that at the oxidation temperature, the impurities in the aluminosilicate, in particular K and Fe as oxides, were responsible for the formation of a liquid phase and again, the result was enhanced transport of oxygen.

An additional study on hot-pressed SiC with Al as a sintering additive, by Costello and Tressler,[24,27] demonstrated that samples which exhibited higher degrees of crystallinity indicated a major phase of cristobalite and a minor phase of mullite, $3Al_2O_3 \cdot 2SiO_2$. The resultant microstructure consisted of an extremely fine particulate structure surrounded by a matrix phase that appeared to be glassy. The oxidation behavior of this hot-pressed SiC initially dropped, presumably caused by the formation of a layer of cristobalite crystals, but longer oxidation times resulted in the kinetics actually increasing. For longer times, more Al^{3+} had an opportunity to be redistributed in the oxide; thus, mullite began to form at the expense of cristobalite. Costello and Tressler attributed the increase in the oxidation rate to mullite being a less effective oxidation barrier.

The aforementioned discussion on the effects of impurities suggests that, in general, increasing the amounts of impurities (sintering additives) increases the oxidation kinetics. There are several mechanisms by which the oxidation rate may be accelerated, and these mechanisms may be system specific since the discussed experiments were all performed on different materials. It appears that redistribution of the impurities into the oxide, and subsequent effect on the physical properties of the scale, is the dominant problem associated with the impurities. Thus, the natural solution to improving the

oxidation behavior of the current ABC-SiC system would be to lower the amounts of the sintering additives; several processing issues must be addressed before this conclusion can be reached. The primary concern of such an approach is that the proper microstructure will not develop, and the advantageous mechanical properties of the material will be lost. The β to α-SiC phase transformation, essential for generating a microstructure with elongated grains, is extremely sensitive to the amounts of Al and B in the starting green compact. Since the primary effect of Al and B is to decrease the temperature at which the transformation begins, it is conceivable that a similar microstructure could be obtained by hot-pressing for longer times, or at higher temperatures, if less Al and B were in the starting powders. Should it be possible to achieve the same microstructure as the standard ABC-SiC by utilizing a lower concentration of additives, the improvement in the oxidation may not be dramatic. Evaluating the data by Singhal and Lange[44] for SiC with alumina, the parabolic rate constant only decreased by ~ 30% when the additive concentration was reduced from 6.1 wt% to 2.5 wt%. Due to the nature of the phase transformation, it probably would not be possible to drop the additive quantity to less than the latter value from the ~ 5wt% used in the standard ABC-SiC. Therefore, merely reducing the amounts of additives would likely only yield minor improvements in the oxidation resistance; this processing approach does not address the issue of bubble formation which is observed in ABC-SiC.

C. Oxide Morphology of ABC-SiC

The standard ABC-SiC, 3% Al, 0.6% B, and ~ 2%C, hot-pressed at 1900°C for 1 hr and oxidized at 1300°C for 75 hours in an air atmosphere is shown in Figure 18. The feature immediately notable, besides the ~ 8 μm oxide layer, was the presence of bubbles

in the oxide. The dominant characteristic of the bubbles was that nearly every bubble spanned the thickness of the oxide scale. Of the numerous samples oxidized during the present experiments this was always the case. For every sample the entire SiC/oxide interface was examined to try to find bubbles in the early stages of formation. The absence of small bubbles indicated that the bubbles might have formed when the oxide was thin and then grown as the oxide thickened. Alternatively, nucleation may have been difficult but growth was fast. A plan view of an oxidation layer is provided in Figure 19. This SEM micrograph shows numerous bubbles, and the bubbles slightly bulge out of the oxide surface. However, none of the bubbles appeared to be ruptured. Costello and Tressler[57] showed that hot-pressed SiC exhibited parabolic kinetics which increased for long times at elevated temperatures. The morphology of the oxide exhibited bubbles, as well as craters, where bubbles had burst. The ruptured bubbles exposed new, unpassivated surfaces, and the increased oxidation rate was attributed to the ruptured bubbles. In contrast, the bubbles in the ABC-SiC were readily apparent in all of the micrographs, but not a single bubble in the standard SiC was determined to have ruptured. The samples were viewed both normal to the oxide surface and at various angles, but it was not possible to focus on the edge of the bubbles as would be possible for a ruptured bubble. This suggested that the bubbles shown in Figure 19, and supported by the cross-sectional view in Figure 18, were subsurface and had not ruptured (despite bulging out of the oxide). This conclusion was further supported by observations at lower accelerating voltages. When the microscope was operated at 5 kV the bubbles could not be detected, indicating that the features were indeed subsurface.

The micrographs of the oxide surface did not show the oxide to be crystalline in nature. The smooth appearance of the surface and the bulging bubbles suggested the SiO_2 was predominantly amorphous (vitreous). In contrast, the XRD spectrum of the oxide showed a small, but definite, peak at a 2θ of ~ 22° which corresponds to cristobalite. Small crystals of cristobalite were not observed in the SEM and this is likely caused since the crystallization nucleates at the oxide/carbide interface[57] and there was not a very strong crystalline signal from the XRD spectrum. This was supported by TEM observations.

Examining the bubbles in oxide also reveals an interesting feature. The oxide does not appear to be very thick below the bubbles. This would be expected for the regions near the high diffusion paths. However, it is believed that the lifetime of the bubbles is not very long and this accounts for the absence of a thicker oxide under the bubbles.

D. TEM of Oxides (in collaboration with Dr. W. J. MoberlyChan)

Reflected and transmitted optical micrographs of the cross-section TEM oxide specimen are shown in Figure 20. The upper region is the ABC-SiC while the bottom half of the micrograph shows the thin oxide for the Ar annealed SiC. The center stripe is the glue layer that was used to hold the two oxides together.

Figure 21 is a low magnification TEM micrograph, without an objective aperture, of the sample depicted in Figure 20. The crystalline nature of the oxide on the Ar heat treated material was observed and appeared to span the entire thickness of the oxide. In contrast, the oxide on ABC-SiC was much thicker and appeared to be primarily

amorphous. However, higher magnification imaging revealed a thin crystalline, ~ 0.5 μm thick, region near the SiC/oxide interface.

The electron beam was focused to a spot and EDS spectra, Figure 22, were obtained at the various points A-F in Figure 21. Figure 22a corresponds to point A, which was obtained from the SiC. It should be noted that the Al signal in this spectrum was less than the bulk of the SiC, consistent with Al being depleted from the substrate during the oxidation process. Point B, from the thin crystalline region of ABC-SiC, showed only a small Al signal and no Na or K impurities. In contrast, point C was acquired in the amorphous region just beyond the thin crystalline region and now a strong Al signal, as well as Na and K impurities, was observed. The Al signal from the amorphous region of the oxide remained constant out to the edge of the oxide.

E. Bubbles in ABC-SiC

As shown with the standard SiC, where the bubbles did not burst, the oxidation would still be expected to follow parabolic kinetics despite bubbles with only an increase in the oxidation rate. This was confirmed by Figure 15, which showed the standard material indeed followed parabolic kinetics.

There are primarily two bulk secondary phases found in SiC hot-pressed with Al, B,and C. The major phase is $Al_8B_4C_7$ and the minor phase is Al_4O_4C. Occasionally, some Al_2O_3, Al_4C_3, and C inclusions (graphite) were identified by TEM.[5,7,8] Figure 23 shows a polished surface of SiC and the oxidized surface of the same area, respectively. The dark regions in Figure 23 correspond to these bulk secondary phases and the grain boundaries of the SiC grains are clearly delineated. As indicated by the markers in the figure, a bubble corresponds to each of the secondary phase regions. The bubble density

is actually higher than the density of secondary phases, and this is believed to result from the secondary phases just below the SiC surface, which may also generate enough gaseous by-products to form a bubble. Also, a higher magnification SEM micrograph of the polished surface, Figure 24, shows the numerous triple point materials and these may be responsible for the enhanced bubble density. Since it appeared the bulk secondary phases were responsible for bubble formation, two-step processing was employed to try to improve the oxidation behavior. Again, the premise of two-step processing was to homogenize the material, hopefully breaking apart the secondary phases, by utilizing an extended hold at a temperature lower than the hot-pressing temperature.

F. Oxidation Behavior of Two-Step Processed SiC

The two-step processed materials were oxidized at 1400°C for 25 hours and Table 4 lists the oxide thickness for each sample. Specimens with a hold between 600°C and 1400°C for 48 hours, prior to hot-pressing, exhibited no improvement in the oxidation behavior, within the error of the measurements. However, the sample heat treated at 1600°C for 48 hours showed a ~ 25% decrease in the oxide thickness. Figure 25 compares the oxide thickness of standard SiC, standard plus 1600°C pre-anneal, and Hexoloy. While the oxide thickness for the annealed sample decreased, bubbles were still present. The feature of the bubbles spanning the thickness of the oxide in the standard material was also true for the annealed materials. A plan view of the oxides for the standard material, along with those annealed at 1400°C and 1600°C, are provided in Figure 26. The specimen annealed at 1400°C actually exhibited a slight decrease in the bubble density while showing no improvement in the oxidation rate. In contrast, the sample annealed at 1600°C clearly exhibited an increase in the bubble density.

Material	Oxide Thickness ± Standard Deviation (μm)
ABC-SiC	4.8 ± 0.4
ABC-SiC + 1000	4.8 ± 0.4
ABC-SiC + 1200	4.7 ± 0.3
ABC-SiC + 1400	4.6 ± 0.4
ABC-SiC + 1600	3.5 ± 0.3
Hexoloy	~ 0.5
SiC + 10 wt% YAG	> 17

Table 4: Oxide thickness' after 25 hours at 1400°C in air.

An understanding of the enhanced bubble density for the 1600°C material is obtained by evaluating the distribution of the secondary phases. Figure 27 compares the polished surfaces of standard ABC-SiC with SiC+1600°C/48 hours and their corresponding WDS x-ray maps for Al. The dark regions in the polished samples correspond to the bulk secondary phases in the standard SiC as well as most of the regions in the annealed specimen. The bright regions denote the presence of Al in the x-ray maps at the bottom of the figure. The bright, Al rich regions, clearly are located at each of the darker regions from the polished surface for the standard material. In contrast, the dark regions in the SEM image (secondary phases), for the annealed samples appeared to be much smaller and this was confirmed by the Al x-ray map. The WDS maps of samples annealed at 1400°C and below exhibited a distribution of secondary phases which was indistinguishable from the standard material. The vapor pressure of the Al metal is ~ 1.33×10^{-3} atm at 1540°C.[58] Therefore, provided the Al had not already formed a compound, it is likely that some of the Al metal was removed from the specimen by the pre-heat treatment at 1600°C. The Al map also indicated that there may be less Al but still there are significant Al rich regions. Thus, it appeared that the two-

step processing at 1600°C successfully redistributed the secondary phases, thereby creating smaller, but more numerous, secondary phase regions. The higher density of secondary phases results in a greater number of nucleation sites. Hence, the bubble density increased for the two-step processed material. The two-step process actually performed as anticipated, but the smaller secondary phases were still large enough to evolve a sufficient volume of gas to form bubbles. The fact that the material annealed at 1600°C exhibited a lower oxidation rate, while increasing the bubble density, indicates that the chemistry of the glass oxide is a critical parameter in the oxidation behavior.

G. Comparison of ABC-SiC Oxidation with Other Silicon Carbides

Standard ABC-SiC was compared to two reference materials, commercial Hexoloy and YAG-SiC. The latter material, YAG-SiC (SiC sintered with alumina and yttria in the proper ratio to form yttrium aluminum garnet (YAG)), has been studied and reported to have a high toughness.[2,3,4] However, there have been no reports on the high temperature stability of these materials. Hexoloy, a brittle SiC with moderate strength, presumably free sintered with only B and C, was also studied as a reference material. Figure 28 compares the plan view of the oxides for the three materials. Figure 28a demonstrates that Hexoloy did not develop a very thick oxide and bubbles were formed. Again, this is consistent with the work of Costello and Tressler[57] for sintered and hot-pressed SiC with B and C additives. Whereas the ABC-SiC exhibited moderate to good oxidation resistance, the YAG-SiC showed a very thick oxide scale with a glassy morphology. The oxide thickness for YAG-SiC was approximately 20 times greater than the reference Hexoloy. In contrast, the ABC-SiC exhibited an oxide thickness ~ 5 times larger than Hexoloy. In addition to the enhanced oxidation rate in the YAG-SiC, this

material may not be stable with these sintering additives. The standard processing of the YAG-SiC involves sintering the material in a closed crucible packed in Al rich powders since the tendency to react and to lose weight is a problem.[2,3,59] The apparent reactivity of the YAG-SiC, and poor oxidation behavior, suggests that this material is not suitable for high temperature oxidizing environments. The oxide thickness on the Hexoloy material is less than 1 μm and exhibits excellent oxidation resistance. When examined in cross-section, the bubbles were located on top of the oxide for Hexoloy, Figure 28a, and thus it appeared an excellent passivating layer was formed. The excellent high temperature behavior is consistent with the low amount of sintering additives likely used in this material.

H. Oxidation Behavior of SiC Annealed in Various Environments

Chemistry was identified as an important processing parameter in the oxidation rate of SiC. Thus, various heat treatments were performed on the ABC-SiC subsequent to hot-pressing to alter the surface chemistry. The first heat treatment, anneal, was actually a reoxidation experiment. The work of Clarke[60] on the Si_3N_4 system showed that the oxidation rate continued to decrease as a sequence of reoxidation experiments were performed. This was attributed to impurities segregating to the oxide; thus, the last oxidation experiments displayed lower rates. The redistribution of the additives, leaving the oxide rich and the substrate depleted of impurities, was also observed in the SiC system. Therefore, a sample was oxidized at 1300°C for ~ 25 hours and the oxide was stripped with HF acid. However, there was virtually no change in the scale thickness, compared to the standard material, upon subsequent reoxidation, Figure 29. Costello and Tressler[57] obtained similar results for reoxidation experiments on sintered α-SiC. These

results indicated that while the substrate may be depleted of impurities from the initial oxidation, the concentration gradient was not maintained for very long after a new oxide was formed and thus the new oxide collected additional impurities. This diffusion was likely rapid through the grain boundaries, which are amorphous in ABC-SiC.[5,7,8] Therefore, it was not possible to obtain a high purity oxide with reoxidation experiments. Utilizing longer initial oxidation times, and/or higher temperatures, likely would not dramatically improve the reoxidation behavior since the amount of impurities would probably not be very different than the oxide in the standard ABC-SiC. Oxidizing the material and stripping the oxides numerous times could be an effective way to ultimately remove the impurities from the surface, but this was not explored in the current experiments. However, it may not be feasible from a processing standpoint (too expensive) to submit the material to so many processing steps. A reference sample, exposed to the same HF solution as the oxidized sample, also showed no improvement in the oxidation behavior, Figure 30. As seen in Figure 31, the oxide thickness was not uniform for the sample exposed to an HF dip.

Changing the chemistry in the system can also be achieved by inducing a reaction layer at the surface that could serve as a protective coating. Naturally, depositing a thin film of pure SiC would be a feasible method for improving oxidation resistance but this would only be realized by increasing the cost of components. In contrast, a simple heat treatment should not add excessive cost to SiC products. Thus, a sample was heated in a N_2 atmosphere to induce the formation of a Si_3N_4 surface layer. Si_3N_4 exhibits excellent oxidation resistance and is chemically compatible with SiC, thus the high temperature properties with a thin Si_3N_4 layer should be excellent. The oxidation of the sample

annealed in N_2 showed a 40% reduction in the oxide thickness compared to the standard SiC.

ABC-SiC annealed at 1800°C for 1 hour in vacuum exhibited a four-fold decrease in the oxide thickness compared to the standard material. Also, the sample annealed in Ar demonstrated a four-fold decrease in the oxide thickness. Figure 32 shows low magnification SEM images of the various oxides (in cross-section), while higher magnification examination is shown in Figure 33. Figure 34 shows the oxide thickness for the annealed samples and standard ABC-SiC.

The nitrogen annealed specimen resulted in an oxide thickness that was 40% thinner, but bubbles were still present in the material. In contrast, the samples annealed in vacuum and Ar decreased the oxide thickness by a factor of 4 and also eliminated the bubbles that are observed in the standard material. There are indications that small bubbles may have formed in these oxides. However, they do not span the thickness of the oxide and thus, as supported by the dramatic increase in oxidation resistance, small bubbles should not disrupt the passivating nature of the oxide.

J. Oxide Morphology and Chemistry after Heat Treatments

The plan view of the oxides for the standard SiC, nitrogen anneal, vacuum annealed, and Ar annealed SiC are provide in Figures 35 & 36 with the corresponding EDS spectra. The general morphology of the standard and nitrogen annealed materials is distinctly different from the other two specimens. The former two samples appeared to have an oxide that was glassy in appearance and numerous bubbles were clearly present. In contrast, the vacuum and Ar annealed SiC produced oxides that appeared to be crystalline in nature. The vacuum annealed indicated that bubbles may be sitting on top

of the oxide similar to the Hexoloy material. However, the examination of the entire cross-section did not reveal any large bubbles in the oxide itself. This specific oxide morphology is very similar to that obtained by Costello and Tressler[24] which was described as a fine particulate structure in a glassy matrix. The nature of the small particles arranged in rings was not identified. EDS spectra from these regions did not exhibit a chemistry different than the rest of the oxide.

An additional feature in the Ar annealed sample was the presence of many small "mud" cracks. These likely were introduced upon cooling the sample from elevated temperatures by the thermal expansion mismatch between SiC and cristobalite. Crack healing would likely assure the integrity of the oxide upon thermal cycling; thus, the oxidation rate should not be accelerated by the cracks formed upon cooling. For SiC, the kinetics of oxidation were indeed verified to be the same for isothermal exposures and 5 hour cyclic exposures.[61]

The chemistry of the oxide was suggested to be critical in the oxidation behavior of SiC. This was confirmed by the EDS spectra accompanying Figures 35 & 36. The standard and nitrogen annealed samples exhibited bubbles and only moderate oxidation resistance. The EDS spectra for these two materials were virtually identical. The ratio of the Al and Si peaks was essentially identical, and Na and K impurities were detected in both samples. These impurities likely came from the mullite reaction tube used during the oxidation experiments. In contrast, the vacuum and Ar annealed samples showed only a minimal Al EDS signal. A significant difference, in addition to the extremely small Al concentration, is that the Na and K impurities were not detected in these oxides. All four of the samples were oxidized during the same high temperature exposure. Na

contamination is documented to be deleterious to the oxidation resistance of a silica formers.[54] Thus, K would likely exhibit similar detrimental affects since it is chemically very similar to Na. As seen by the Stokes-Einstein equation, (7), since Na and K reduce the viscosity of silica, the diffusion rates will increase. Examination of the Na_2O-SiO_2-Al_2O_3 phase diagram, Figure 37, shows that the melting point of SiO_2 is lowered by the presence of Na and Al, and presumably the viscosity would exhibit a similar decrease. Hence, impurities in ABC-SiC lower the viscosity of the passivating layer and increase the oxidation rate.

The EDS spectra that did not show Al did not reveal measurable quantities of Na, despite being oxidized at the same time as ABC-SiC, which had a strong Na signal. This is explained by the different valence of Si and Al. Al has a valence of +3 and Si is +4. Therefore, if Al_2O_3 tetrahedra are to be incorporated into the glass network an additional positive charge is required to maintain charge neutrality. This is accomplished by the incorporation of Na into the oxide when Al is present.

The TEM micrograph for the Ar annealed SiC is shown in Figure 21. The EDS spectra for the thin crystalline oxide were similar throughout the oxide and are illustrated in Figure 22f. The Al signal is very small and the Na and K impurities are not observed. This EDS spectrum is very similar to the Figure 22b, corresponding to the crystalline region in the oxide of the standard ABC-SiC.

A higher magnification TEM micrograph of the oxide from the SiC annealed in Ar is shown in Figure 38. This BF image clearly revealed the crystalline nature of the oxide, and many stacking faults and/or twins were present. The two electron diffraction patterns are consistent with the cubic silica phase, cristobalite. The diffraction patterns

are consistent with the [100] and [1$\bar{1}$2] zone axis orientations with the extra reflections being attributed to double diffraction and {111} twin planes for the upper and lower patterns, respectively.

The XRD spectra of the oxides, Figure 39, for the standard SiC and that annealed in nitrogen were virtually identical. The cristobalite peak with the strongest intensity was present and indicated that crystalline silica was present. An additional peak at $2\theta \sim 26.5°$ was also present and this corresponds the strongest tridymite peak. However, with only one weak peak present it is not possible to definitively state that tridymite is present in addition to cristobalite. Figure 39 also shows the oxide XRD patterns for samples annealed in vacuum and Ar. The spectra indicated that the Ar annealed material exhibited a higher degree of crystallinity than the standard ABC-SiC despite having thinner oxides. Here, the secondary peaks begin to become distinct, thus confirming that the crystalline silica was cristobalite. The final spectrum, for the vacuum anneal, exhibited the greatest degree of crystallinity and this is consistent with the observations from the SEM.

K. Effects of Annealing on Chemistry and Surface Morphology

The surface layer of the materials annealed in vacuum and Ar at 1800°C, after hot-pressing, was effectively thermally etched. The bulk secondary phases present in the standard material, Figure 27a, are not seen for the vacuum and Ar anneals. Figure 40 for the vacuum annealed SiC exhibited dark regions where the bulk secondary phases were removed during the heat treatment. The higher magnification SEM micrograph illustrated that while material was clearly removed from the surface large voids do not appear. The vacuum heat treatment would be anticipated to be a more aggressive thermal

etch than the Ar atmosphere. Consequently, the vacuum annealing process would be expected to remove more material. This was confirmed by both the high and low magnification micrographs after a vacuum anneal, Figure 40. Large voids are clearly evident at the triple junctions where material has been removed, and the bulk secondary phases also appear to have been removed by this heat treatment.

The chemistry of the surfaces after being thermally etched is consistent with the chemistry of the oxides. Figure 41 shows the EDS spectrum for ABC-SiC (for a low magnification image). The ratio of Al to Si in this spectrum was less than the ratio for the oxides grown on ABC-SiC and the SiC annealed in nitrogen. This strongly suggested that the Al was redistributing during the oxidation process and thus the oxide became rich in Al, while the SiC substrate near the surface was depleted of Al. This is the exact phenomenon observed for B redistribution during oxidation. Comparing the EDS spectra for the SiC annealed in vacuum and Ar, Figures 40 & 41, respectively, with the standard material shows that Al was removed from the surface region. The presence of B and C could not be detected with the window on the EDS detector so these concentrations were not monitored. Also, the initial B concentration is low since the material was processed with only 0.6 wt%, and variations in such a small quantity would not be possible to accurately monitor. However, it is believed that since the bulk secondary phases were removed with the thermal etch, and the B and C concentration likely decreased in a similar fashion as Al. This is also consistent with the observed oxidation rates since if B was not removed a borosilicate glass with a low viscosity would probably form and the material would still display poor oxidation behavior (even though Al had been removed). Since the impurities apparently were removed from the surface layer, an oxide of higher

purity was formed on the samples annealed in vacuum and Ar. The higher purity silica and the crystalline nature of the scale both contributed to dramatically reducing the oxidation rate.

L. Microstructure after Annealing

The post hot-pressing anneals must not have a significant effect on the overall microstructure of the SiC. The degree of grain growth is critical and overaging the system will result in the aspect ratio being decreased below the optimum value.[5] XRD, Figure 42, provides a comparison of the standard and annealed samples. The strongest SiC peaks are labeled for the standard SiC with the strongest peaks corresponding to 3C, 4H, and 6H phases. The small peak at $2\theta \sim 27°$ may correspond to the graphite inclusions as seen in the TEM. The annealed samples, especially for an Ar heat treatment, displayed a stronger graphite peak than the standard material. While SiC will not melt at 1800°C, the SiC may begin to decompose. In the Ar atmosphere this carbon may stay on the surface while in vacuum the volatile species are more likely to be removed. Large graphite regions are not seen on the surface after heat treatment in Ar, Figure 40. This indicates that the carbon is distributed relatively homogeneously across the surface. In this event, the carbon will readily oxidize and be removed from the surface prior to the formation of a passivating silica scale. The critical aspect of the XRD spectra, to ensure the microstructure has not undergone significant changes with the heat treatments, is the relative ratios of the SiC peaks. In each of the annealed samples the relative peak intensities appeared to be comparable to the standard material. Therefore, the bulk microstructure of annealed samples was similar to the standard ABC-SiC and

thus should possess similar mechanical properties. Both materials exhibited a microstructure with 46% 6H, 49% 4H, and 5% 3C.

M. Mechanical Properties

Since the microstructure, from XRD, showed little change as a result of the heat treatments, the mechanical properties would be expected to exhibit similar properties to standard ABC-SiC. However, as illustrated in Figure 32, the fracture mode appeared different in the standard ABC-SiC compared to the SiC annealed in Ar and vacuum prior to oxidation. The predominant intergranular fracture present in ABC-SiC was evident from the center of the specimen to the outer edge near the oxide. In contrast, the Ar and vacuum annealed materials displayed a predominant transgranular fracture surface near the oxide in Figure 32. Low magnification SEM micrographs of the same oxides demonstrated that the surface of the annealed samples was altered and there was a switch back to the intergranular fracture mode near the center of the sample. For the Ar heat treatment, the transgranular fracture regions was ~ 25 μm thick, while the SiC annealed in vacuum had a transgranular fracture region of ~ 100-125 μm thick.

To further examine the fracture morphology the vacuum annealed sample was evaluated at low magnification, Figure 43, and high magnification, Figure 44. A region of transgranular fracture is exhibited in the first ~ 100-125 μm, as measured from the oxide/SiC interface, whereas the fracture mode switched to the typical intergranular fracture near the center of the specimen. A higher magnification SEM micrograph of the transgranular surface, region A, is shown in Figure 44. The micrograph illustrates that the grains were still elongated in this region. Additionally, the presence of numerous voids was readily observed. The result of annealing the samples apparently removed the

bulk secondary phases and altered the chemistry of grain boundary phase. It has been reported that it is not possible to remove the grain boundary phase in Si_3N_4 ceramics[62] and this behavior would be expected to be similar in the SiC system. Therefore, it appears that the heat treatments altered the chemistry of the grain boundaries, as opposed to removing these boundaries, and this resulted in the change in fracture mode near the surface. Characterization of the effect of the heat treatments on the grain boundaries is continuing. The affected region was thicker for the sample annealed in vacuum, which is consisted with the lower pressure system resulting in an more aggressive thermal etch and removing more material (deeper into the specimen).

The effect of the transgranular fracture was a reduction in the four-point bend strength compared to standard ABC-SiC. Figure 45 plots the strength of the Ar and vacuum annealed SiC's with the standard material and commercially available Hexoloy. The ABC-SiC tested in these experiments demonstrated a strength of ~ 550 MPa while the strength dropped to ~ 490 MPa for the Ar heat treated specimen (~15% reduction in strength). The strength dropped even further for samples annealed in vacuum and resulted in values of ~ 400 MPa, similar to Hexoloy. The reduction in strength for heat treated materials is consistent with introducing a thin layer of brittle material on the surface of the flaw tolerant ABC-SiC, Figure 43. Since the transgranular region is more extensive for the sample annealed in vacuum a greater decrease in strength is expected, and indeed was observed. Additionally, the heat treatments resulted in voids near the surface, Figure 44a, and this enhanced porosity would be expected to reduce the strength. Finally, the strength of ceramics is dictated by the size the initial flaws. The voids

resulting from the annealing procedure likely increased the size of the initial flaw. Thus, the combination of these factors accounts for the reduction in strength.

Two parameter Weibull plots for standard ABC-SiC and the Ar annealed sample are shown in Figure 46. The Weibull modulus, m, for ABC-SiC was 13 and dropped to 9 for the heat treated material. The decrease in the modulus is the result of the initial flaw size increasing. Since these plots were generated with only eight data points, a minimum for generating a Weibull plot, the absolute value in the modulus will contain a significant uncertainty, but the trend of a decreasing modulus is still valuable for evaluating the decrease in the strength.

The toughness of the heat treated samples, although not tested to date, should not be completely compromised. Once the crack extends beyond the initial region of transgranular fracture, the remaining flaw tolerant material will possess a greater resistance to crack propagation and likely lead to stable crack growth. This is true provided that the initial crack size is not small compared to the thickness of the transgranular region. Likewise, if the heat affected layer is thin compared to dimensions over which stable crack growth will occur the material will exhibit good flaw tolerance. Since the transgranular region is ~ 25 μm for the Ar annealed SiC, compared to stable crack growth of 600 μm,[6] the flaw tolerance of heat treated SiC's should be retained.

IV. CONCLUSION

Initial kinetic data have been obtained on the oxidation behavior of SiC sintered with Al, B, and C additives (ABC-SiC). The oxidation rate was consistent with other polycrystalline SiC's and higher than single crystalline SiC. The oxidation kinetics at 1200°C were parabolic, suggesting the rate-limiting step in the oxidation reaction was diffusion. The oxide surface was smooth, but the presence of numerous bubbles in the passivating silica scale was observed.

Two-step processing was employed and resulted in an ~ 25% reduction in the oxidation rate for samples held at 1600°C for 48 hours prior to hot-pressing at 1900°C for 1 hour. Two-step sintering, between 600°C and 1400°C for 48 hours, did not show a measureable improvement in the oxide integrity or thickness. Samples processed at 1400°C showed a slight decrease in the bubble density, but no improvement in the oxidation rate was realized. In contrast, the SiC processed at 1600°C for 48 hours reduced the subsequent oxidation rate, but the bubbles were smaller and more numerous. Therefore, chemistry appears to be the dominant variable in the oxidation rate of SiC, even when bubbles are observed in the SiO_2 scale.

Post hot-pressing anneals on SiC sintered with Al, B, and C in an Ar and vacuum (2×10^{-4} torr) environment reduced the oxide thickness by a factor of 4 by changing the chemistry of the oxide. Most notably, the concentration of Al was dramatically reduced by the heat treatments and subsequent oxides formed with only a minimal amount of Al. The Al impurities likely result in a lower viscosity passivating scale; thus, diffusion rates and oxidation rates are accelerated. Therefore, by removing the impurities by thermally etching the surface in an Ar or vacuum environment, the oxidation behavior was

dramatically improved. Additionally, the heat treatments removed the bulk secondary phases, which are believed to enhance bubble formation. Hence, the bubbles, which could compromise the integrity of the passivating layer, were eliminated. Also, the crystalline nature of the silica scale grown on heat treated samples contributed to reducing the oxidation rate.

The SiC annealed in Ar and vacuum resulted in the surface chemistry being altered and thus the fracture mode changed in this region. Near the surface a transgranular mode of fracture was observed with a switch to the typical intergranular fracture for ABC-SiC at the center of the sample. This thin brittle region near the surface, ~ 25 μm thick for Ar annealed ABC-SiC and ~ 100-125 μm for vacuum annealed ABC-SiC, resulted in the four-point bend strength being reduced. However, the strength only dropped by ~ 15 % for the SiC annealed in Ar at 1800°C for 1 hour. At the same time the flaw tolerance of the SiC should not be compromised.

Annealing ABC-SiC in Ar or vacuum is an effective method for reducing the oxidation rate while retaining good mechanical properties. Optimization of the processing schedule should lead to similar oxidation resistance while sacrificing little of the excellent mechanical properties of SiC sintered with Al, B, and C.

References

[1] N.S. Jacobson, "Corrosion of Silicon-Based Ceramics in Combustion Environments", J. Am. Ceram. Soc., **76**[1] 3-28 (1993).

[2] D.-H. Kim and C.H. Kim, "Toughening Behavior of Silicon Carbide with Additions of Yttria and Alumina," J. Am. Ceram. Soc., **73**[5] 1431-34 (1990).

[3] S.K. Lee and C.H. Kim, "Effects of α-SiC versus β-SiC Starting Powders on Microstructure and Fracture Toughness of SiC Sintered with Al_2O_3-Y_2O_3 Additives," J. Am. Ceram. Soc., **77**[6] 1655-58 (1994).

[4] N.P. Padture, "*In Situ*-Toughened Silicon Carbide," J. Am. Ceram. Soc., **77**[2] 519-23 (1994).

[5] J.J. Cao, W.J. MoberlyChan, L.C. De Jonghe, C.J. Gilbert, and R.O. Ritchie, "*In Situ* Toughened Silicon Carbide with Al-B-C Additions," J. Am. Ceram. Soc., **79**[2] 461-69 (1996).

[6] C.J. Gilbert, J.J. Cao, W.J. MoberlyChan, L.C. De Jonghe, and R.O. Ritchie, "Cyclic fatigue and resistance-curve behavior of an in situ toughened silicon carbide with Al-B-C additions," Acta Materialia, **44** [8] 3199-214 (1996).

[7] W.J. MoberlyChan, J.J. Cao, M.Y. Niu, and L.C. De Jonghe, "Toughened β-SiC Composites with Alumina-Coated α-SiC Platelets," in *High Performance Composites* (edited by K.K. Chawla, P.K. Liaw, and S.G. Fishman), TMS Conference Proceedings (1994).

[8] T.D. Mitchell, L.C. De Jonghe, W.J. MoberlyChan, and R.O. Ritchie, "Silicon Carbide Platelet/Silicon Carbide Composites," J. Am. Ceram. Soc., **78**[1] 97-103 (1995).

[9] N.J. Shaw et al., "Materials for Engine Applications Above 3000°F-An Overview," NASA Rept. No. TM-100169, NASA Lewis Research Center, Cleveland, OH, 1987.

[10] J.L. Smialek and G.H. Meier, "High-Temperature Oxidation; pp. 293-326 in Superalloys II, Edited by C.T. Sims, N.S. Stoloff, and W.C. Hagel, Wiley, New York, 1988.

[11] G. Ervin, "Oxidation Behavior of Silicon Carbide," J. Am. Ceram. Soc., **41** [9] 347-52 (1958).

[12] E. Fitzer and R. Ebi, "Kinetic Studies on the Oxidation of Silicon Carbide"; pp. 320-28 in Silicon Carbide 1973. Edited by R.C. Marshall, J.W. Faust, Jr., and C.E. Ryan, University of South Carolina Press, Columbia, SC, 1974.

[13] N.S. Jacobson, "Corrosion of Silicon-Based Ceramics in Combustion Environments", J. Am. Ceram. Soc., **76**[1] 3-28 (1993).

[14] R. Pampuch, W. Ptak, S. Jonas, and J. Stoch, "Formation of Ternary Si-O-c Phases(s) During Oxidation of SiC," *Mater. Sci. Monogr.*, **6**, 435-48 (1980).

[15] F.J. Kohl, D.M. Leisz, G.C. Fryburg, and C.A. Stearns, "Thermochemical Analyses of the Oxidative Vaporization of Metals and Oxides by Oxygen Molecules and Atoms," NASA Rept. No. TM X-73682, NASA Lewis Research Center, Cleveland, OH, 1977.

[16] N.S. Jacobson, K.N. Lee, and D.S. Fox, "Reactions of SiC and SiO_2 at Elevated Temperatures," J. Am. Ceram. Soc., **75** [6] 1603-11 (1992).

[17] K. Motzfeld, "On the Rates of Oxidation of Silicon and Silicon Carbide in Oxygen and Correlation with Permeability of Silica Glass," *Acta Chem. Scand.*, **18** [7]1596-606 (1964).

[18] B.E. Deal and A.S. Grove, "General Relationship for the Thermal Oxidation of Silicon," *J. Appl. phys.*, **36** [12] 3770-78 (1965).

[19] Z. Zheng, R.E. Tressler, and K.E. Spear, "Oxidation of Single-Crystal Silicon Carbide, Part I. Experimental Studies," *J. Electrochem. Soc.*, **137** [3] 854-58 (1990).

[20] Z. Zheng, R.E. Tressler, and K.E. Spear, "Oxidation of Single-Crystal Silicon Carbide, Part II. Kinetic Model," *J. Electrochem. Soc.*, **137** [9] 2812-16 (1990).

[21] D.M. Mieskowski, T. E. Mitchell, and A.H Heuer, "Bubble Formation in Oxide Scales on SiC," *J. Am. Ceram. Soc.*,**67**[1] C-17-C-18 (1984).

[22] K.L. Luthra, "Some New Perspectives on Oxidation of Silicon Carbide and Silicon Nitride," *J. Am. Ceram. Soc.*,**74**[5] 1095-1103 (1991).

[23] Tables of Interatomic Distances and Configuration in Molecules and Ions; Special Publication No. 11; London: The Chemical Society, Burlington House, WI (1958).

[24] J.A. Costello and R.E. Tressler, "Oxidation Kinetics of Silicon Carbide Crystals and Ceramics: I, in Dry Oxygen," *J. Am. Ceram. Soc.*,**69**[9] 674-81 (1986).

[25] W.H. Zachariasen, *J. Am. Ceram. Soc.*, **54**, 3841 (1932).

[26] N.P. Bansal, Handbook of Glass Properties, Academic Press, Inc., pp. 7-28 (1986).
[27] P.J. Jorgensen, M.E. Wadsworth, and I.B. Cutler, "Effects of Water Vapor on Oxidation of Silicon Carbide," *J. Am. Ceram. Soc.*, **44** [6] 258-61 (1961).
[28] H.Cappelen, K.H. Johansen, and K. Motzfeld, "Oxidation of Silicon Carbide in Oxygen and Water Vapor at 1500°C," *Acta Chem. Scand. A*, **35**, 247-54 (1981).
[29] T. Narushima, T.Goto, Y. Iguchi, and T. Hirai, "High-Temperature Oxidation of Chemically Vapor-Deposited Silicon carbide in Wet Oxygen at 1823 to 1923K," *J. Am. Ceram. Soc.*, **73** [12] 1580-84 (1990).
[30] M.Maeda, K. Makamura, and T. Ohkubo, "Oxidation of Silicon Carbide in a Wet Atmosphere," *J. Mater. Sci.*, **23**, 3933-38 (1988).
[31] R.E. Tressler, J.A. Costello, and Z.Zheng, "Oxidation of Silicon Carbide Ceramics"; pp. 307-14 in *Industrial Heat Exchangers*. Edited by A.J. Hayes, *et al.*American Society of Metals, Warrendale, PA, 1985.
[32] E.A. Irene and R. Ghez, "Silicon Oxidation Studies: the Role of H_2O," *J. Electrochem. Soc.*, **124** [11] 1757-61 (1977).
[33] W.D. Kingery, H.K. Bowen, and D.R. Uhlmann, Introduction to Ceramics, 2nd ed., John Wiley&Sons, New York, (1976).
[34] T. Narushima, T.Goto, and T. Hirai, "High-Temperature Passive Oxidation of Chemically Vapor Deposited Silicon Carbide," *J. Am. Ceram. Soc.*, **72** [8] 1386-90 (1989).
[35] L.U. Ogbuji, "Development of Oxide Scale Microstructures on Single-Crystal SiC," *J. Mater. Sci.*,**16**, 2753-59 (1981).
[36] Concise Encyclopedia of Advanced Ceramic Materials, Edited by R.J. Brook (1990).
[37] J. Schlichting, "SiC as an Oxidation-Resistant Refractory Material. Resistance to Oxidation and Corrosion at High Temperatures. I and II," *Ber. Dtsch. Keram. Ges.*, **56**, 196-200, 256-61 (1971).
[38] J.W. Fergus and W.L. Worrell, "Effect of Carbon and Boron on the High-Temperature Oxidation of Silicon Carbide," *J. Am. Ceram. Soc.*,**78**[7] 1961-64 (1995).
[39] S.C. Singhal, "Oxidation Kinetics of Hot-Pressed Silicon Carbide," *J. Mater. Sci.*, **11**. 1246-53 (1976).
[40] J. Schlichting and J. Kriegesmann, "Oxidation Behavior of Hot-Pressed Silicon Carbide," *Ber. Dtsch. Keram. Ges.*, **56** [3-4],72-75 (1975).
[41] A.H. Heuer, L.U. Ogbuji, and T.E. Mitchell, "The Microstructure of Oxide Scales on Oxidized Si and SiC Single Crystals," *J. Am. Ceram. Soc.*,**63**[5-6] 354-55 (1980).
[42] J.W. Hinze, W.C. Tripp, and H.C. Graham; pp. 409-419 in Mass Transport Phenomena in Ceramics (Materials Science Research, Vol. 9). Edited by A.R. Cooper and A.H. Heuer. Plenum, NY, 1975.
[43] J.E. Hoherty, "Oxidation of Silicon Carbide," *Proc. EMSA*, **30**, 538-39 (1972).
[44] S.C. Singhal and F.F. Lange, "Effect of Alumina Content on the Oxidation of Hot-Pressed Silicon Carbide," *J. Am. Ceram. Soc.*,**58** [9-10]433-35 (1975).
[45] G.H. Schiroky, "Oxidation of Chemically Vapor-Deposited Silicon Carbide," *Adv. Ceram. Mater.*, **2** [2] 137-41 (1987).
[46] J.W. Fergus and W.L. Worrell, "Silicon-Carbide/Boron-Containing Coating for the Oxidation Protection of Graphite," *Carbon*, **33**[4] 537-43 (1995).
[47] J. Cao, "*In Situ* Toughened SiC Ceramics with Al-B-C Additions and Oxide-Coated SiC Platelet/SiC Composites," Ph.D. Thesis, Univerisity of California, Berkeley, pp. 22, (1996).
[48] D.H. Stutz, S. Prochazka, and J. Lorenz, "Sintering and Microstructure Formation of β-Silicon Carbide," *J. Am. Ceram. Soc.*,**68**[9] 478-82 (1985).
[49] M.-Y. Chu, L.C. DeJonghe, M.K.F. Lin, and F.J.T. Lin, "Precoarsening to Improve Microstructure and Sintering of Powder Compacts," *J. Am. Ceram. Soc.*,**74**[11] 2902-11 (1991).
[50] T. Ohji and L.C. DeJonghe, "Presintering Heat Treatment, Densification, and Mechanical Properties of Silicon Carbide," *J. Am. Ceram. Soc.*,**77** [6]1685-87 (1994).
[51] S.G. Cook, J.A. Little, and J.E. King, "Etching and Microstructure of Engineering Ceramics," *Materials Characterization*, **34** 1-8 (1995).
[52] J. Ruska, L.J. Gauckler, J.L. Lorenz, and H.U. Rexer, "The Quantitative Calcualtion of SiC Polytypes from Measurements of X-ray Diffraction Peak Intensities," *J. Mater. Sci.*, **14** [8] 2013-17 (1979).
[53] L.U.J.T. Ogbuji and E.J. Opila, "A Comparision of the Oxidation Kinetics of SiC and Si_3N_4," *J. Electrochem. Soc.*,**142** [3]925-30 (1995).

[54] E.J. Opila,"Influence of Alumina Reaction Tube Impurities on the Oxidation of Chemically-Vapor-Deposited Silicon Carbide," *J. Am. Ceram. Soc.*,**78** [4] 1107-10 (1981).
[55] Z. Zheng, R.E. Tressler, and K.E. Spear, *Corros. Sci.*, **33**, 569 (1992).
[56] J.A. Costello, R.E. Tressler, and I.S.T. Tsong, "Boron Redistribution in Sintered α-SiC During Thermal Oxidation," *J. Am. Ceram. Soc.*,**64** [6]332-35 (1981).
[57] J.A. Costello and R.E. Tressler, "Oxidation Kinetics of Hot-Pressed and Sintered α-SiC," *J. Am. Ceram. Soc.*,**64** [6]327-31 (1981).
[58] CRC Handbook of Chemistry and Physics, 68th edition, CRC Press, Inc., Boca Raton, Florida, 1987.
[59] M.A. Mulla and V.D. Krstic, "Low-Temperature Pressureless Sintering of β-Silicon Carbide with Aluminum Oxide and Yttrium Oxide Additives," *Ceramic Bulletin*, **70** [3] 439-43 (1991)
[60] D.R. Clarke and F.F. Lange, "Oxidation of Si_3N_4 Alloys: Relations to Phase Equilibria in the System Si_3N_4-SiO_2-MgO," *J. Am. Ceram. Soc.*,**63** [9-10] 586-93 (1980).
[61] E.J. Opila, D.S. Fox, C.A. Barrett, *Ceram. Eng. Sci. Proc.*, **14**, 367 (1993).
[62] Clarke, "A Comparison of Reducing and Oxidizing Heat Treatments of Hot-Pressed Silicon Nitride," *J. Am. Ceram. Soc.*,**66** [2] 92-5 (1983).

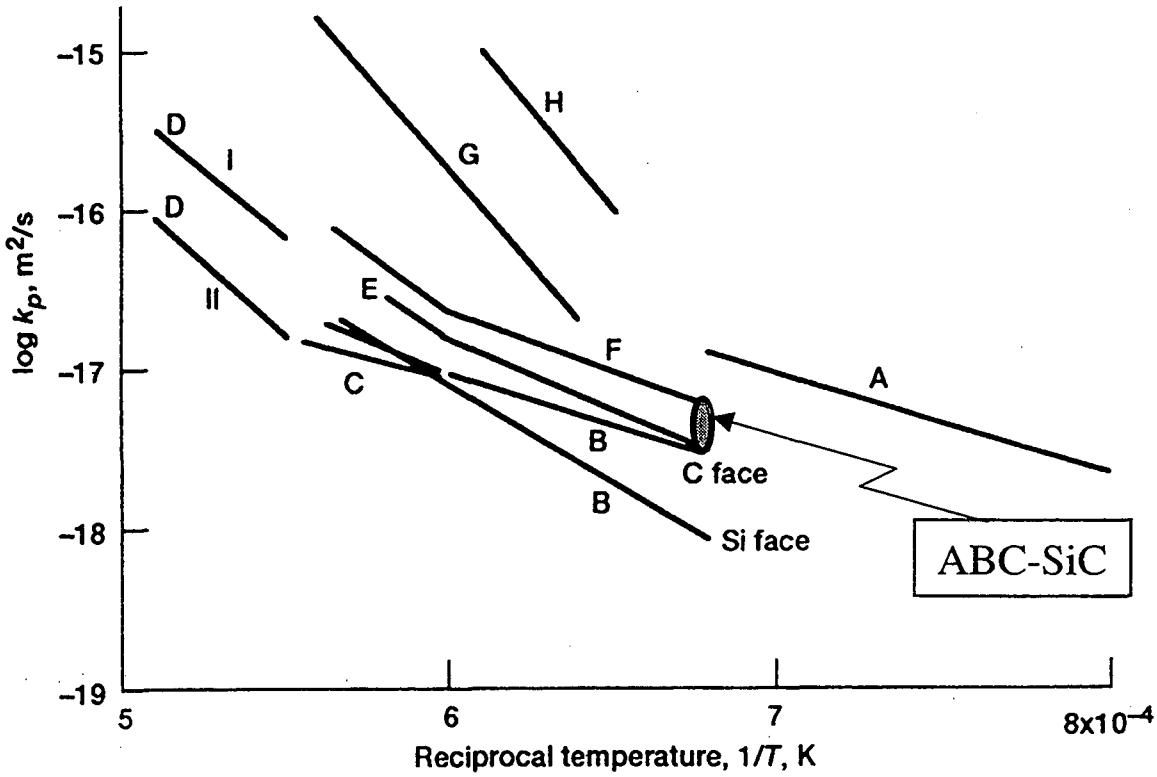

Figure 1: Parabolic rate constants for numerous SiC's.[1]

A: Single-crystal silicon
B: Single-crystal SiC
C: Chemical vapor deposition (CVD) SiC
D: CVD SiC
E: Controlled-nucleation, thermally deposited SiC
F: Sintered α-SiC
G: Hot-pressed SiC (Al_2O_3 additives), 0.2 atm O_2
H: Hot-pressed SiC (Al_2O_3 additives)

The shaded region denotes ABC-SiC. The top of the region corresponds to the standard ABC-SiC while the lower region estimates the improved oxidation resistant by incorporating heat treatments.

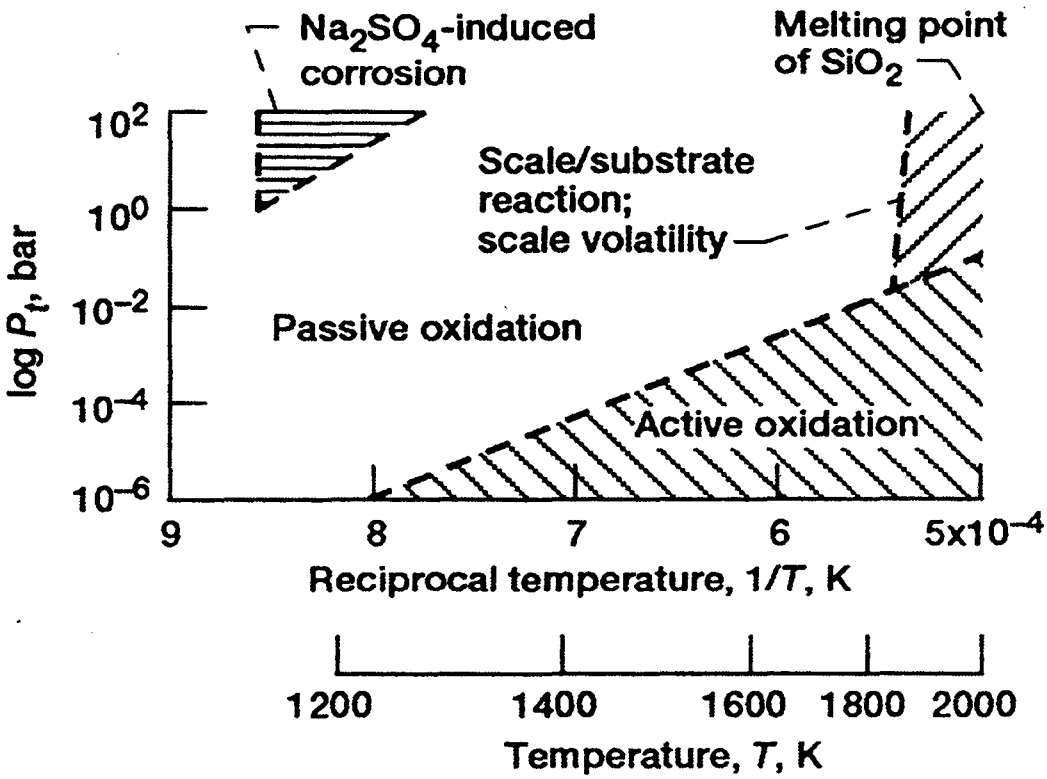

Figure 2: Types of corrosive degradation as an approximate function of reciprocal temperature.[1]

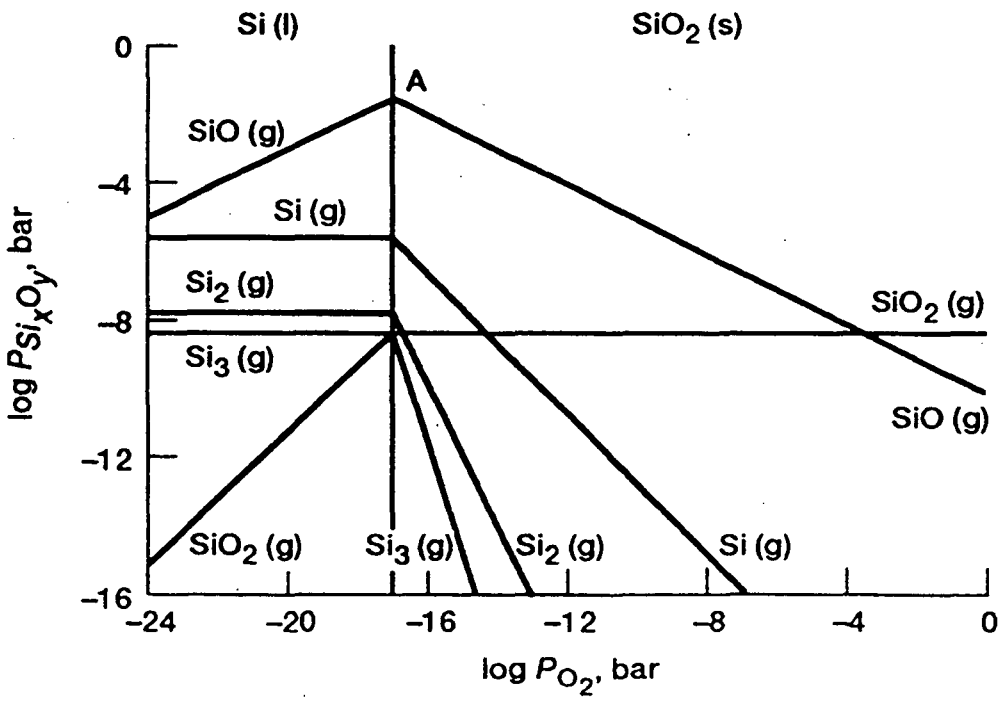

Figure 3: Volatility diagram for the Si-O system at 1800 K.[1]

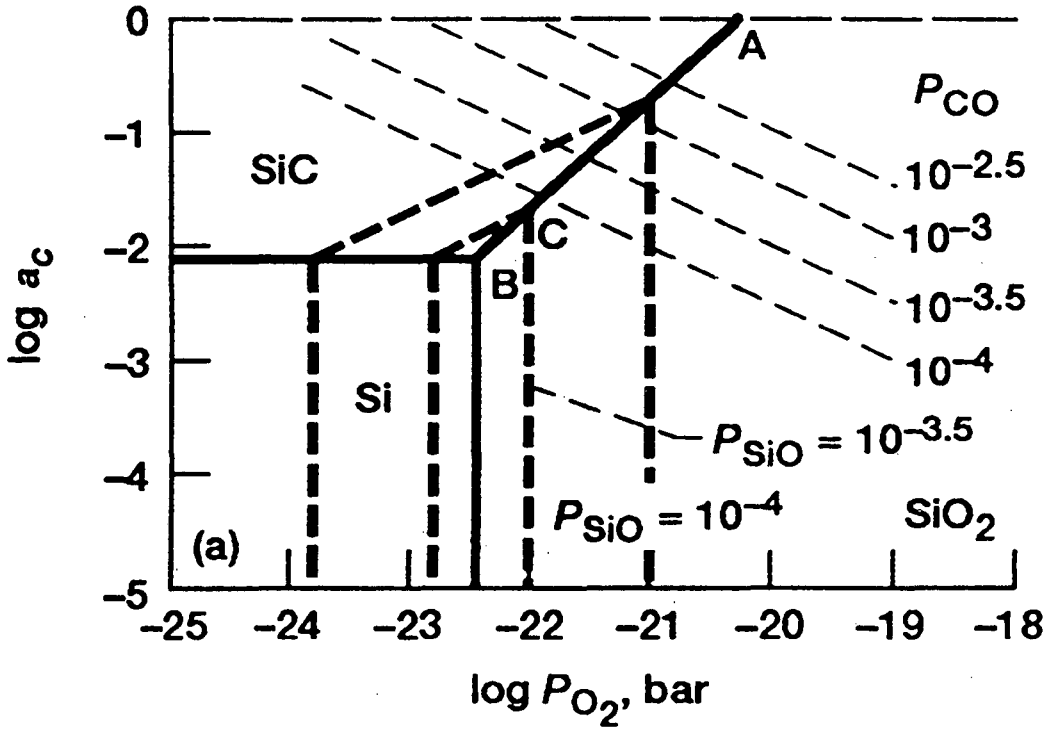

Figure 4: Predominance diagram for the Si-C-O system at 1500K.[1]

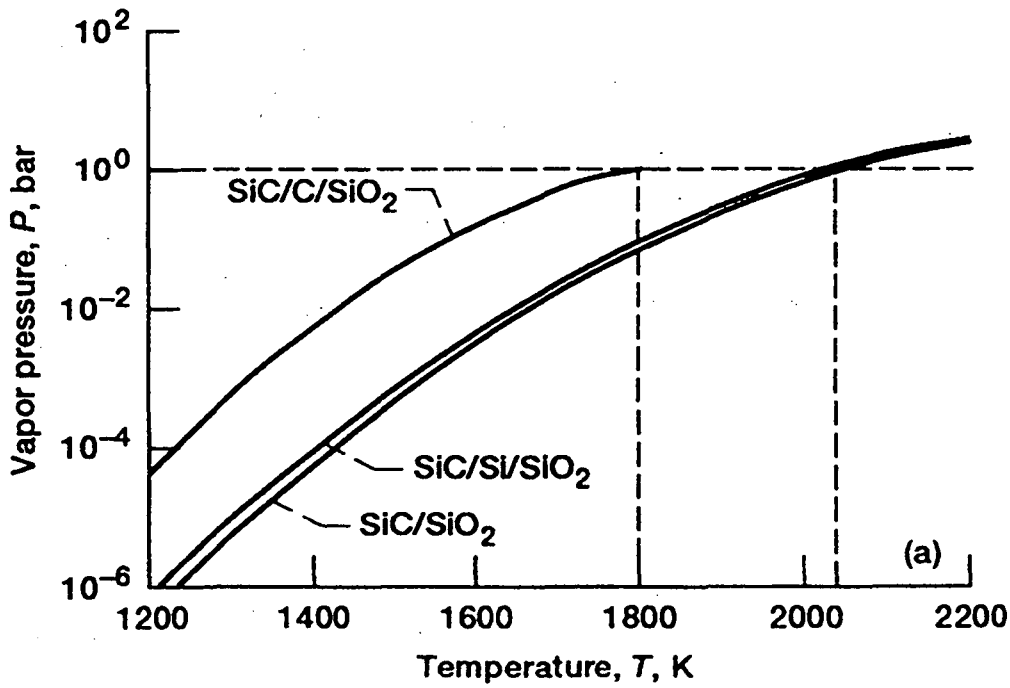

Figure 5: Total vapor pressure at SiC/SiO_2.[1]

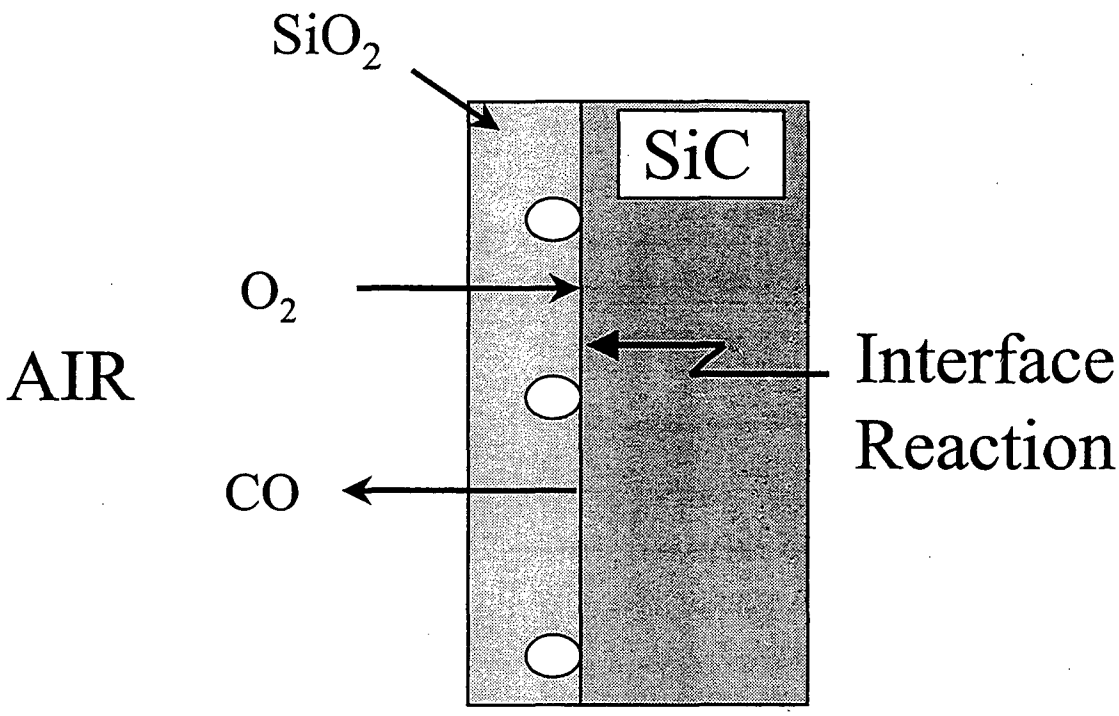

- $SiC(s) + 3/2O_2(g) \longrightarrow SiO_2(s) + CO(g)$
- ABC-SiC follows parabolic kinetics

Figure 6: Schematic diagram showing the oxidation process.

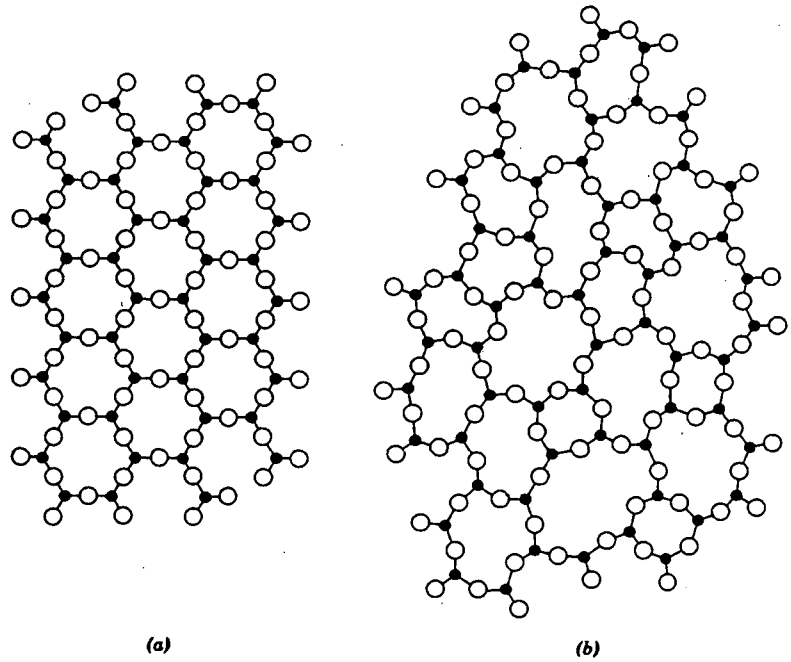

Figure 7: Schematic diagram of a) ordered crystalline structure and b) random glass network.[32]

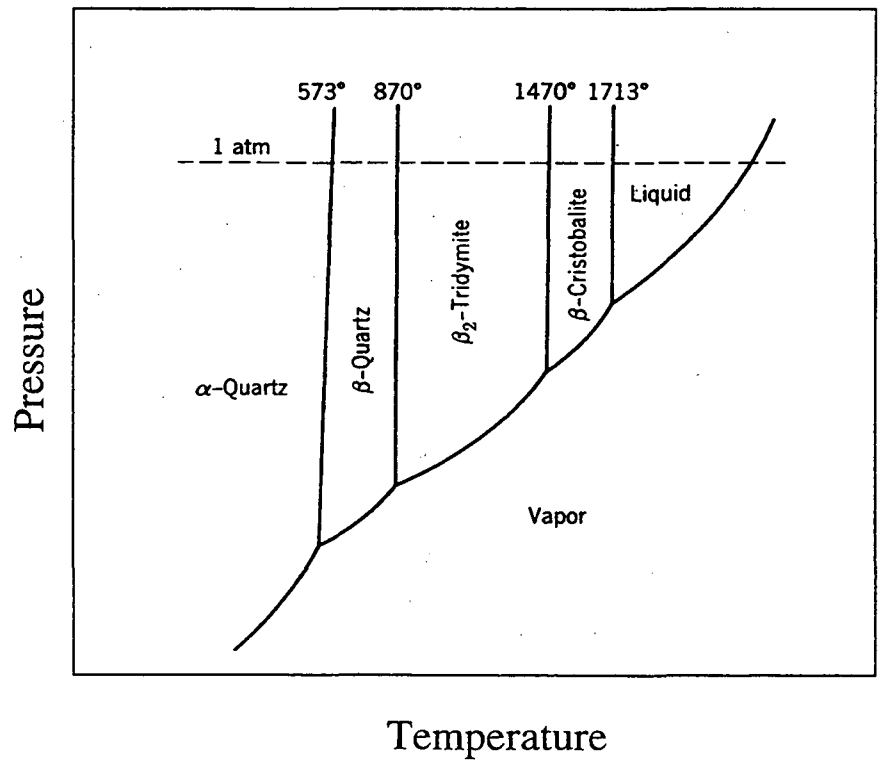

Figure 8: Equilibrium phase diagram for silica.[32]

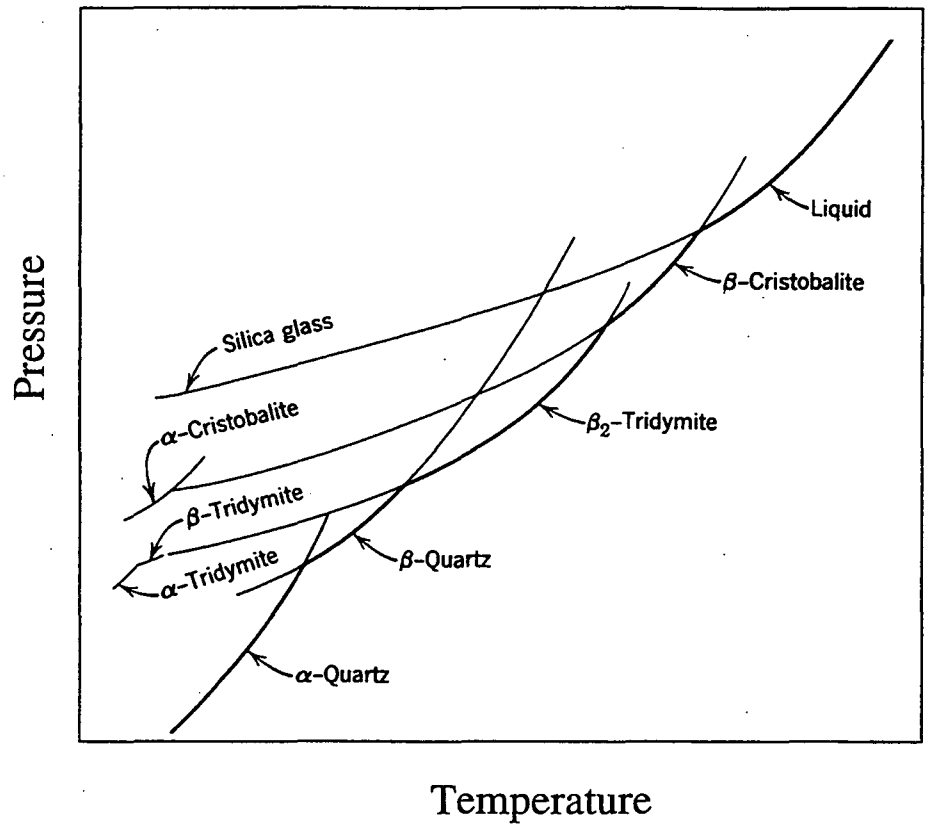

Figure 9: Diagram for silica including metastable phases.[32]

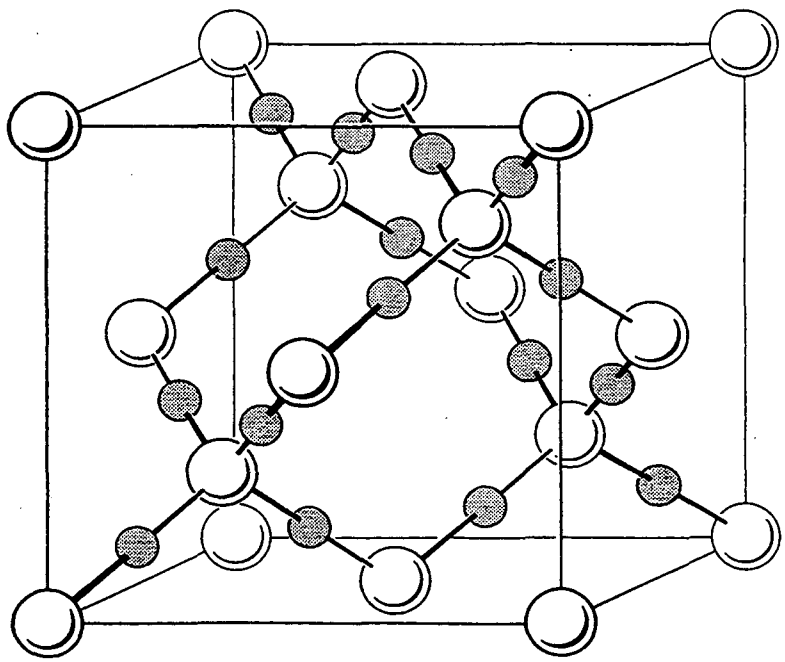

Figure 10: Structure of high cristobalite.[32]

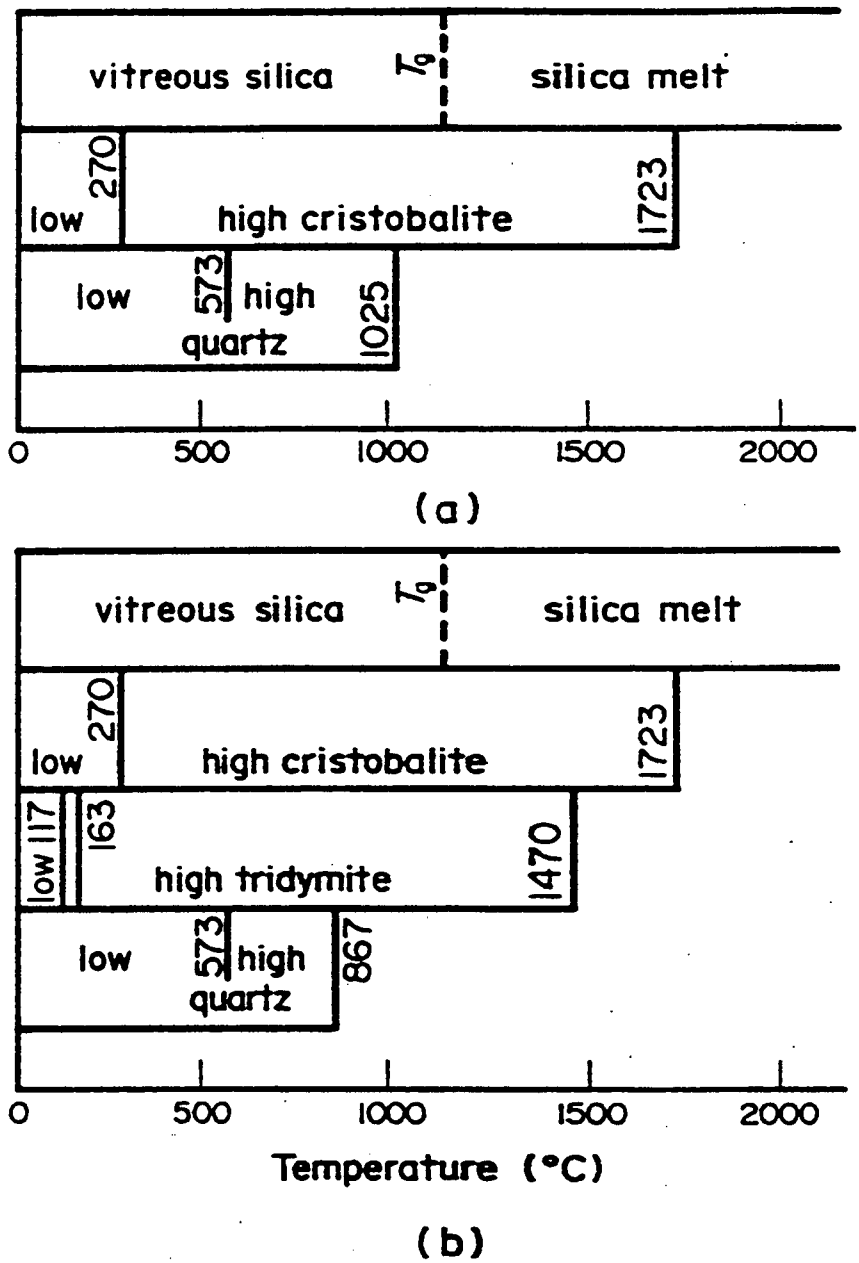

Figure 11: The phases of silica as a function of temperature at atmospheric pressure for a) a pure system and b) an impure system.[35]

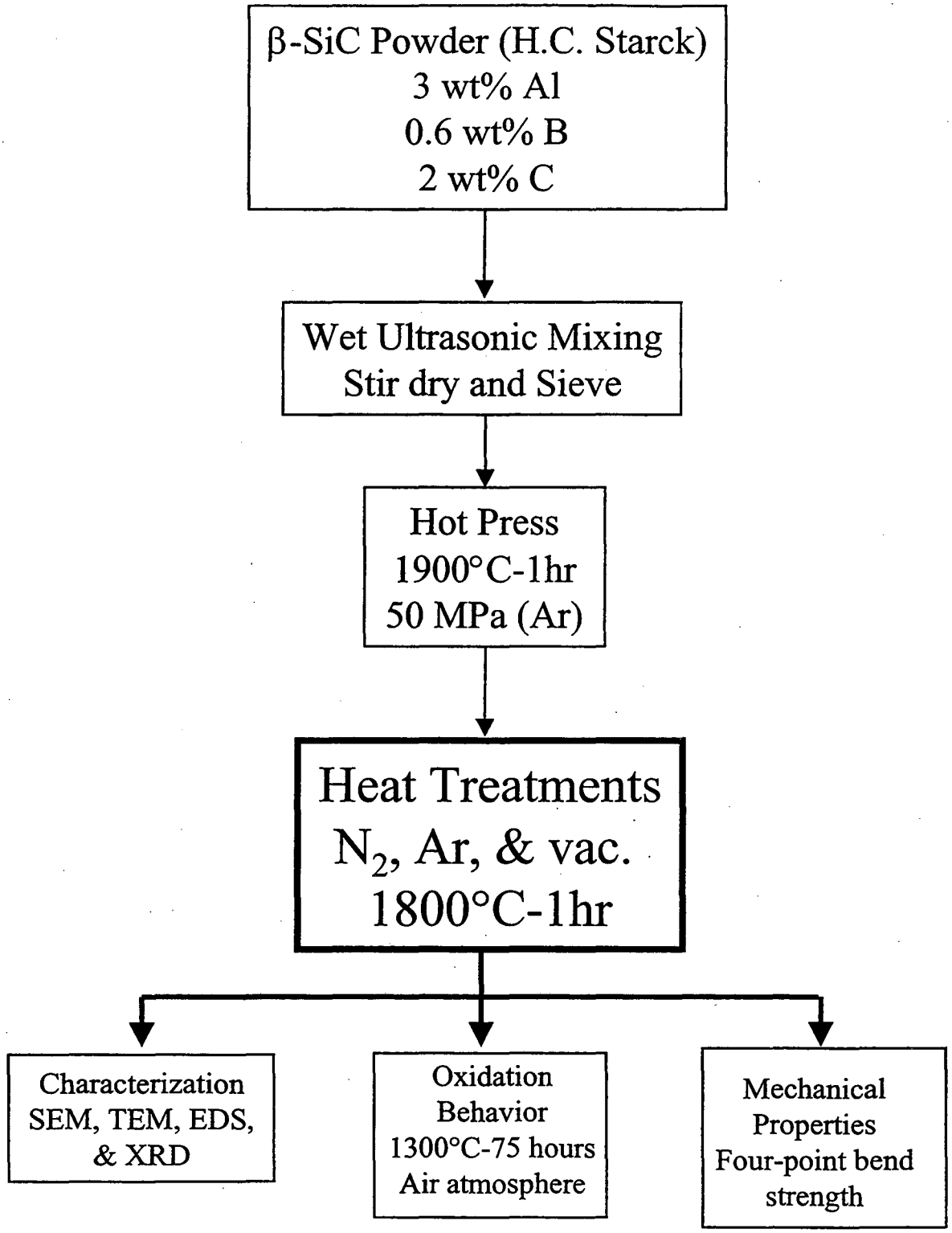

Figure 12: Flow chart for the processing and testing of ABC-SiC.

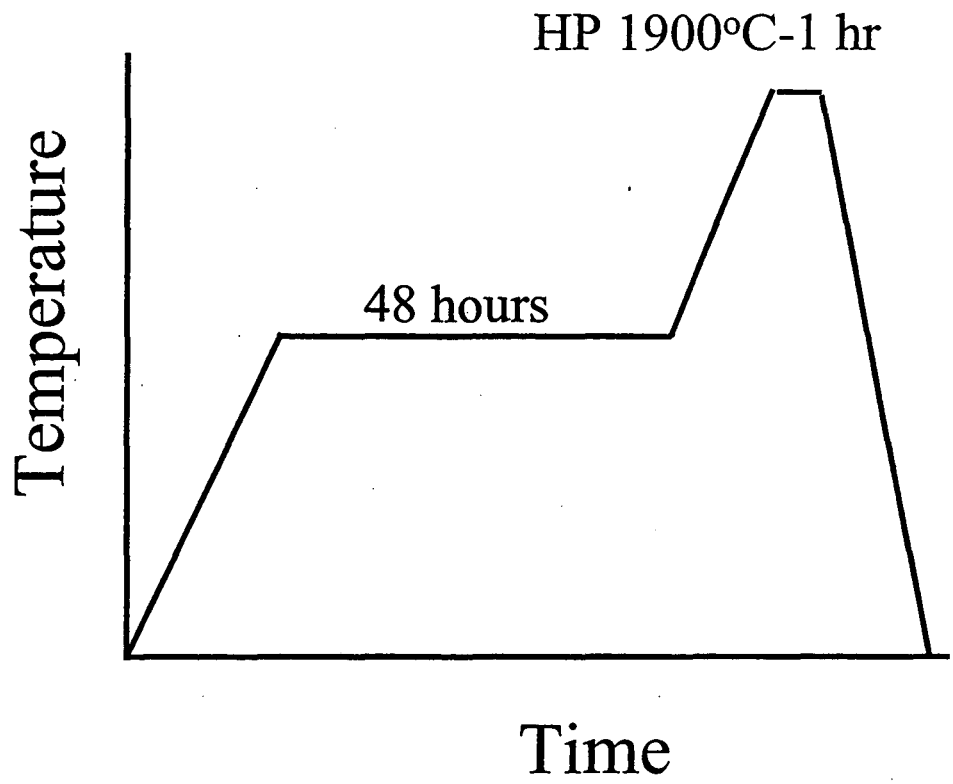

Figure 13: Schematic diagram for the two-step sintering heating schedule.

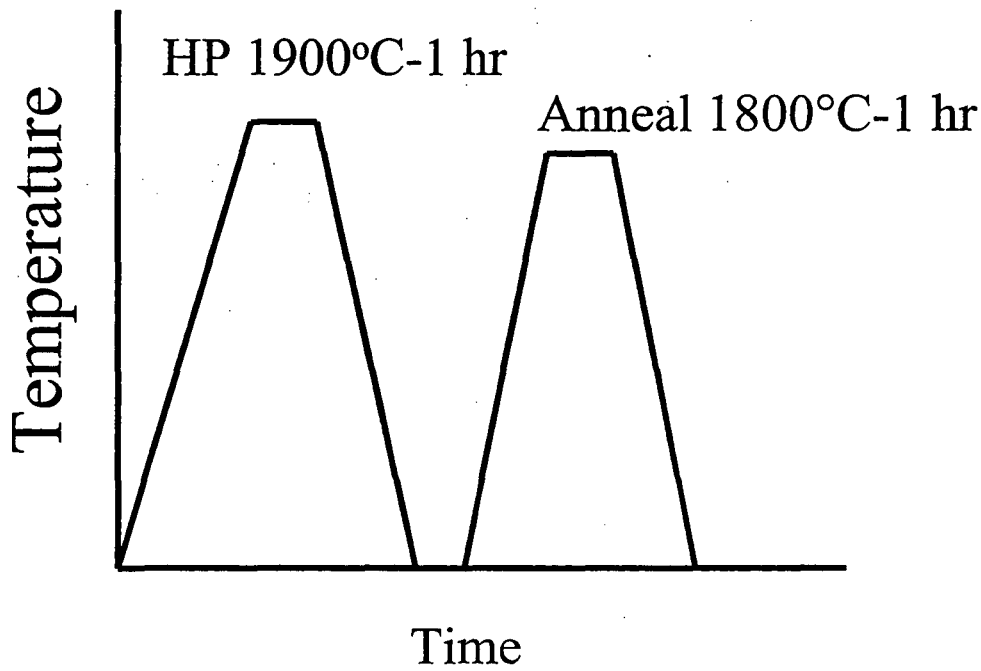

Figure 14: Schematic diagram for the heat treatment heating schedule.

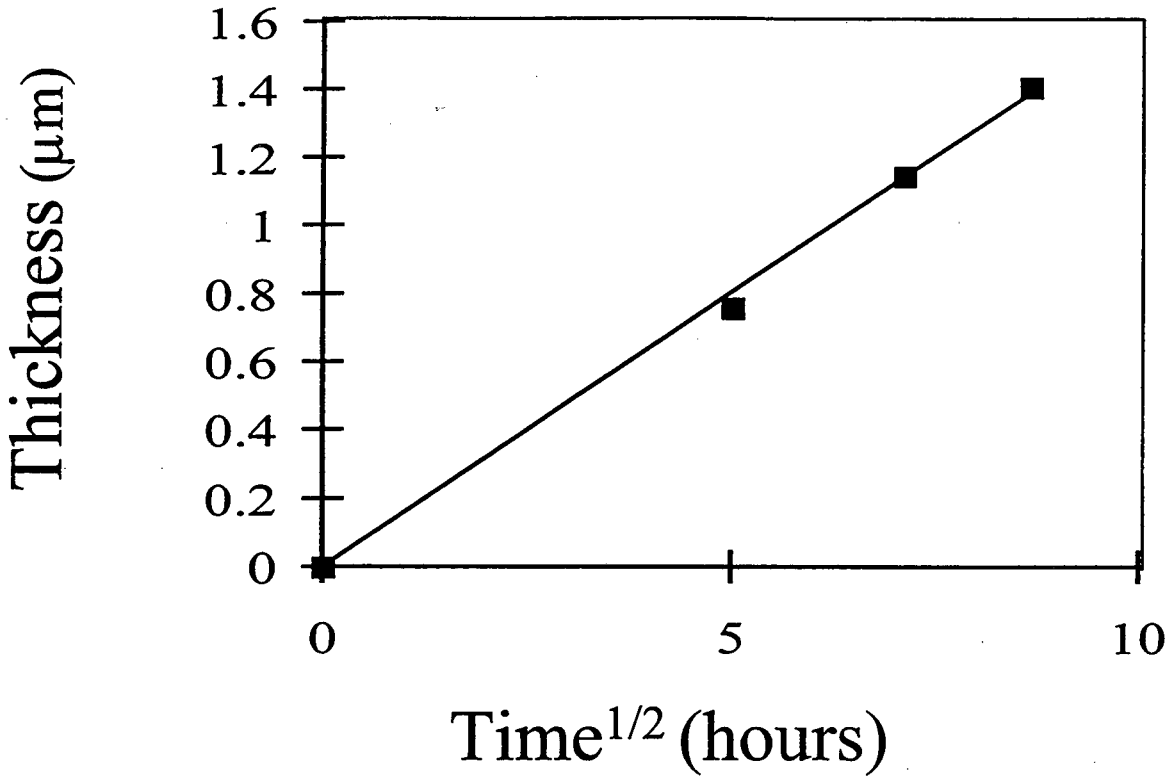

Figure 15: Kinetic data for ABC-SiC oxidized at 1200°C for 25, 50, and 75 hours in air.

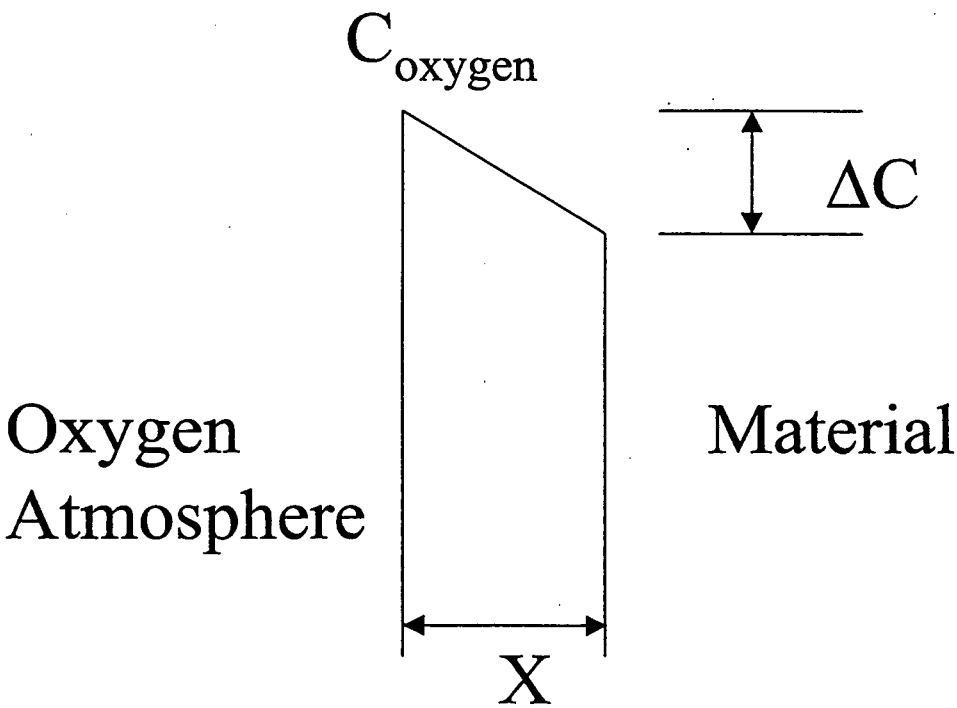

Figure 16: Schematic diagram of the oxygen concentration gradient across the oxide scale

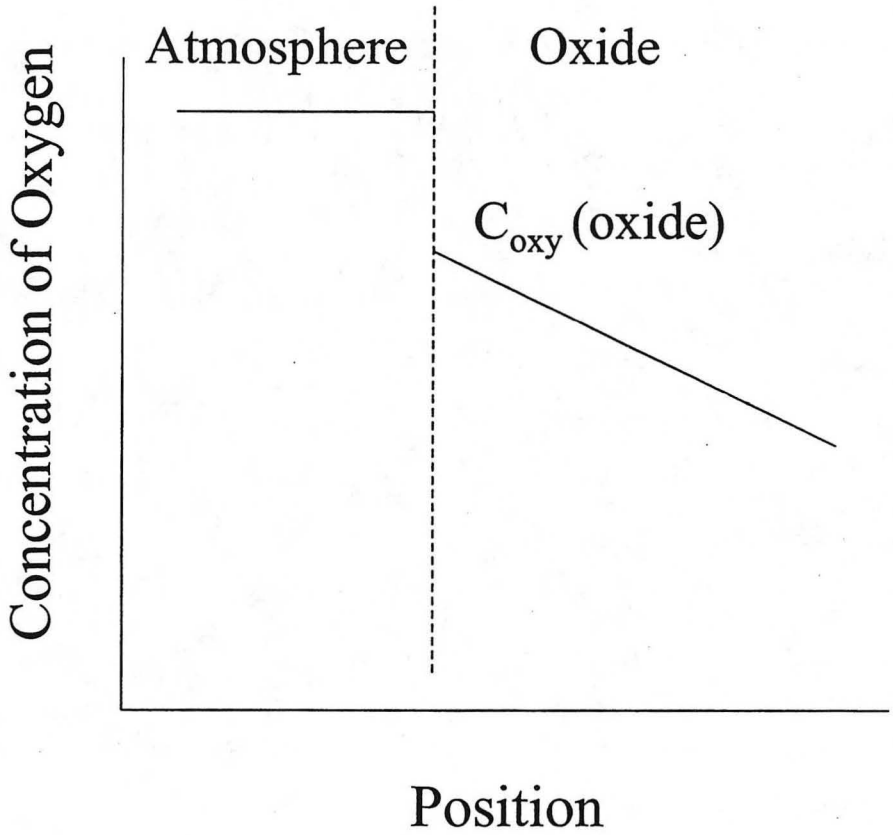

Figure 17: Schematic diagram of oxygen concentration gradient used by Deal and Grove[22] for calculating growth kinetic for Si.

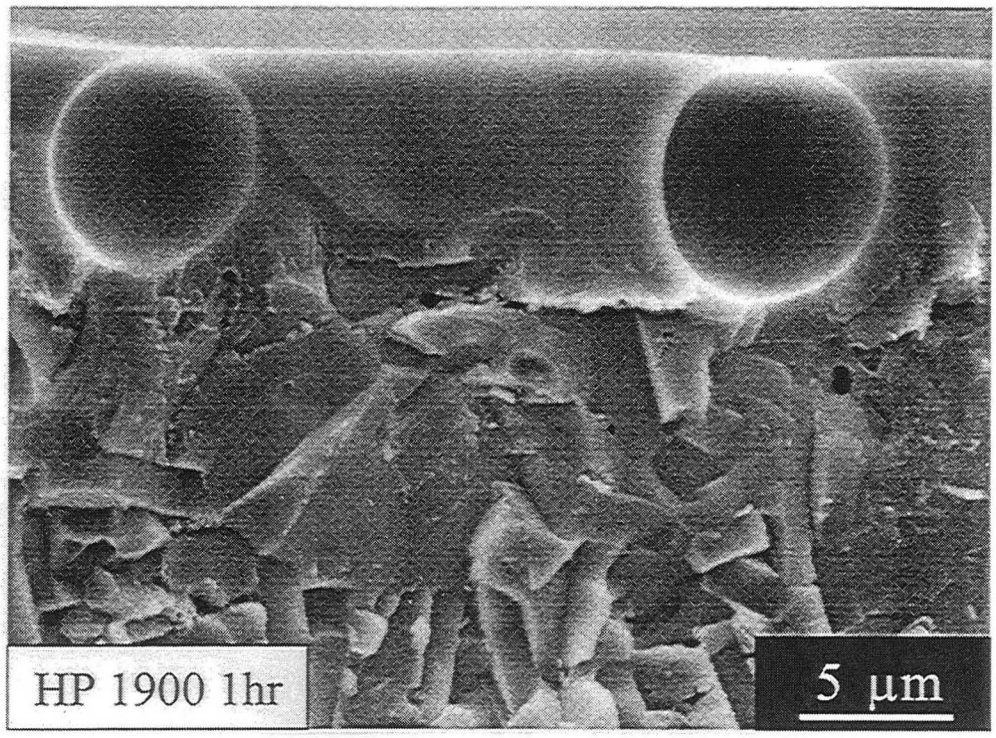

Figure 18: SEM micrograph of Standard ABC-SiC oxide in cross-section after 1300°C exposure for 75 hours in air.

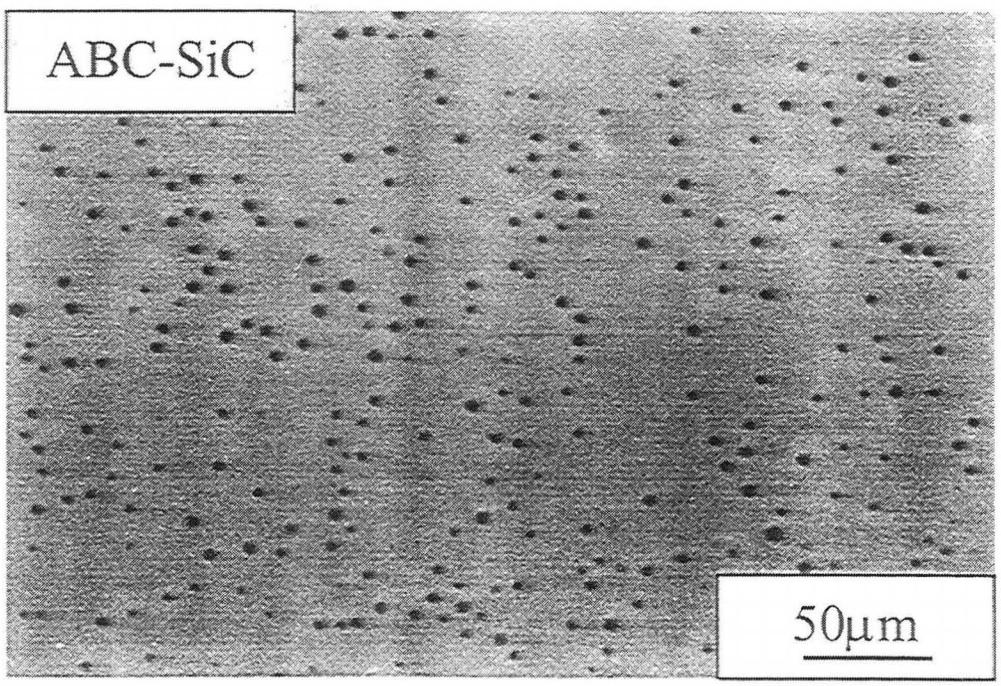

Figure 19: Plan view SEM micrograph of Standard ABC-SiC after oxidation for 25 hours in air.

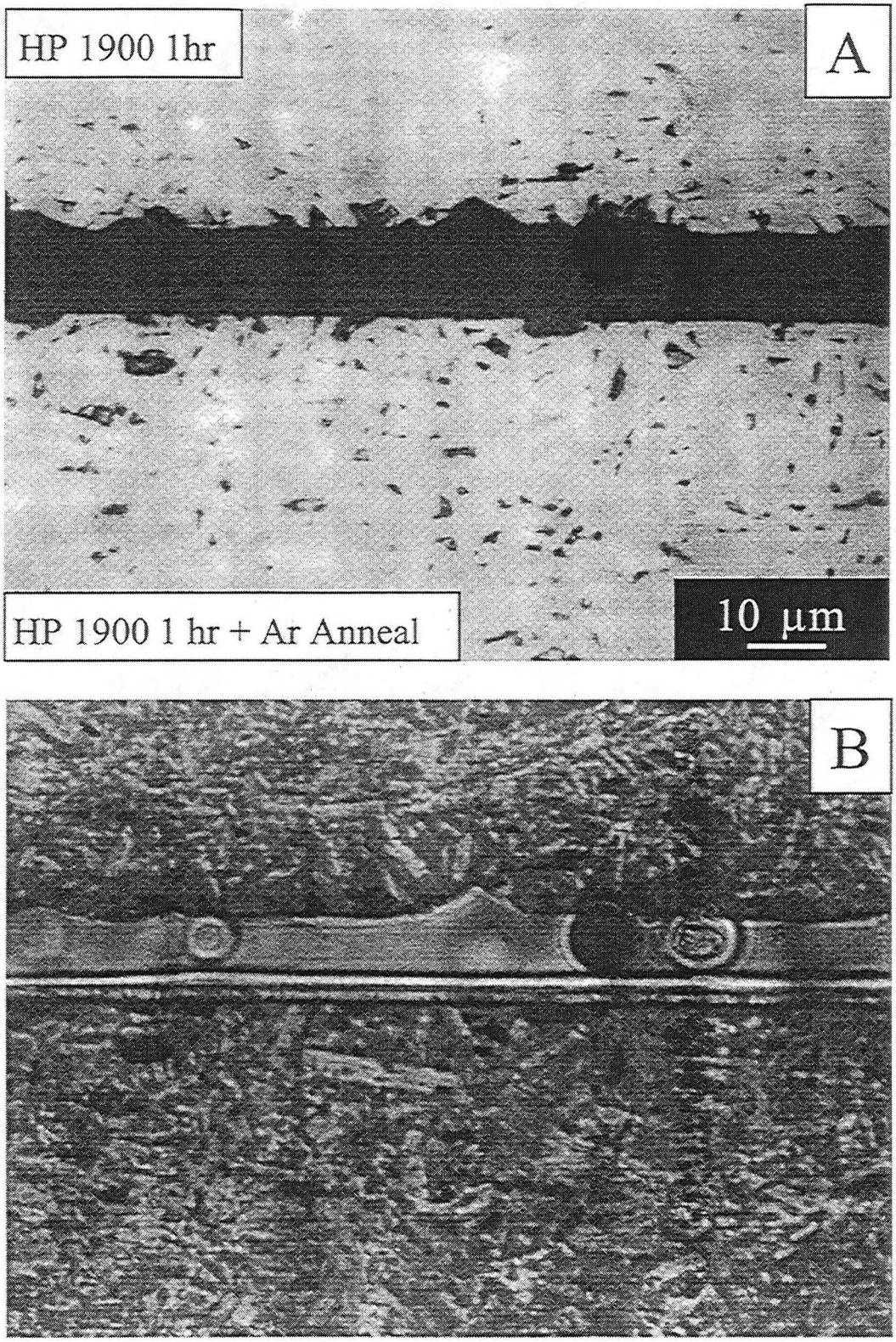

Figure 20: A) Reflected and B) transmitted optical micrographs of cross-section TEM specimen prior to ion milling. Courtesy of Dr. Warren J. MoberlyChan.

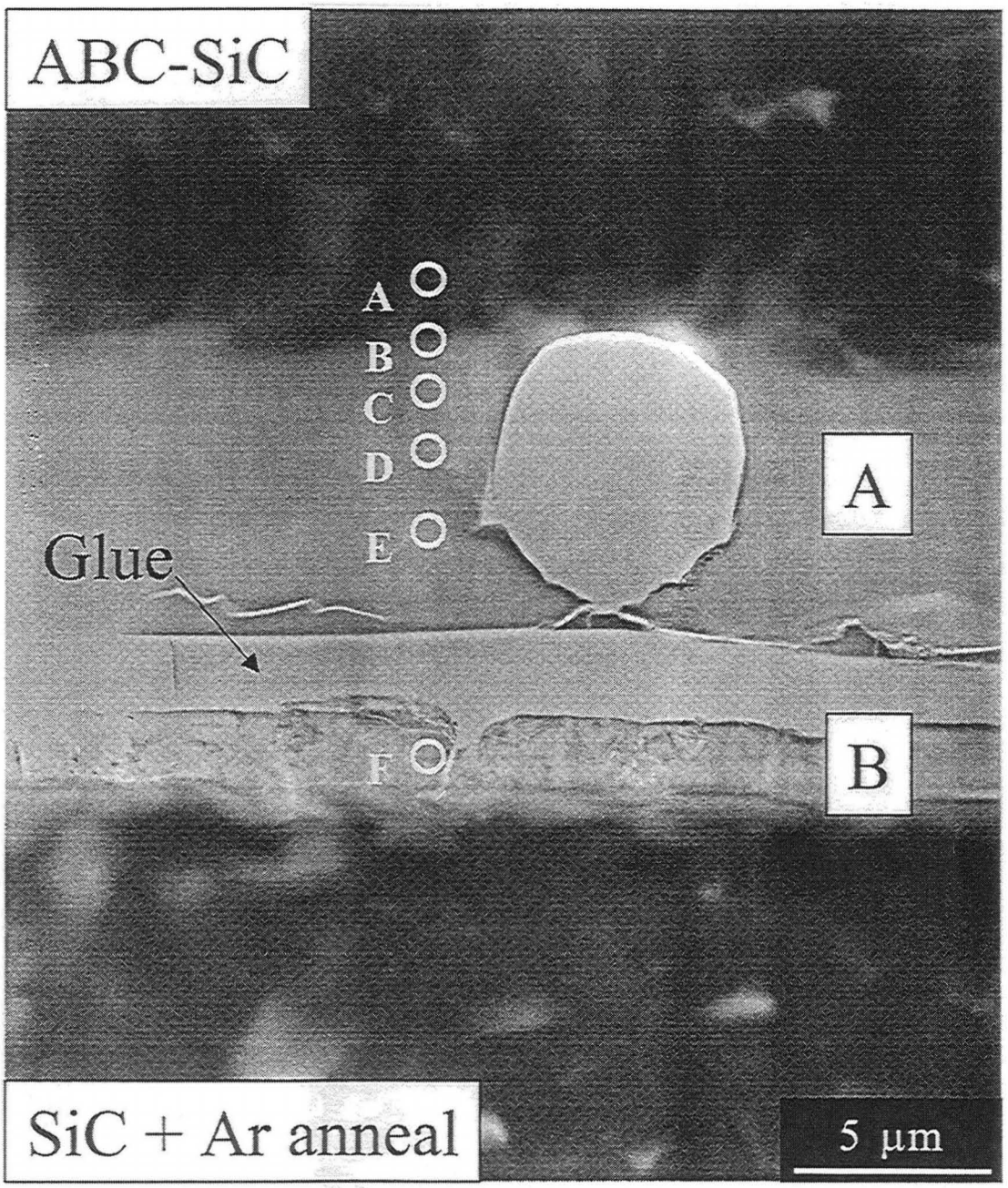

Figure 21: Low magnification TEM micropraph, no objective aperture, of A) standard ABC-SiC and B) ABC-SiC + Ar heat treatment. Both samples were oxidized for 75 hours in air at 1300°C. The dark regions are the SiC substrate and the lighter contrast areas are the oxides (with a thin glue layer in the middle). Courtesy of Dr. Warren J. MoberlyChan.

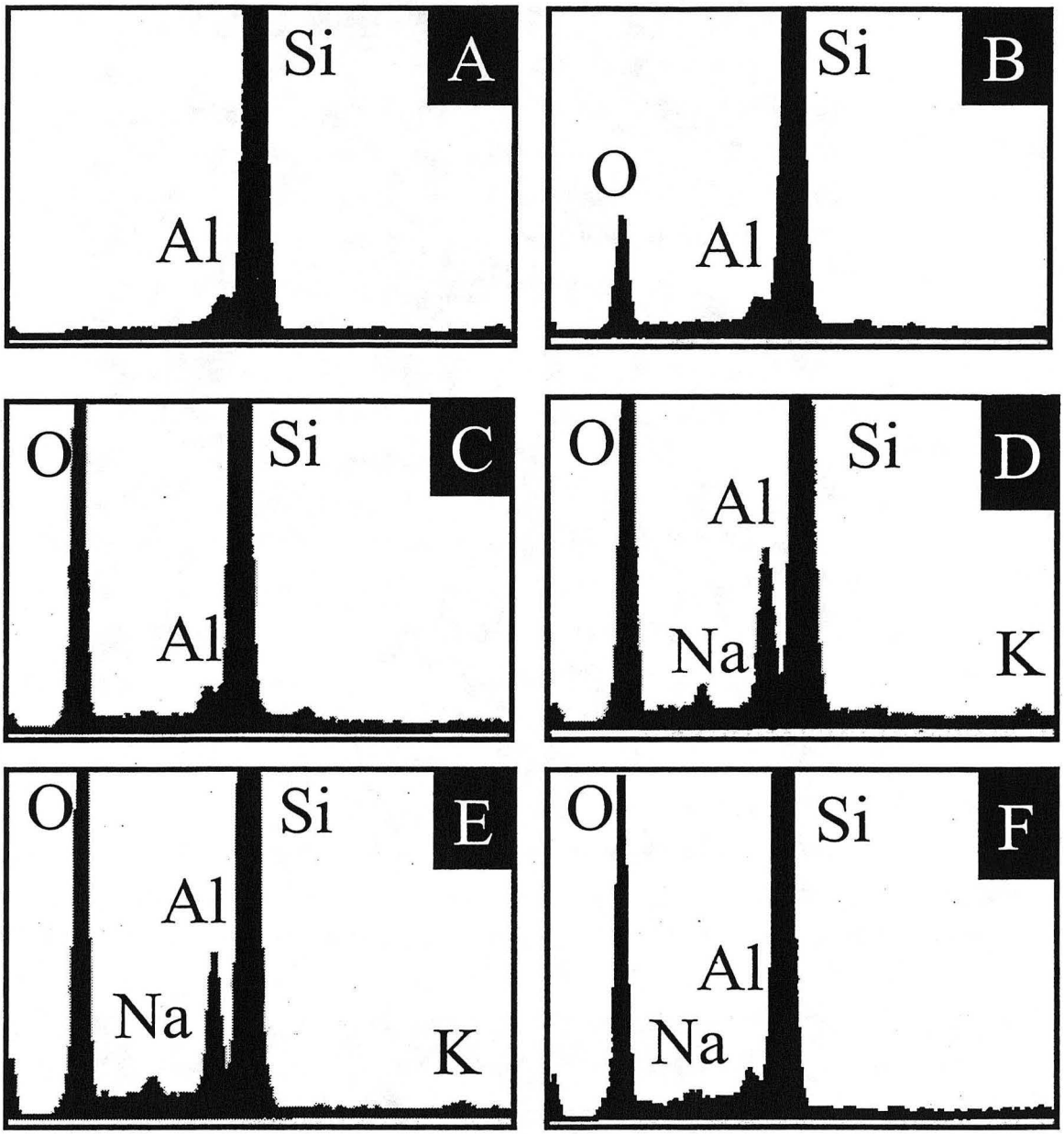

Figure 22: EDS spectra from the regions A-F shown in Figure 41. Spectra A-E are from standard ABC-SiC. F is from ABC-SiC annealed in an Ar environment. Courtesy of Dr. Warren J. MoberlyChan.

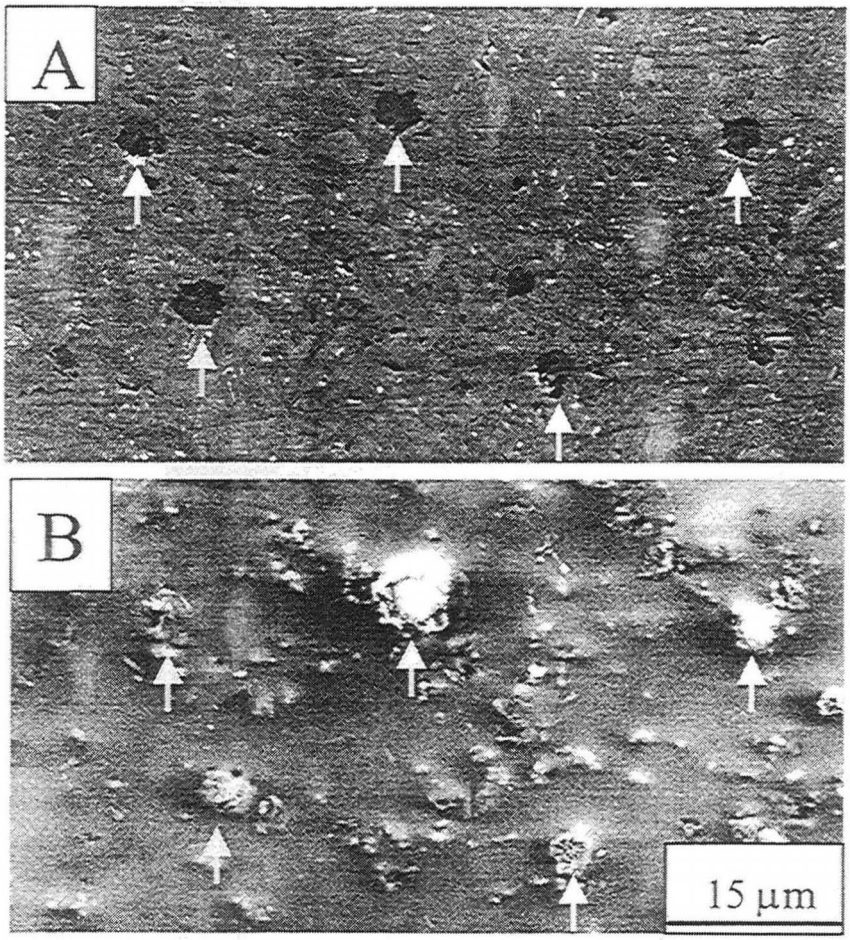

Figure 23: a) SEM micrograph of polished ABC-SiC surface prior to oxidation, b) SEM micrograph of the same region as A after oxidation 1400-20 hours (Courtesy of Dr. Joe Cao).

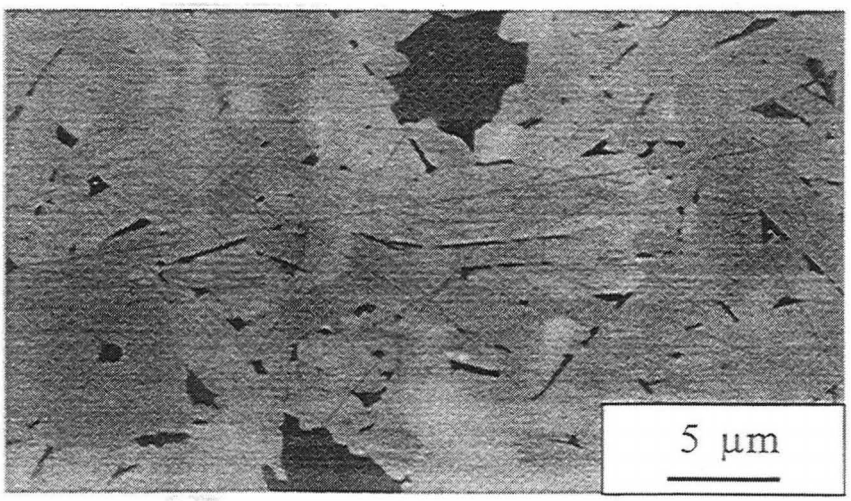

Figure 24: Higher magnification SEM micrograph of polished surface elucidates the numerous triple point materials in addition to the bulk secondary phase.

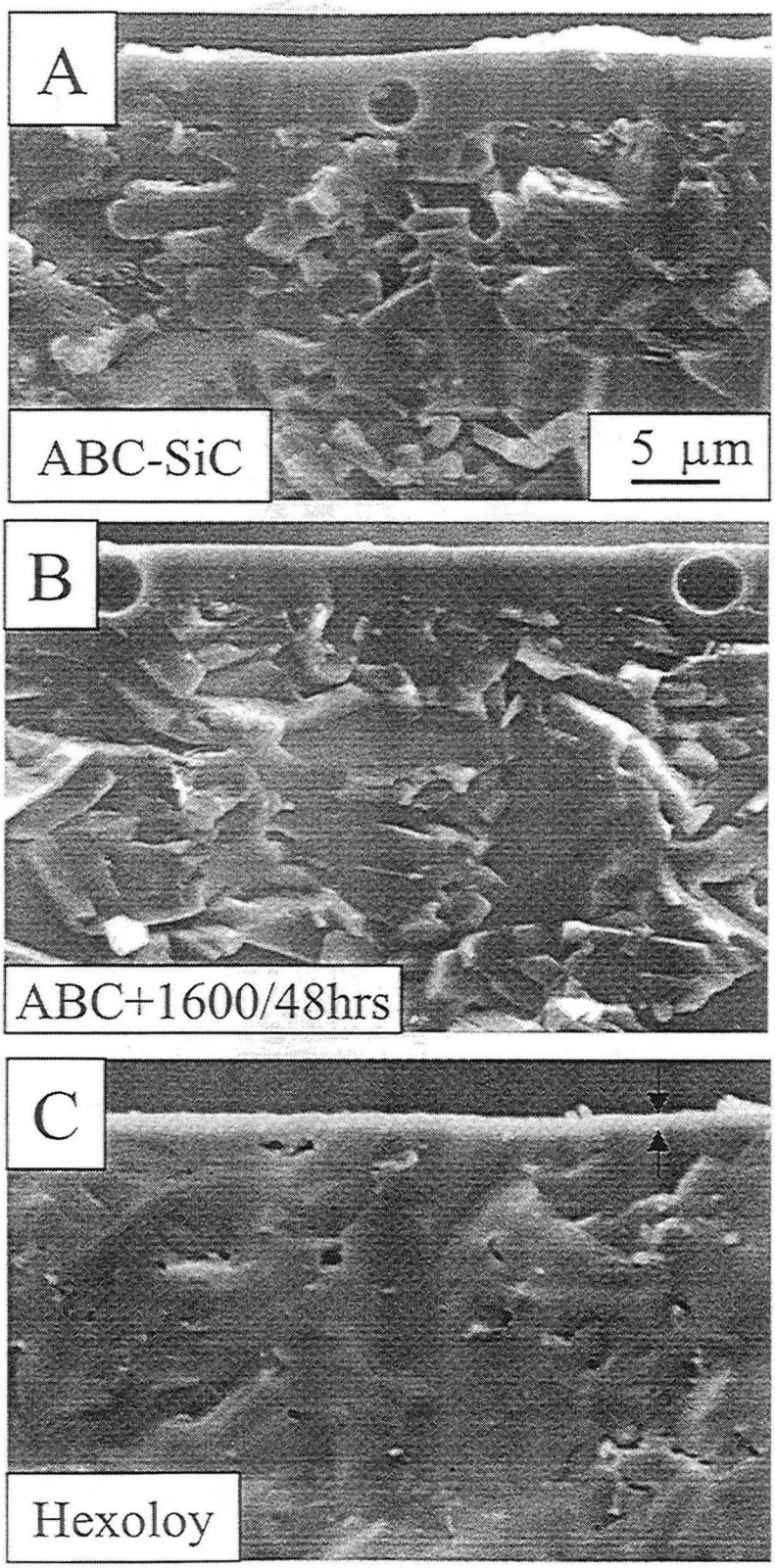

Figure 25: Cross-section SEM micrographs of A) standard ABC-SiC, B) ABC-SiC + 1600-48 hours, and C) Hexoloy after oxidation at 1400°C for 25 hours in air (oxide thickness shown by arrows).

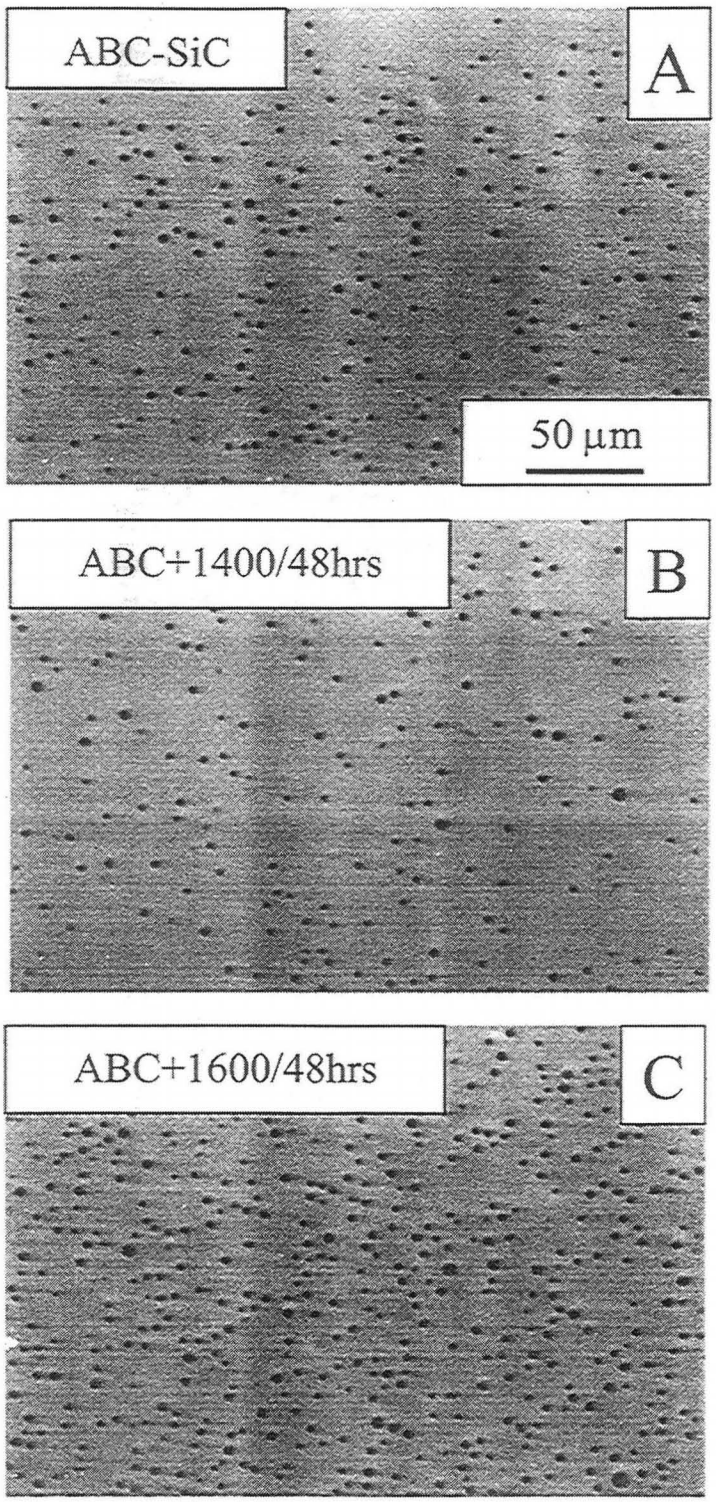

Figure 26: Plan view SEM micrographs of A) standard ABC-SiC, B) ABC-SiC + 1400°C-48 hours two-step processing, and C) ABC-SiC + 1600°C-48 hours two-step processing afteroxidation at 1400°C for 25 hours in air.

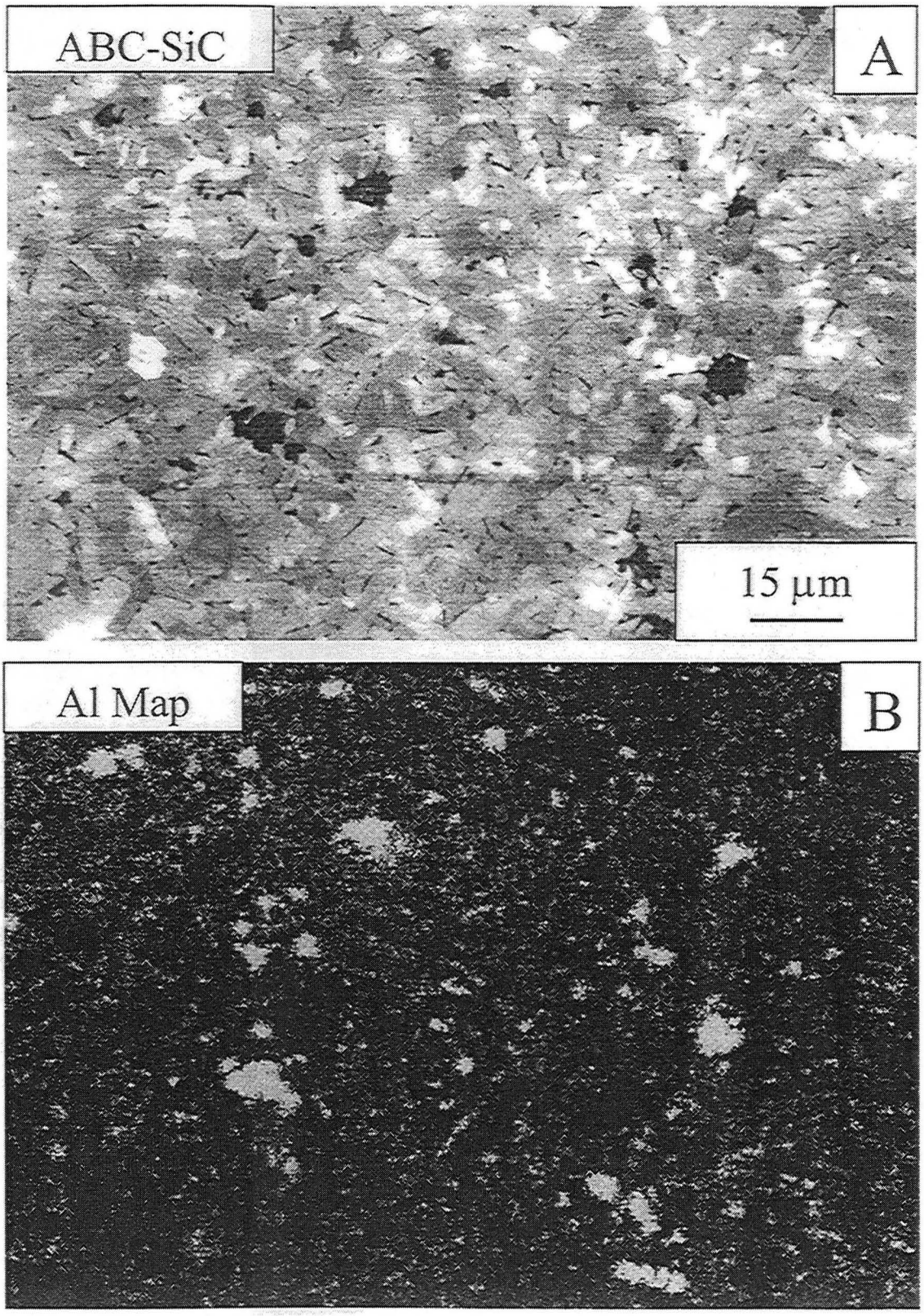

Figure 27: A) SEM micrograph of a polished ABC-SiC surface, B) corresponding WDS Al map of the same region.

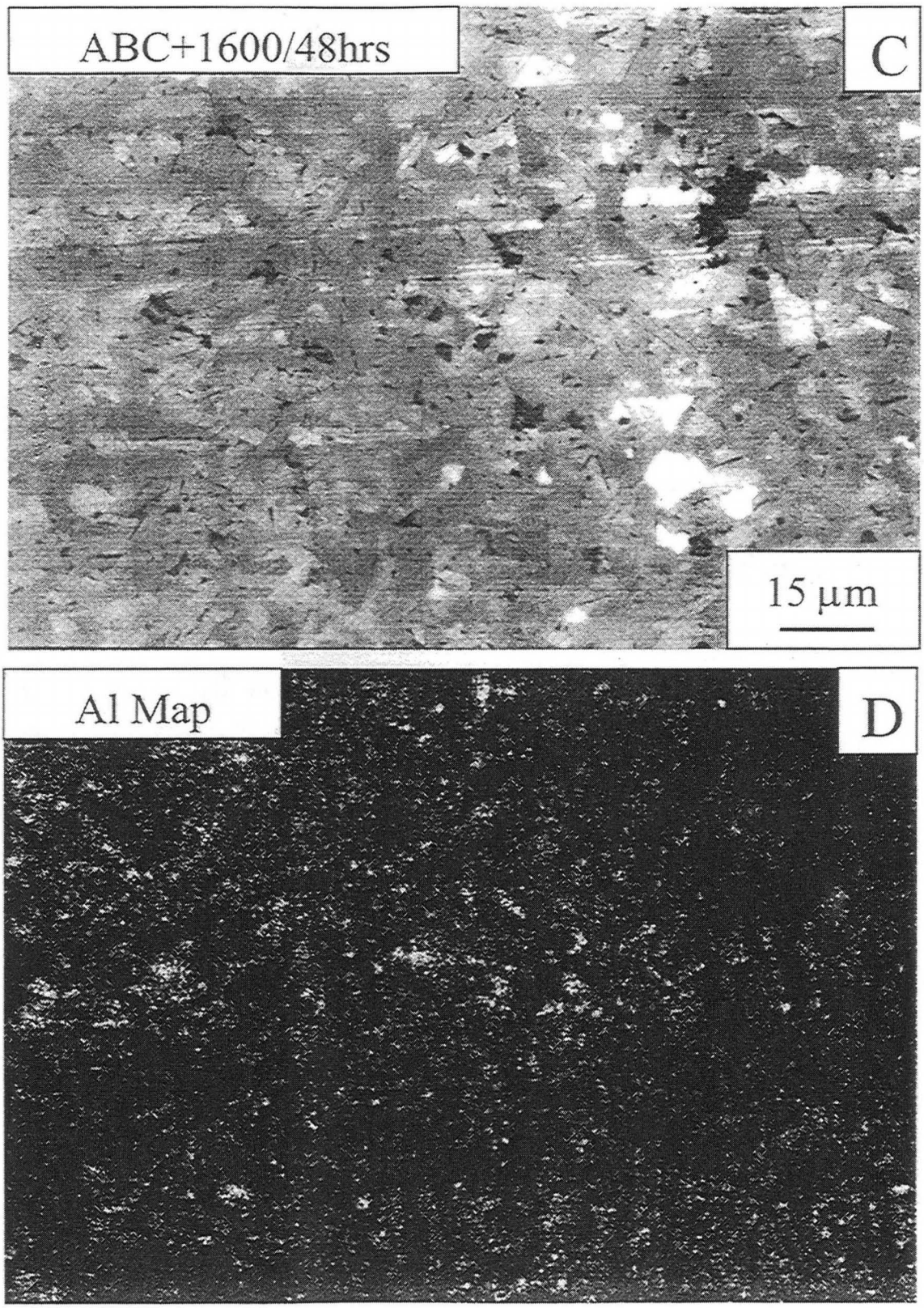

Figure 27: C) SEM micrograph of a polished ABC-SiC + 1600°C-48 hour processed surface, D) corresponding WDS Al map of the same region.

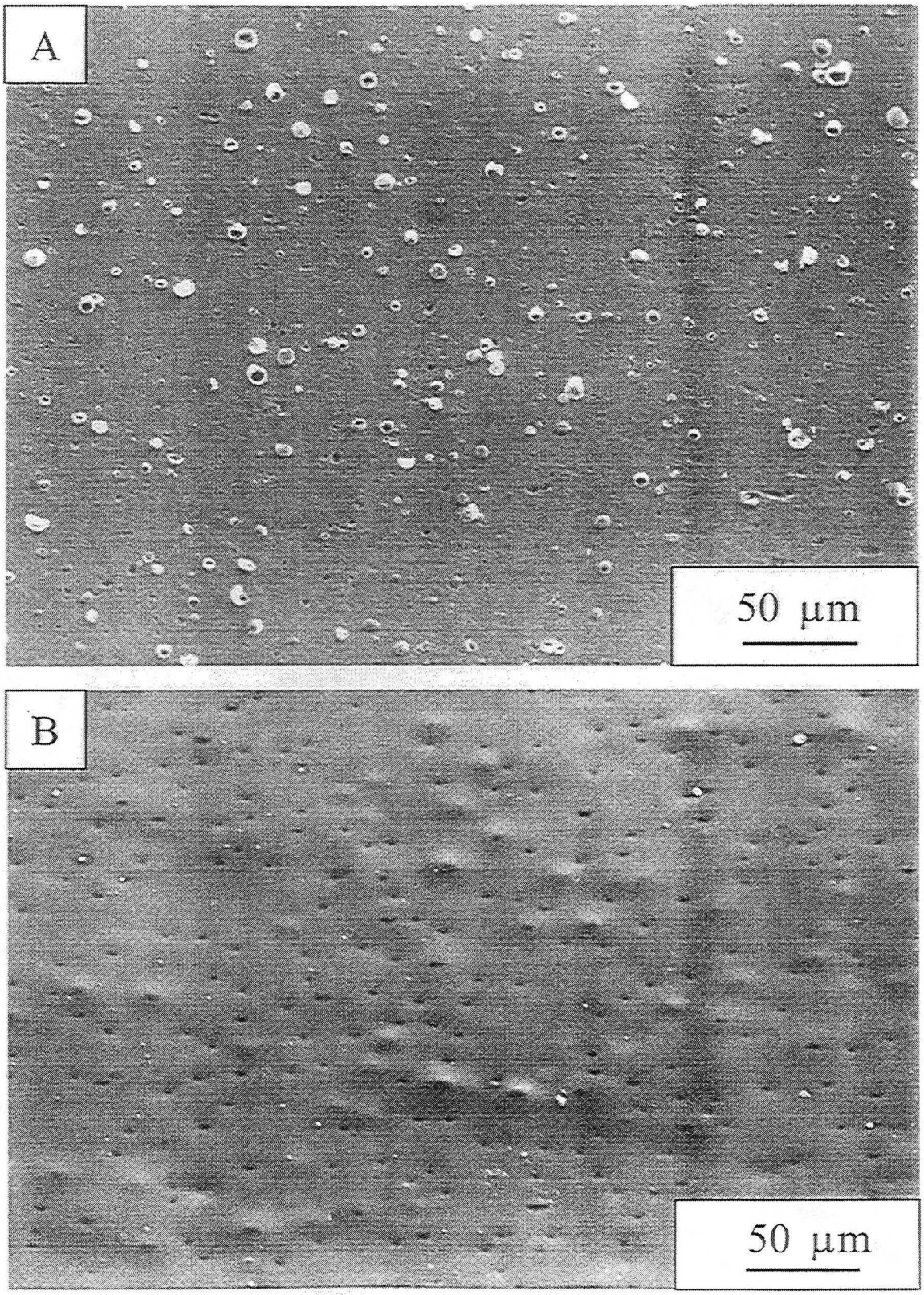

Figure 28: A) Top surface of Hexoloy and B) ABC-SiC after oxidation at 1400°C for 20 hours. Both SEM images taken at a tilt of 45°.

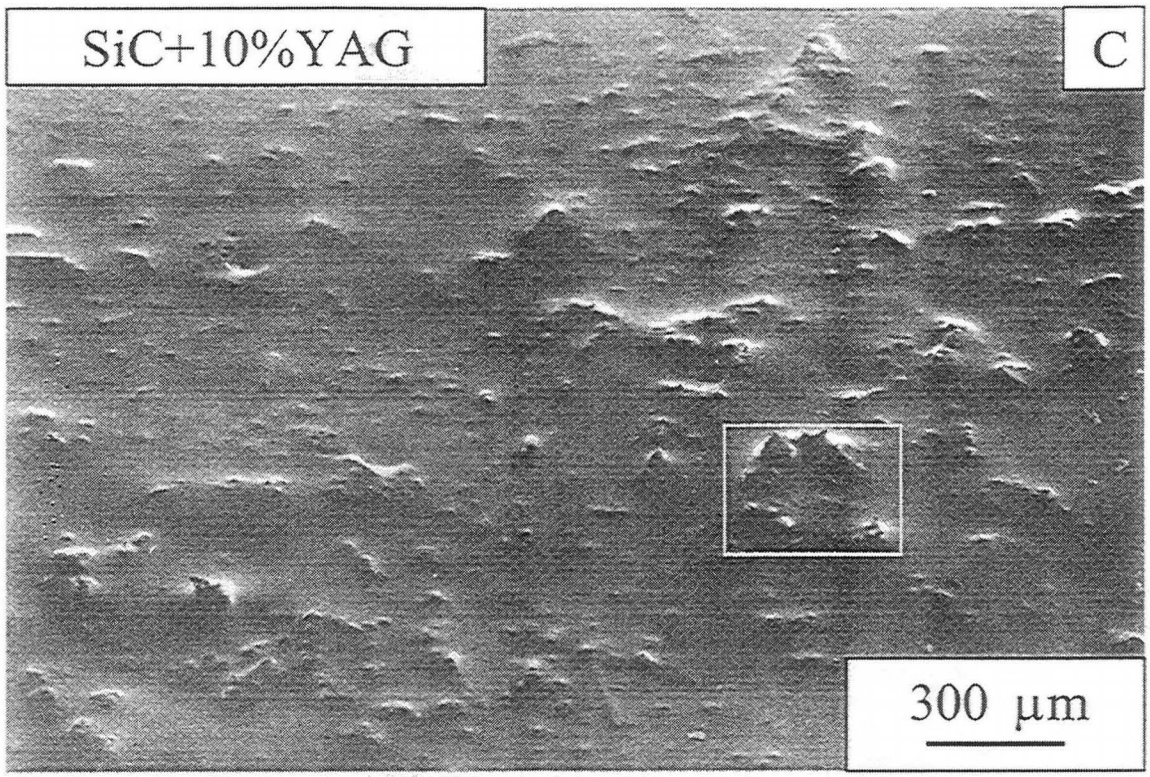

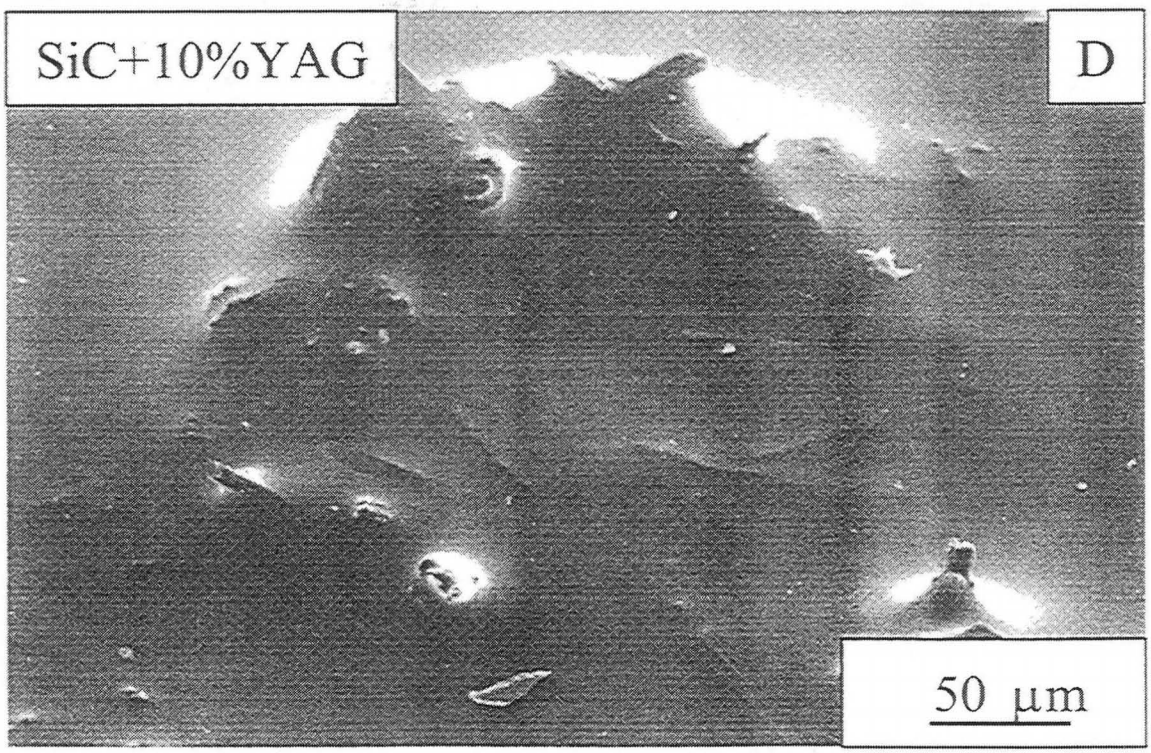

Figure 28: C) Top surface of SiC sintered with yttria and alumina D) high magnification of region marked by the box in C), after oxidation at 1400°C for 20 hours. Both SEM micrographs taken at a tilt of 45°.

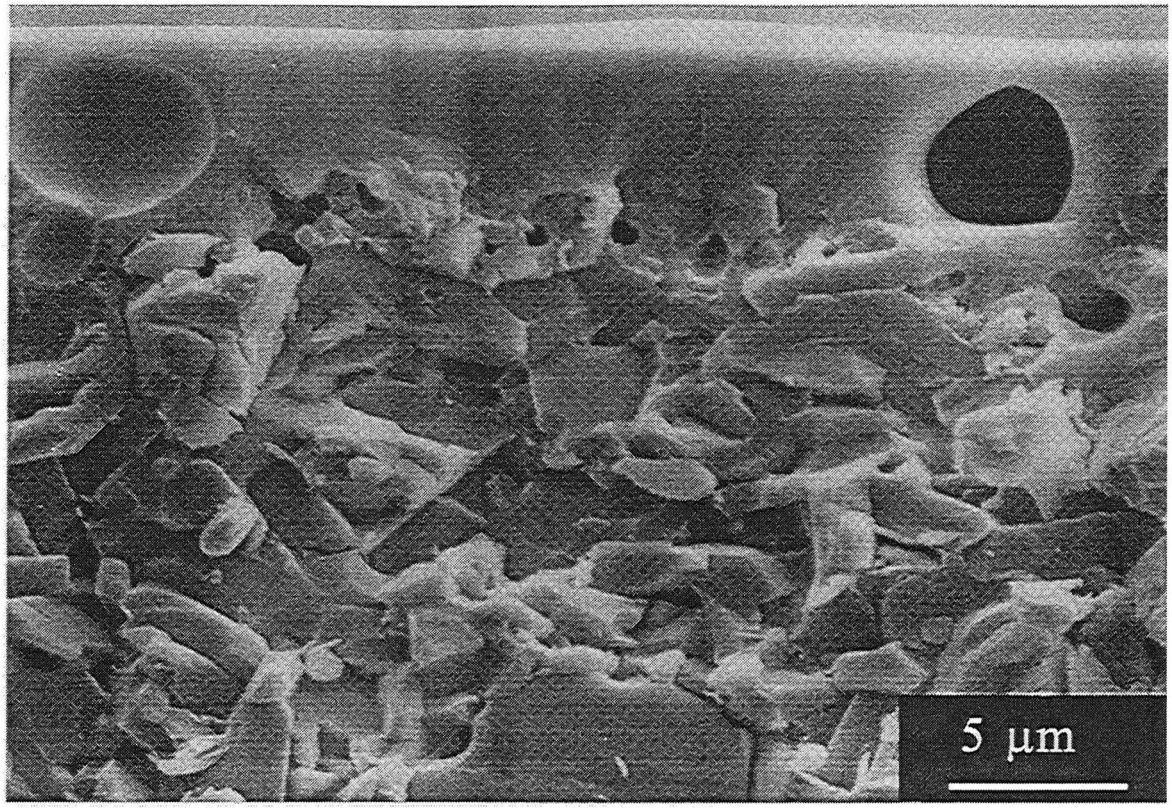

Figure 29: ABC-SiC oxidized at 1300°C for 25 hours in air, oxide stripped in HF solution, and reoxidized at 1300°C for 75 hours in air.

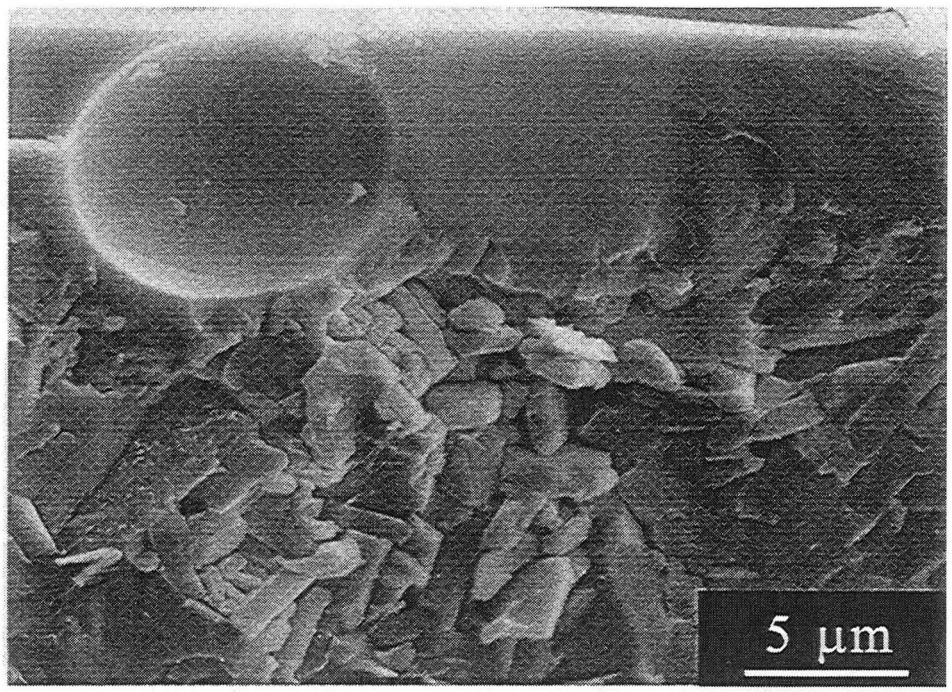

Figure 30: ABC-SiC plus 2% HF exposure for 24 hours. Oxidized at 1300°C for 75 hours in air. The oxide thickness was not uniform and this SEM micrograph shows a thicker region.

Figure 31: ABC-SiC plus 2% HF exposure for 24 hours. Oxidized at 1300°C for 75 hours in air. The oxide thickness was not uniform and this SEM micrograph shows a thin region.

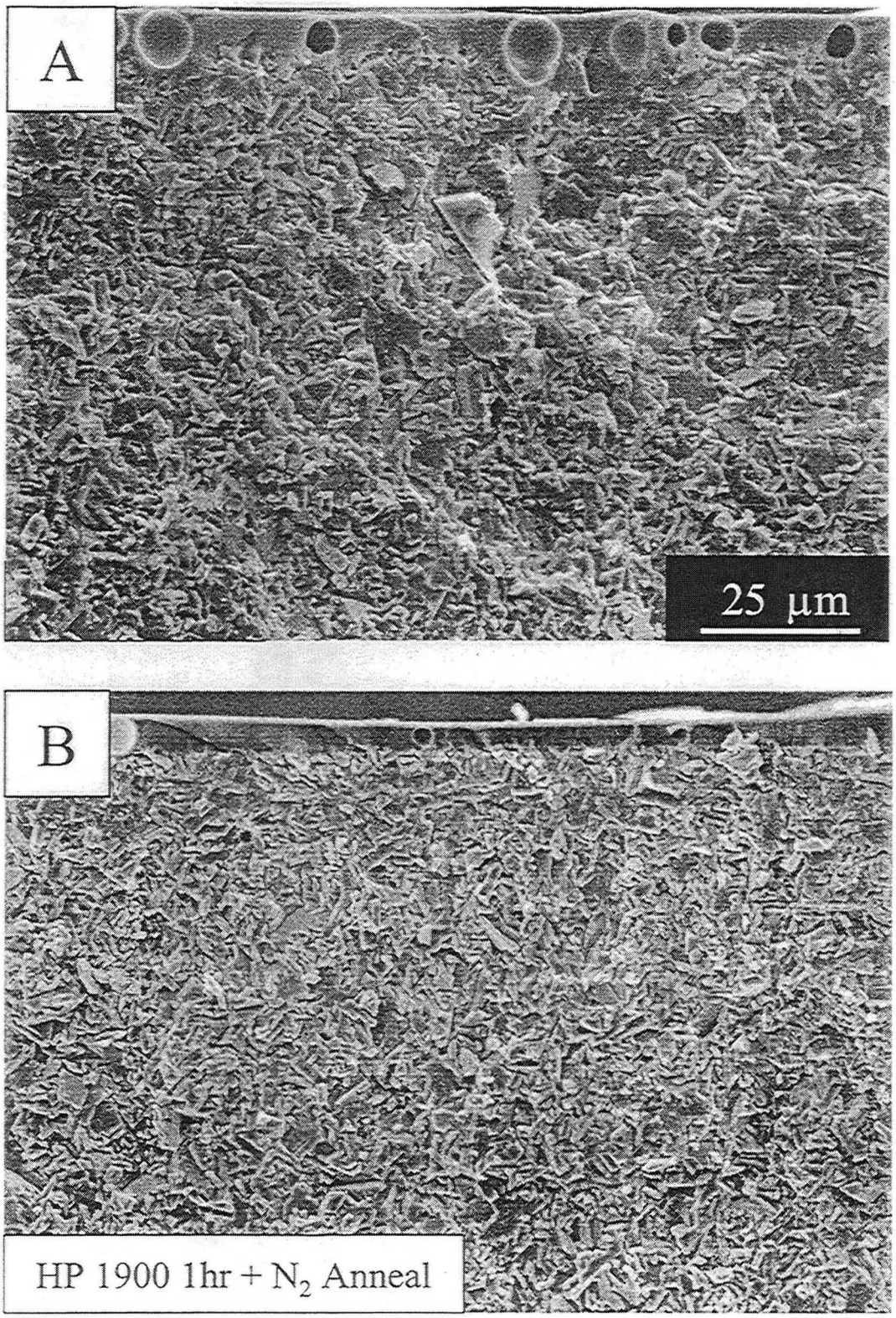

Figure 32: SEM micrographs after oxidation at 1300°C-75 hours in air for A) standard ABC-SiC and B) ABC-SiC + nitrogen heat treatment (1800°C-1 hour prior to oxidation).

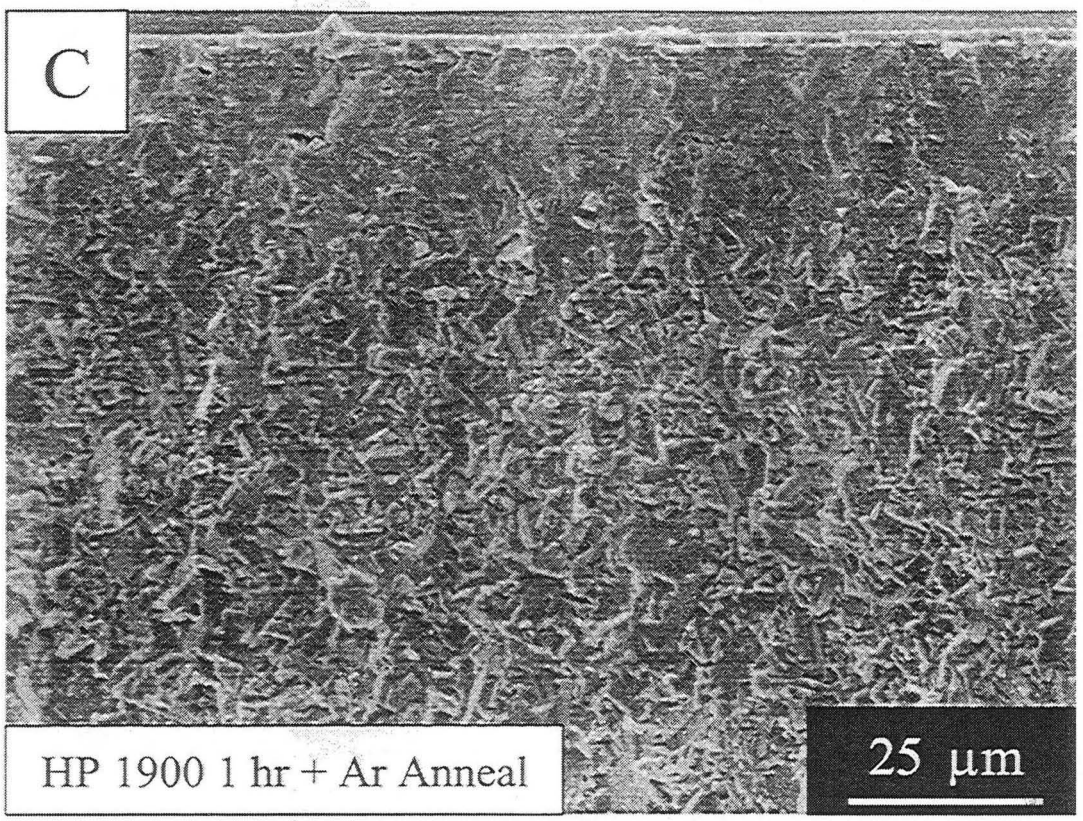

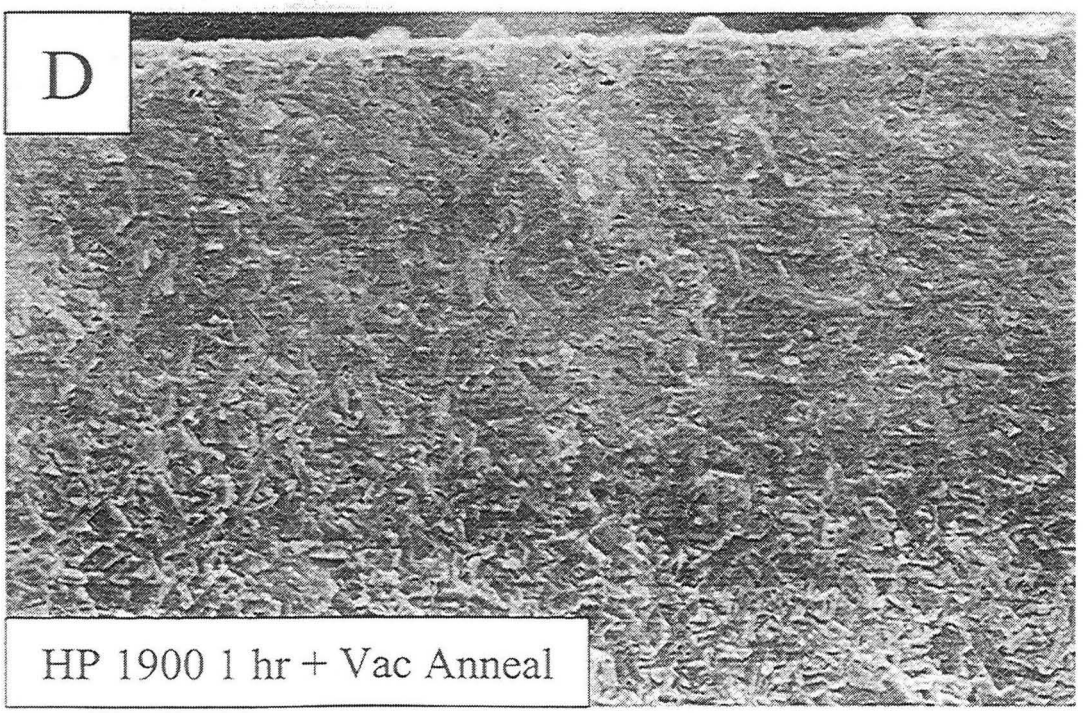

Figure 32: SEM micrographs after oxidation at 1300°C-75 hours in air for C) ABC-SiC +Ar heat treatment and D) ABC-SiC + vacuum heat treatment. Both heat treatments were for 1 hour at 1800°C, prior to oxidation.

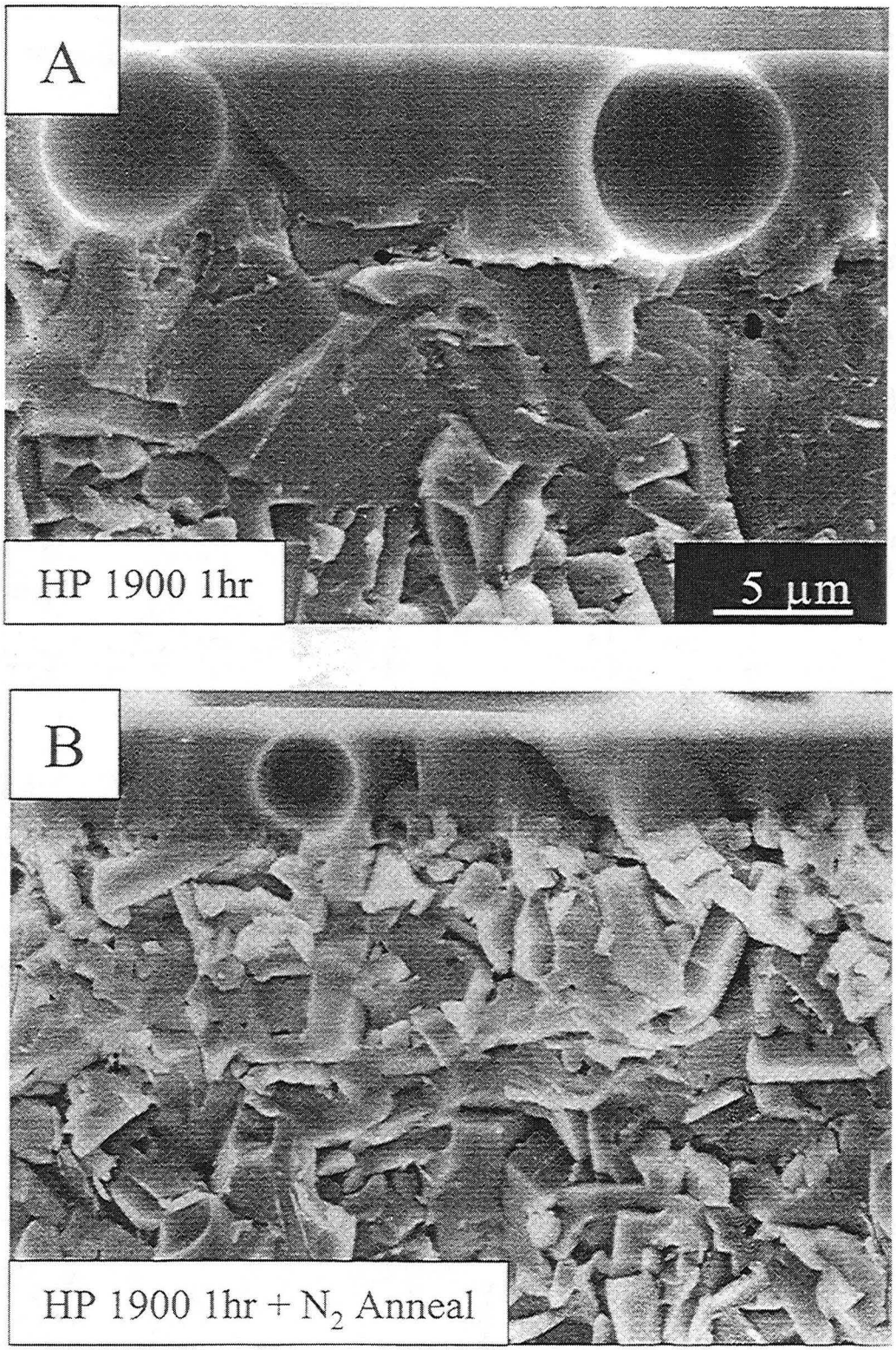

Figure 33: SEM micrographs after oxidation at 1300°C-75 hours in air for A) standard ABC-SiC and B) ABC-SiC + nitrogen heat treatment (1800°C-1 hour prior to oxidation).

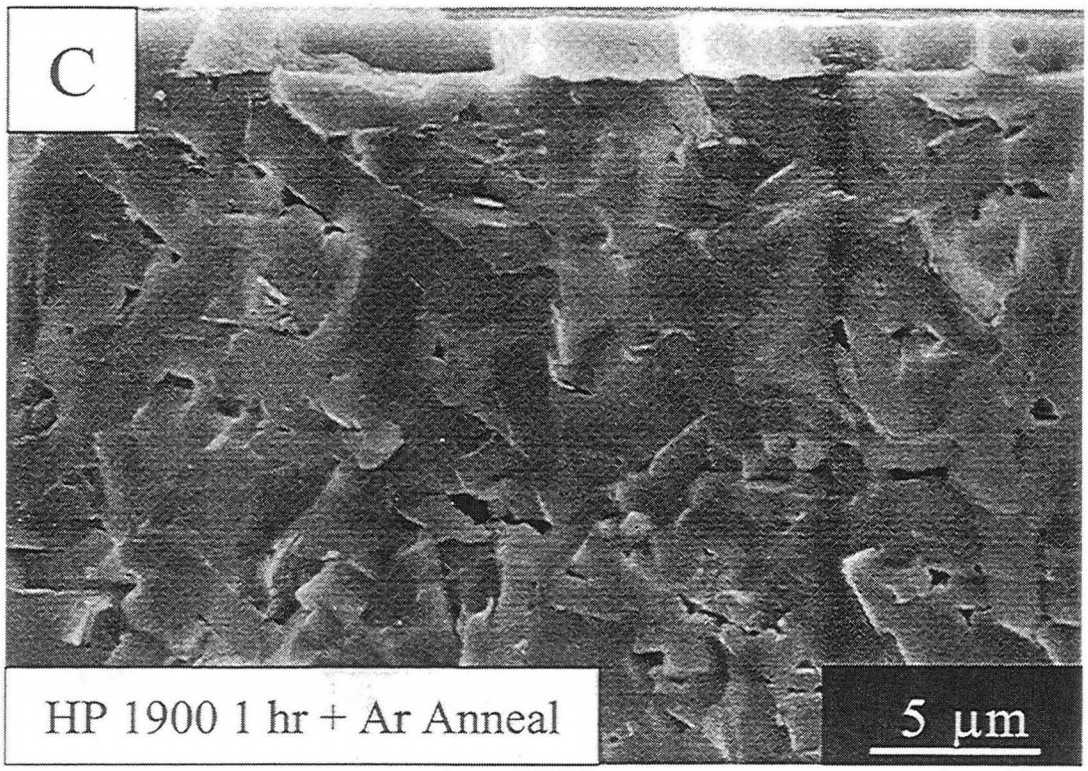

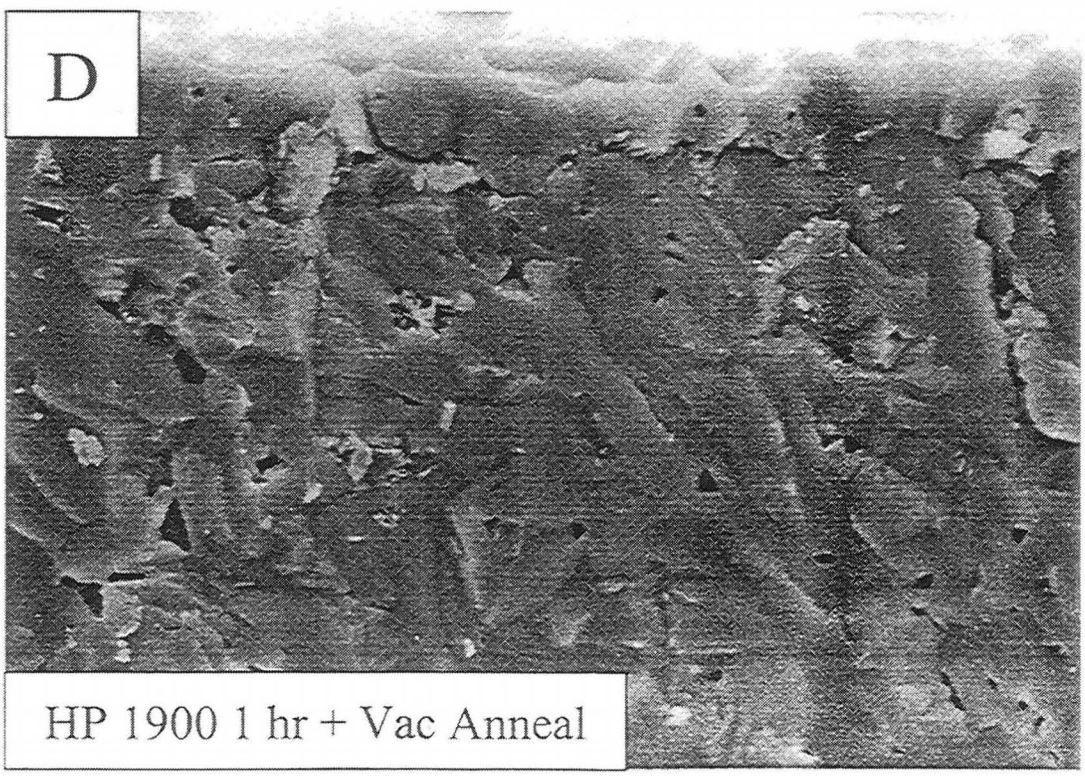

Figure 33: SEM micrographs after oxidation at 1300°C-75 hours in air for C) ABC-SiC +Ar heat treatment and D) ABC-SiC + vacuum heat treatment. Both heat treatments were for 1 hour at 1800°C, prior to oxidation.

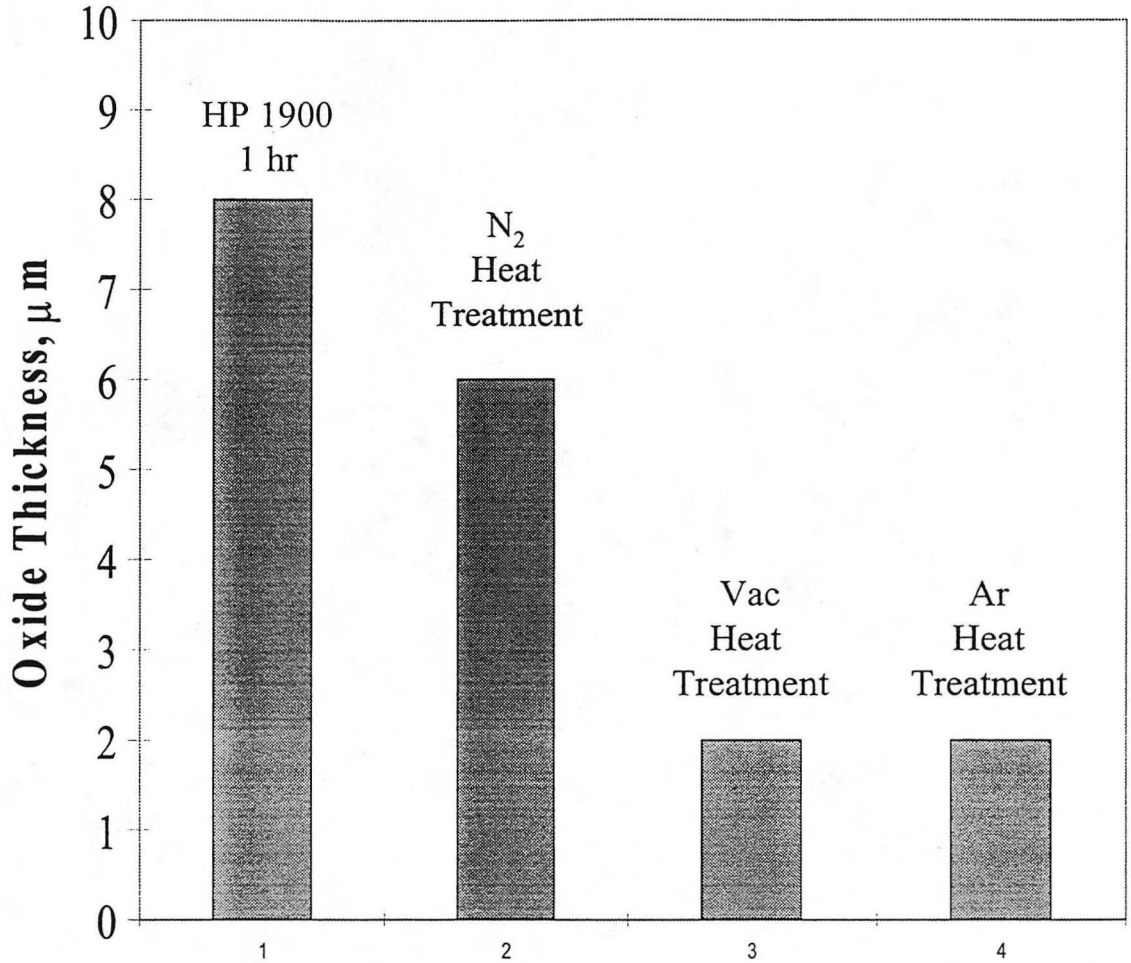

Figure 34: Bar graph comparing oxide thickness', 1300°C-75 hours in air, for standard ABC-SiC, ABC-SiC + nitrogen anneal, ABC-SiC + Ar heat treatment, and ABC-SiC + vacuum heat treatment.

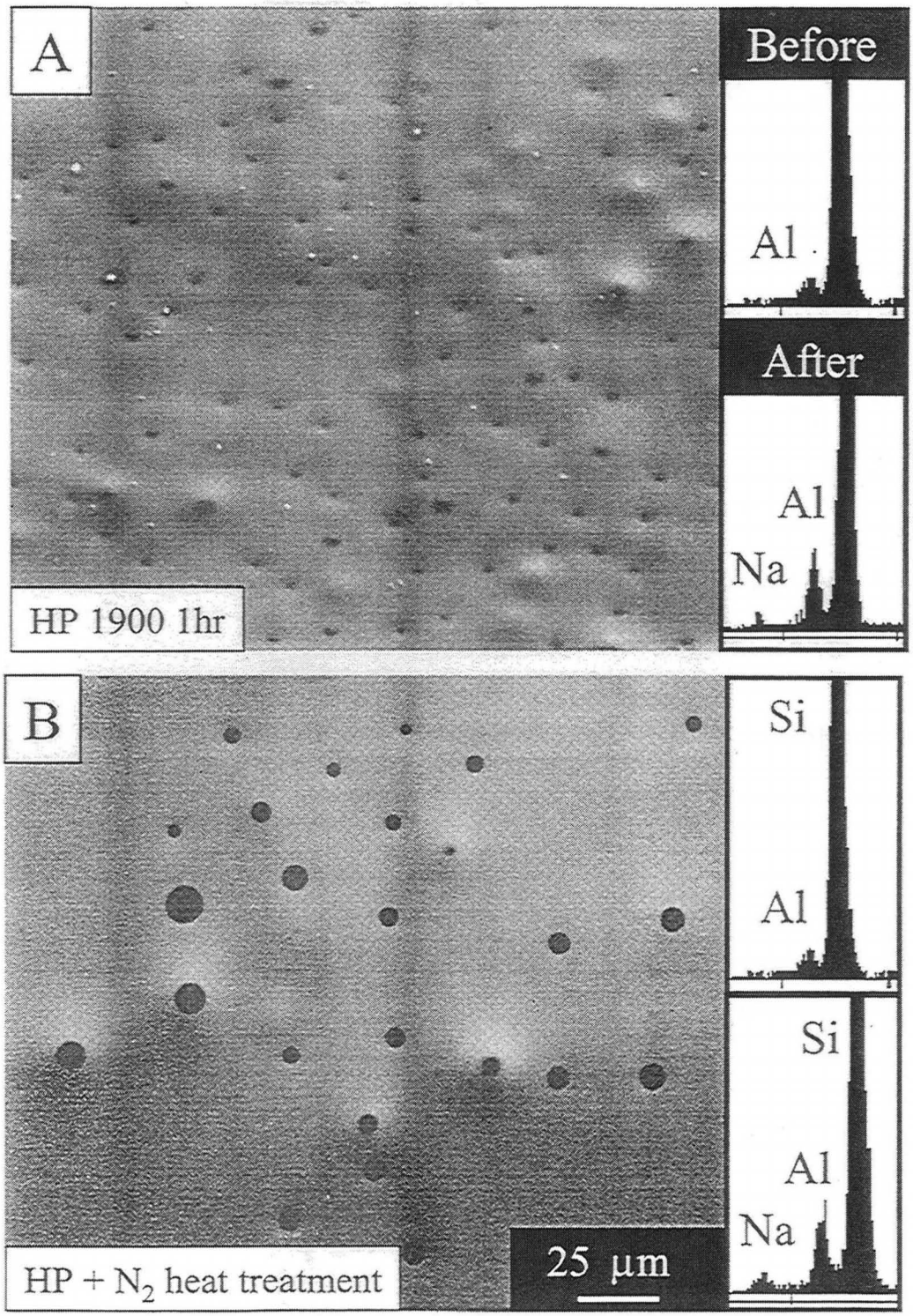

Figure35: Top surfaces of oxides for A) standard ABC-SiC and B) ABC-SiC + nitrogen heat treatment. The upper EDS spectra embedded in the SEM micrographs was obtained from the polished surface prior to oxidation. The lower EDS spectra in each sequence was obtained, at low magnification, from the surface after oxidation at 1300°C-75 hours in air.

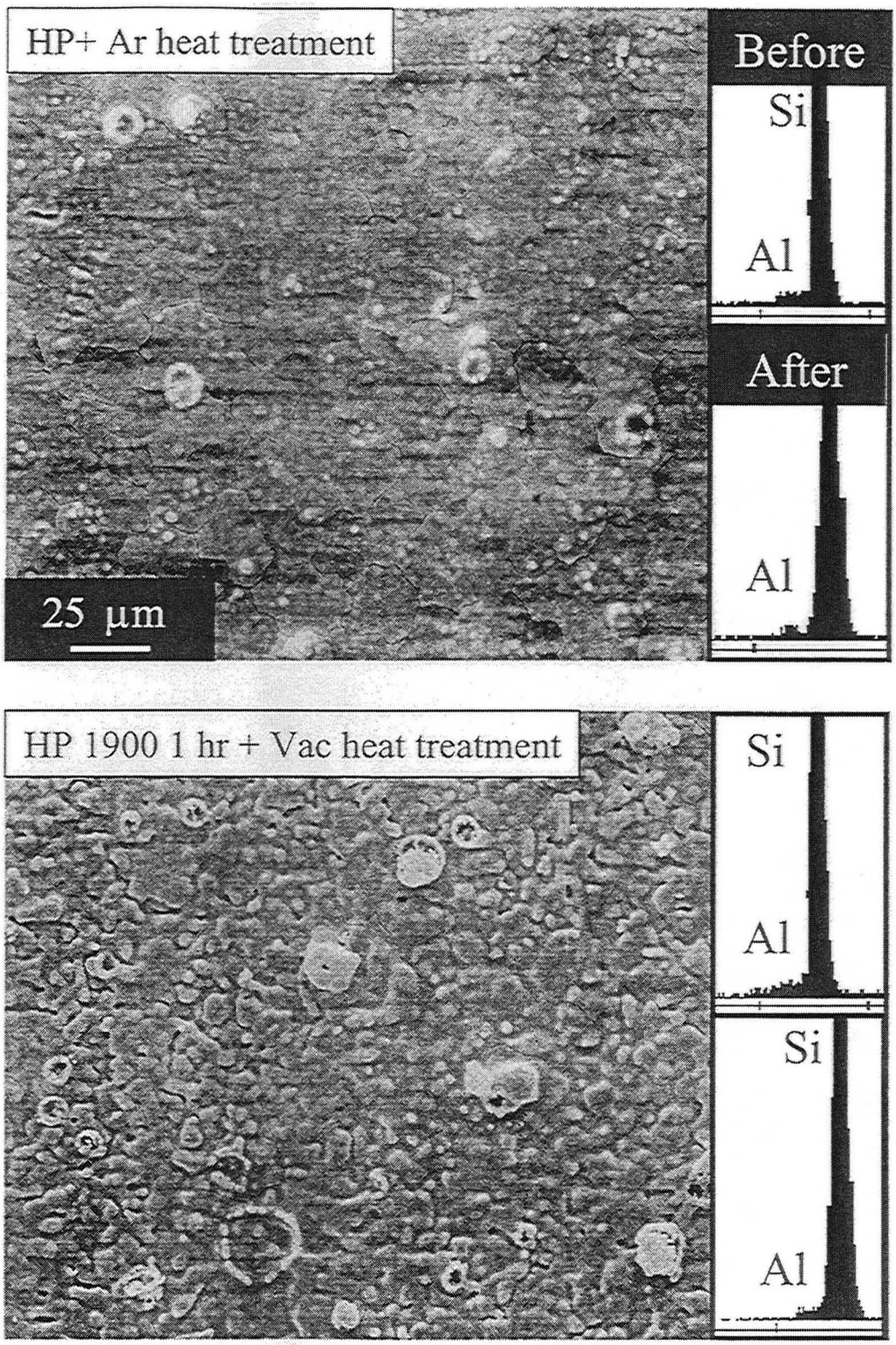

Figure 36: Top surfaces of oxides for A) ABC-SiC + Ar anneal and B) ABC-SiC + vacuum heat treatment. The upper EDS spectra embedded in the SEM micrographs were obtained from the polished surface prior to oxidation. The lower EDS spectra in each sequence was obtained, at low magnification, from the surface after oxidation at 1300°C-75 hours in air.

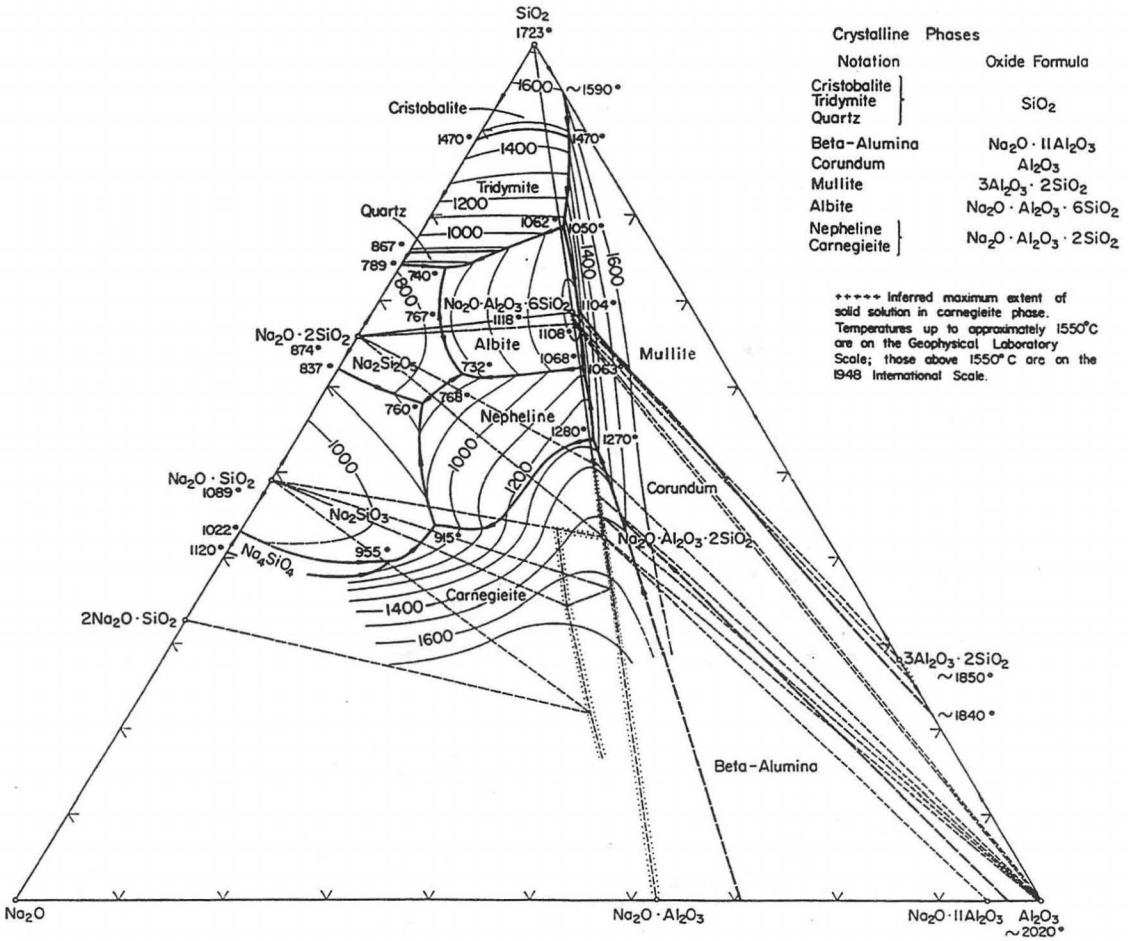

Figure 37: Equilibrium phase diagram for the Na_2O-Al_2O_3-SiO_2 system.

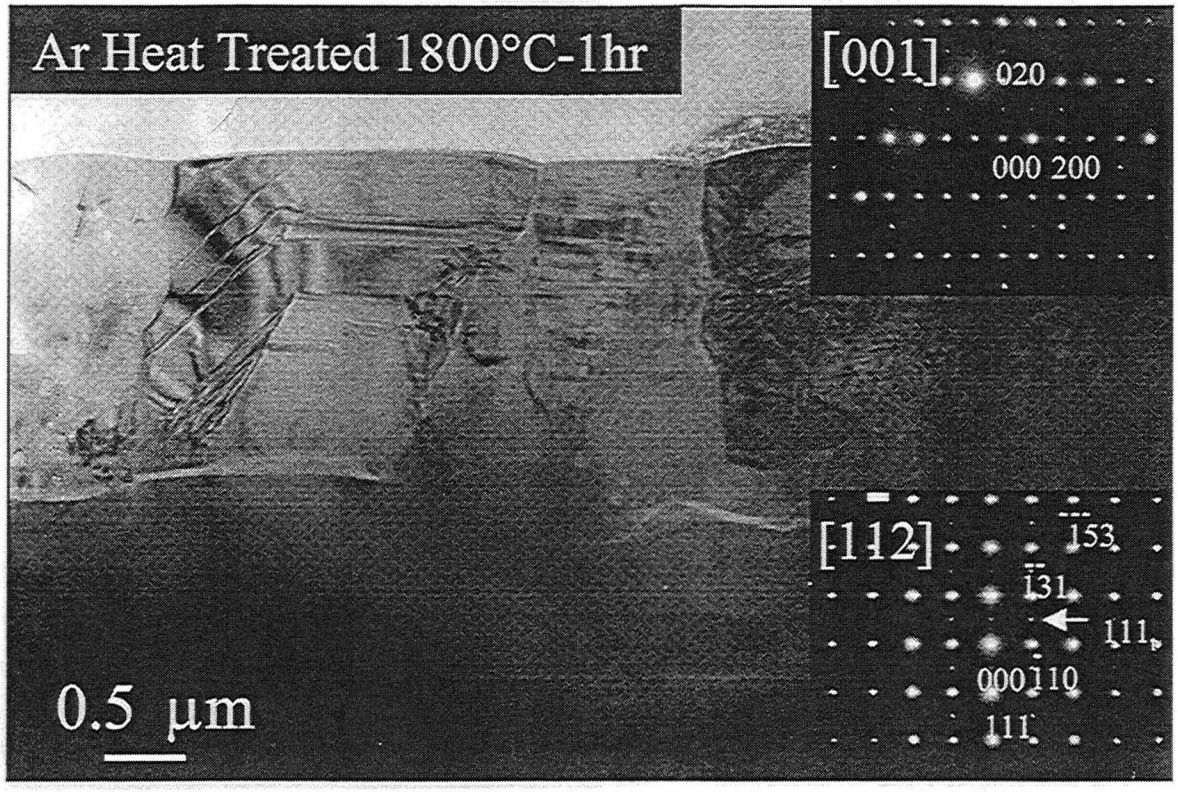

Figure 38: Bright-field TEM micrograph of oxide cross-section. ABC-SiC + Ar heat treatment oxidized at 1300°C for 75 hours in air. Electron diffraction patterns were obtained from two different grains. Courtesy of Dr. Warren J. MoberlyChan.

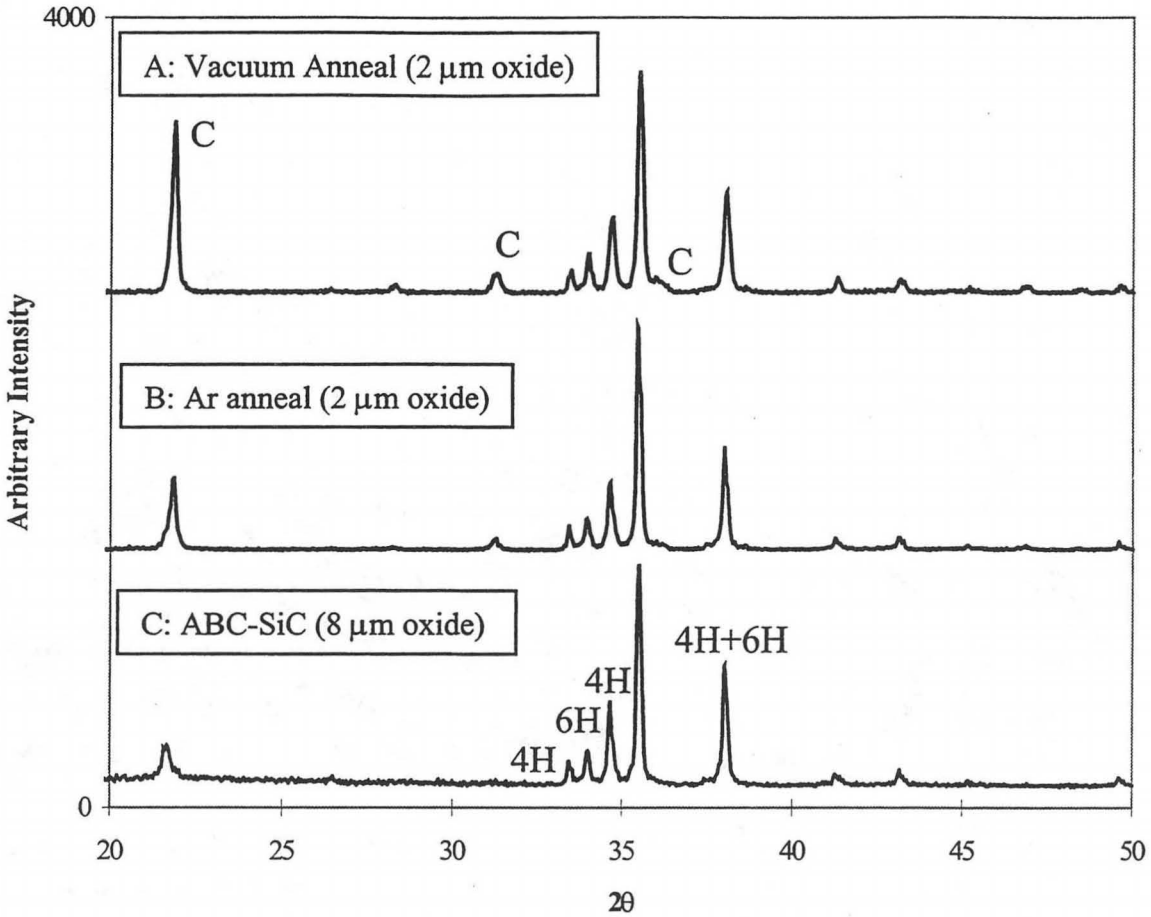

Figure 39: XRD spectra of oxides for A) ABC-SiC + vacuum anneal, B) ABC-SiC + Ar anneal, and C) standard ABC-SiC. The specimens were oxidized for 75 hours at 1300°C.

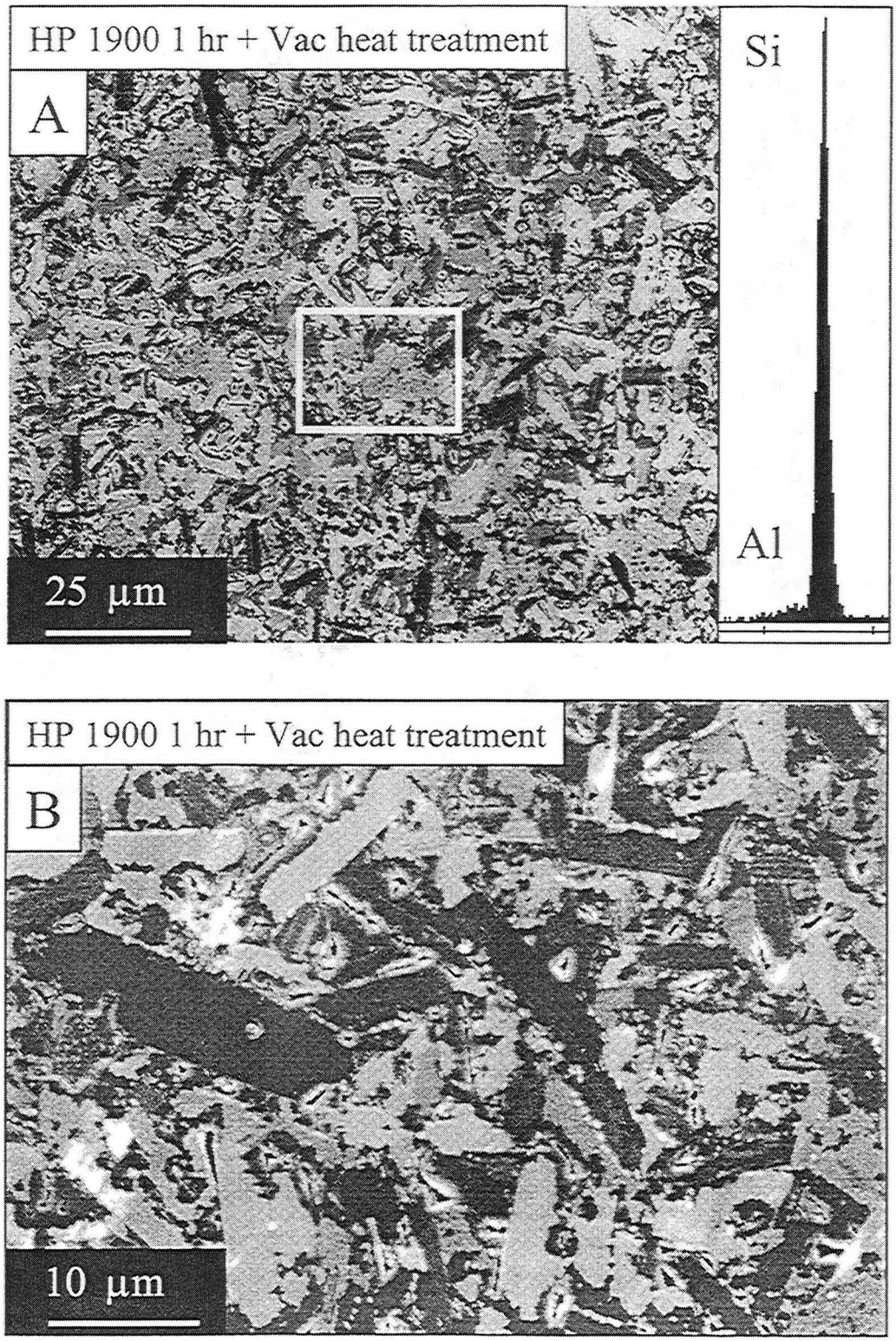

Figure 40: A) SEM micrograph of the surface after heat treating a polished ABC-SiC sample in vacuum (P~2 x 10^{-4} torr) at 1800°C for 1 hour. B) Higher magnification of region denoted by the box in A). The EDS spectra in A) was obtained from a low magnification region of the heat treated sample.

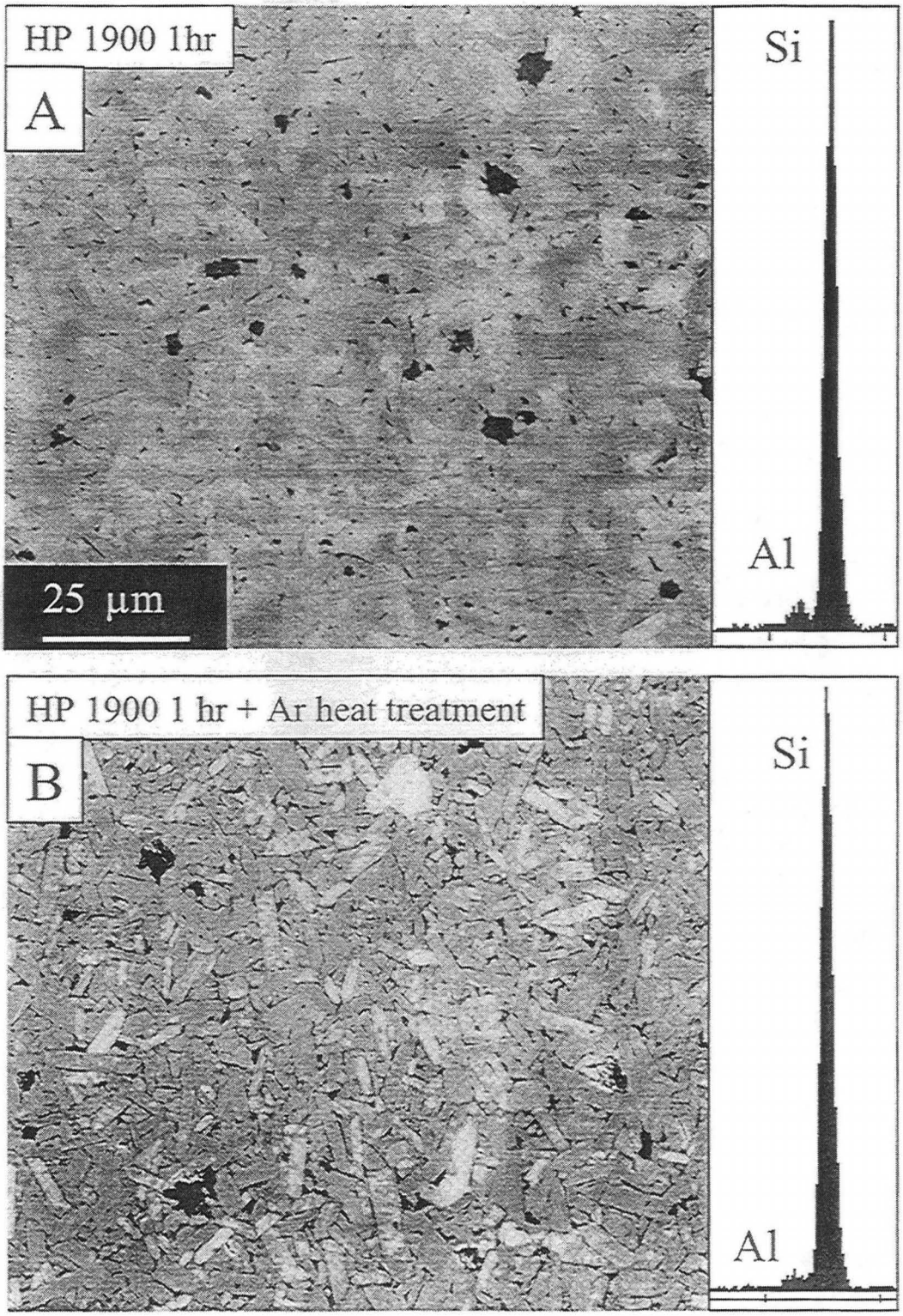

Figure 41: A) SEM micrograph of polished standard ABC-SiC surface. B) Surface of ABC-SiC after being annealed at 1800°C for 1 hour in Ar. The EDS spectra at the right of the micrographs, which show Al and Si signals, were obtained from the surfaces at low magnification.

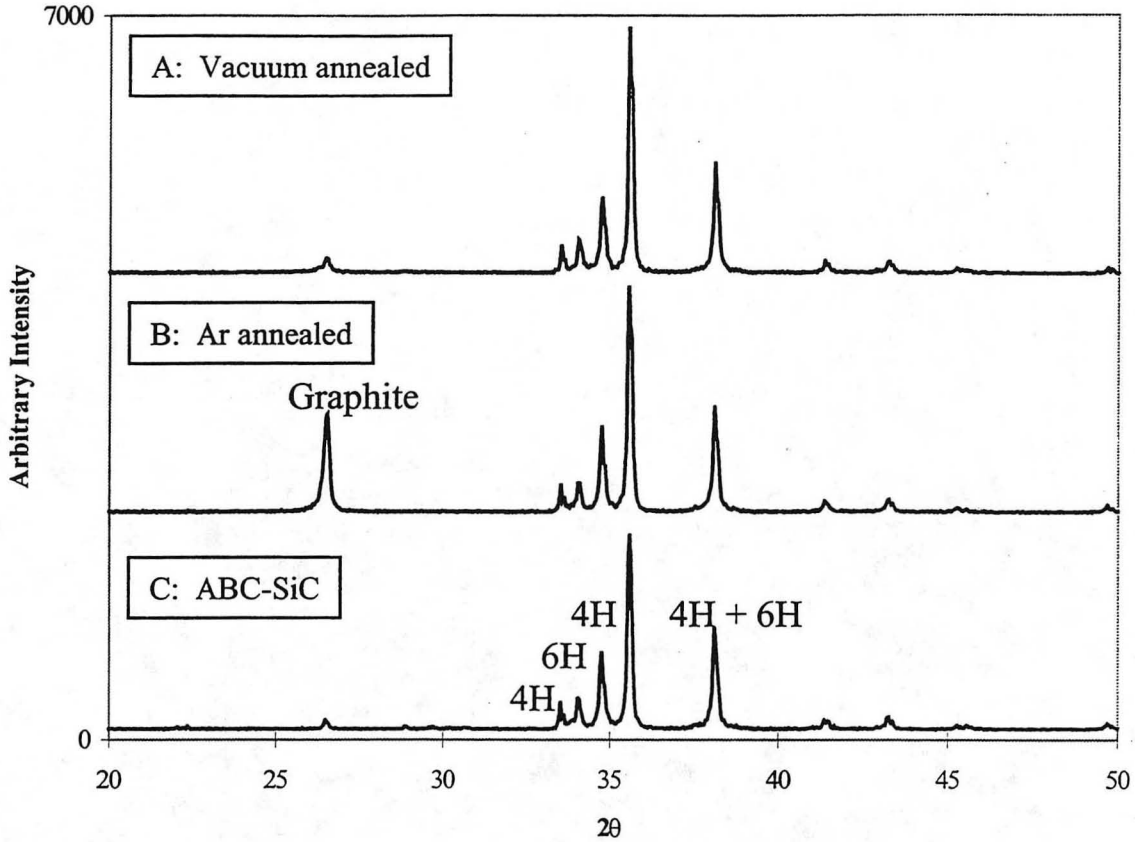

Figure 42: XRD spectra of surface for A) ABC-SiC + vacuum anneal, B) ABC-SiC + Ar anneal, and C) standard ABC-SiC prior to oxidation.

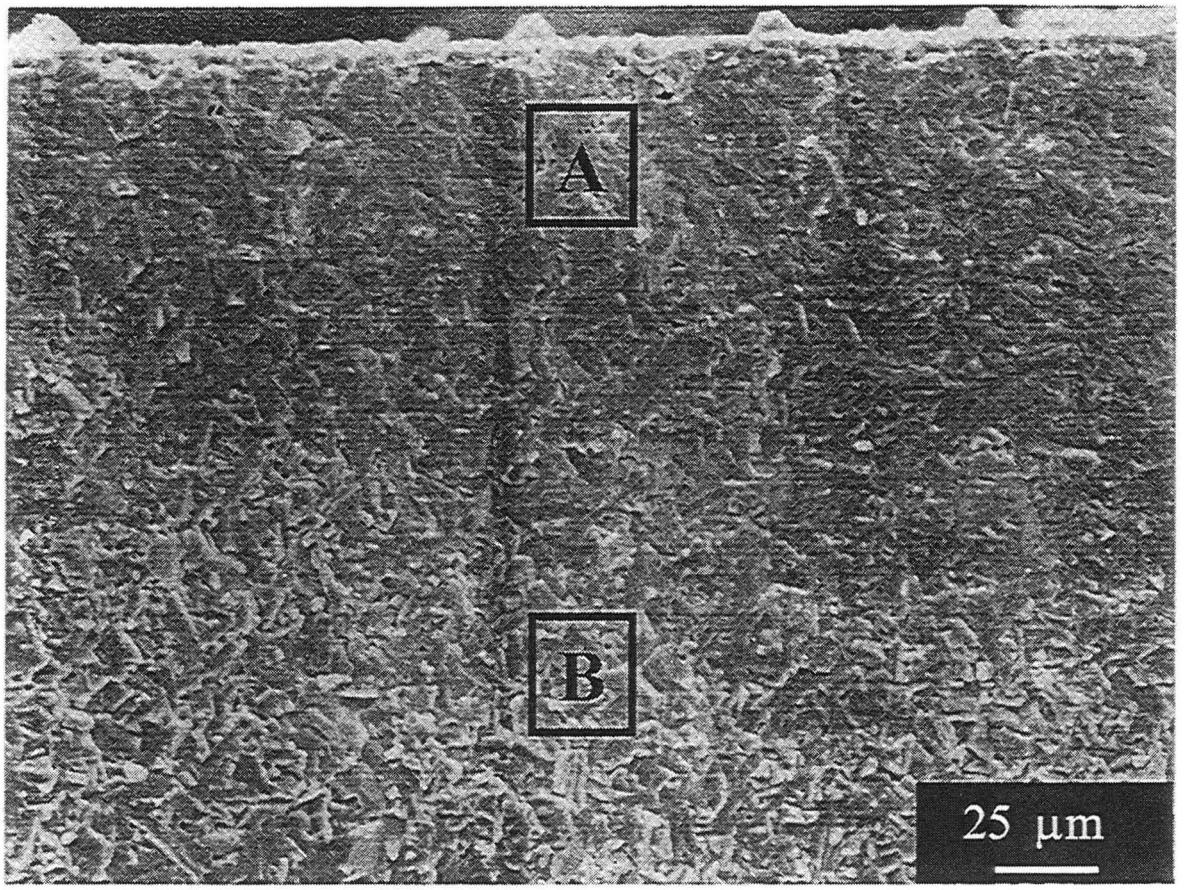

Figure 43: SEM micrograph of fracture surface of ABC-SiC annealed in vacuum and oxidized at 1300°C for 75 hours in air.

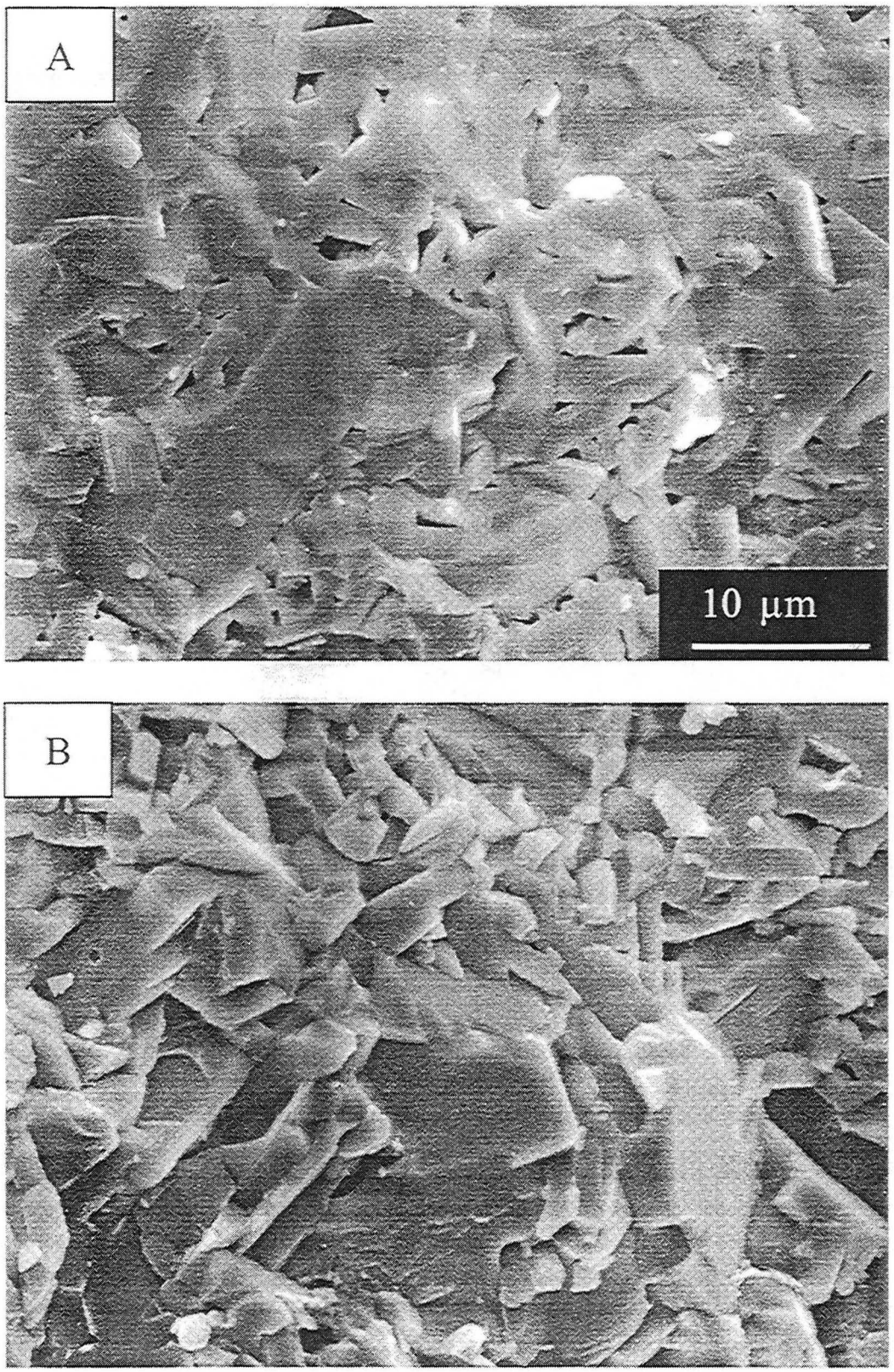

Figure 44: Higher magnification SEM micrographs of the regions corresponding to A & B in Figure 43.

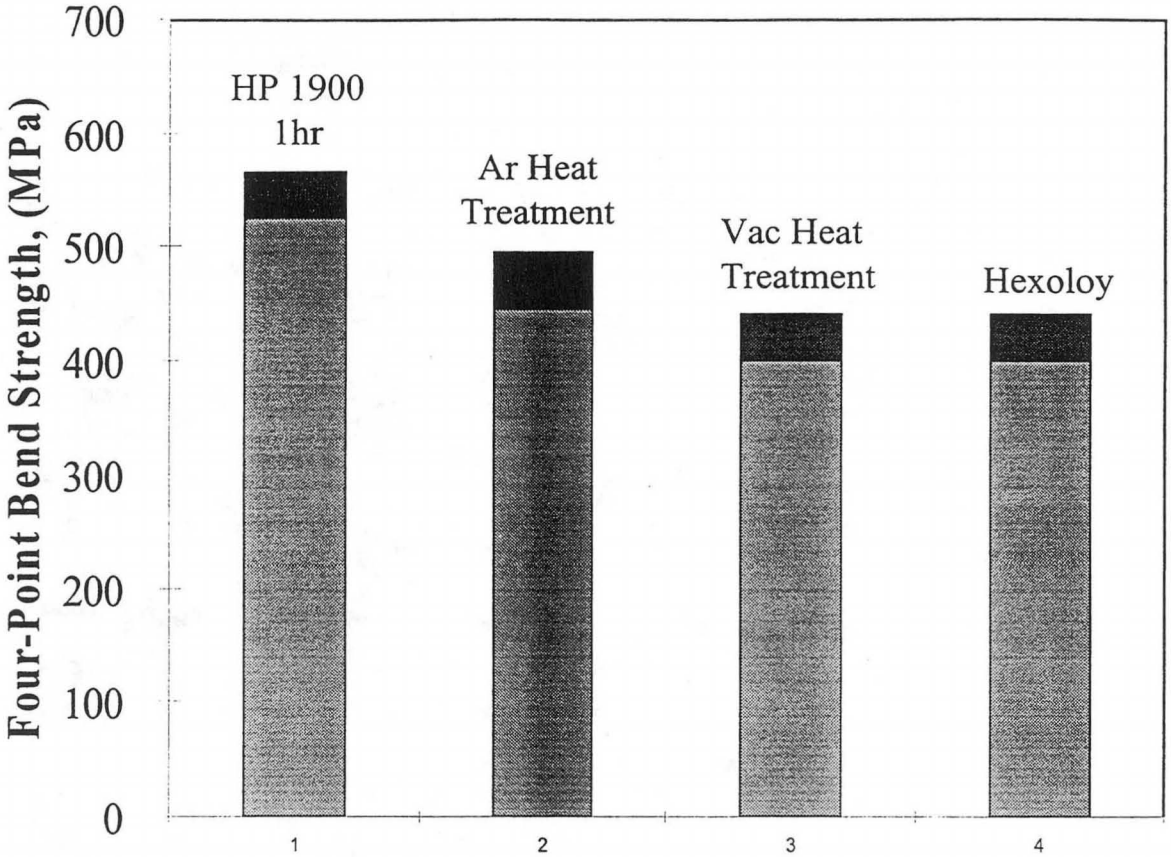

Figure 45: Four-point bend strength for ABC-SiC and SiC annealed in Ar and vacuum. The strength of commercially available Hexoloy is shown for comparison.

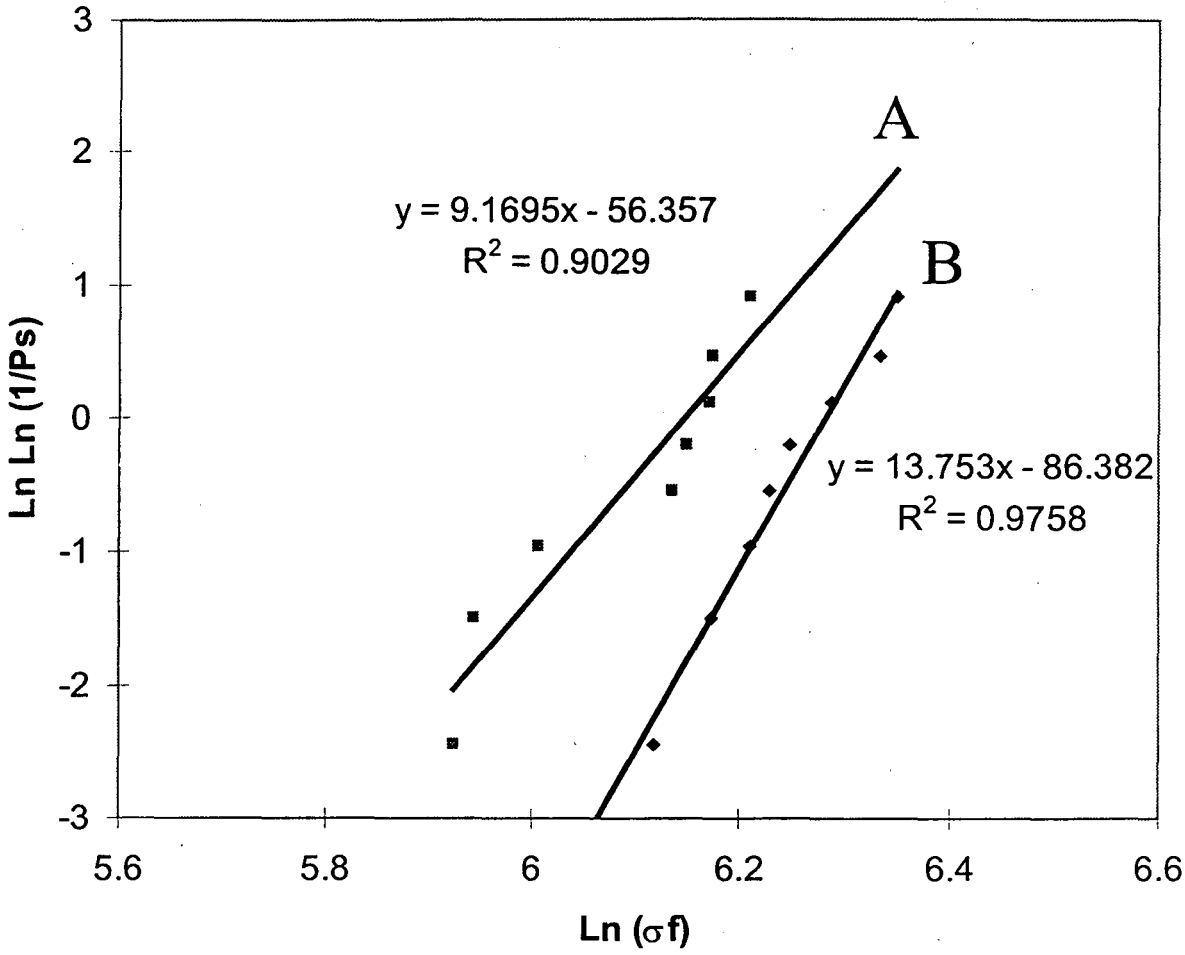

Figure 46: Weibull plots for A) ABC-SiC + Ar heat treatment and B) ABC-SiC.

Ernest Orlando Lawrence Berkeley National Laboratory
One Cyclotron Road | Berkeley, California 94720

Prepared for the U.S. Department of Energy under Contract No. DE-AC03-76SF00098